Dissertation
submitted to the
Combined Faculty of Natural Sciences and Mathematics
of the Ruperto Carola University Heidelberg, Germany
for the degree of
Doctor of Natural Sciences

Presented by: MSc John Brevoort Walden
Born in: New York City, USA
Oral examination: May 4th, 2020

UNRAVELING THE MYSTERIES OF THE PLANT CELL WALL: A CHARACTERIZATION OF THREE NOVEL PROTEINS RELATED TO CELL WALL SIGNALING

Referees: Prof. Dr. Karin Schumacher

Dr. Sebastian Wolf

Table of Contents

Summary

The field of plant cell wall signaling is one that has seen tremendous growth in the last few decades. One result of this has been the identification of many uncharacterized proteins putatively involved in the cell wall signaling network. This thesis outlines the initial characterization of three previously unstudied genes of interest in the model organism *Arabidopsis thaliana* which are loosely tied together by their apparent links, either directly or indirectly, with cell wall signaling. The first gene investigated, named PHYTOSULFOKINE LIKE 1 (PSKL1), is what seems to be a potential preproprotein with possible links to Phytosulfokine (PSK) singling and RECEPTOR-LIKE-PROTEIN 44 (RLP44). PSKL1 was found to contain two of the YIYTQ amino acid motifs found in *PSK* genes and to affect vascular cell identity. This was shown by an increase in the average number of metaxylem cells in the roots of *pskl1* mutant seedlings, a phenotype that was rescued back to wildtype by exogenous PSK treatment. The inverse of this phenotypic trend was observed in a mutant line where both PSK motifs in the gene remained intact, suggesting that PSKL1 might function as more than a possible source of mature PSK's. The second gene investigated is a member of the F-Box/RNI Like family. This gene was identified in a forward genetic screen looking for suppressors of the *RLP44ox* phenotype, where it emerged as the most likely candidate for a Brassinosteroid (BR) signaling independent *RLP44ox* suppressor. Generation of a *f-box/rni like* line in the *RLP44ox* background using the CRISPR/Cas9 system recapitulated the suppression phenotype, supporting its role as the causative mutant gene in the original forward genetic screen. Use of a F-Box/RNI Like:RFP line showed F-Box/RNI Like to be localized to the cytosol and a lack of colocalization with RLP44:GFP, suggesting that it doesn't directly associate with RLP44. The third gene investigated is a receptor like protein named RECEPTOR-LIKE-PROTEIN 46 (RLP46), which has a high degree of genetic conservation throughout the plant kingdom. Available data showed highest *RLP46* expression in mature root tissue, and a strong upregulation of expression upon exposure to the elicitor elf18, suggesting RLP46 might have a role in plant innate immune response. The CRISPR/Cas9 system was used to generate a *rlp46* mutant line which was tested for biotic and abiotic stress phenotypes. *rlp46* at first showed a possible NaCl resistance phenotype, but repetitions of the experiment gave conflicting results. There was however a subtle but consistent phenotype of resistance to elicitor induced growth inhibition in the *rlp46* line. Co-immunoprecipitation and Western Blot showed evidence for an association between RLP46 and SUPPRESSOR-OF-BIR 1 (SOBIR1), providing a strong clue for how RLP46 might interact with the plant immune response signaling network. The experiments outlined in this thesis proved successful in characterizing these three proteins and provide a firm foundation for future research.

Zusammenfassung

Das Feld der Pflanzenzellwandsignale ist in den letzten Jahrzehnten enorm gewachsen. Das führte zur Identifizierung vieler bislang nicht charakterisierter Proteine, die mutmaßlich am Signalnetzwerk der Zellwand beteiligt sind. In dieser Dissertation werden drei bisher nicht untersuchte Gene des Modellorganismus *Arabidopsis thaliana* charakterisiert, die durch ihre scheinbar direkten oder indirekten Verbindungen mit der Signalübertragung an der Zellwand lose miteinander verbunden sind. Das erste hier untersuchte Gen, PHYTOSULFOKINE LIKE 1 (PSKL1), scheint ein potenzielles Preproprotein mit möglichen Verbindungen zu Phytosulfokine (PSK) -Einzelprodukten und RECEPTOR-LIKE-PROTEIN 44 (RLP44) zu sein. PSKL1 enthält zwei der in PSK-Genen gefundenen YIYTQ-Aminosäuremotive, was darauf schließen lässt, dass es die Identität der Gefäßzellen beeinflusst. Eine Zunahme der durchschnittlichen Anzahl von Metaxylemzellen in den Wurzeln von pskl1-mutierten Keimlingen, ein Phänotyp, der durch exogene PSK-Behandlung in den Wildtyp zurückgeführt wurde, bestätigt diese Vermutung. Die Umkehrung dieses phänotypischen Trends wurde in einer Mutante beobachtet, in der beide PSK Motive im Gen intakt blieben, was darauf hindeutet, dass PSKL1 zusätzlich zu seiner potentiellen Rolle als Quelle für reife PSKs noch weitere Funktionen haben könnte. Das zweite untersuchte Gen ist ein Mitglied der F-Box/RNI Like-Familie. Dieses Gen wurde in einem genetischen Vorwärtsscreening auf der Suche nach Suppressoren des RLP44ox-Phänotyps identifiziert, wobei es sich als wahrscheinlichster Kandidat für einen Brassinosteroid (BR)-Signal-unabhängigen RLP44ox-Suppressor erwies. Die Erzeugung einer *f-Box/rni-like* Linie im RLP44ox-Hintergrund unter Verwendung des CRISPR/Cas9-Systems immitierte den Suppressionsphänotyp und untermauerte seine Rolle als ursächliches mutiertes Gen im ursprünglichen genetischen Vorwärtsscreening. Die Verwendung einer F-Box/RNI-Like:RFP-Linie zeigte, dass F-Box/RNI-Like im Cytosol lokalisiert war und dass die Co-Lokalisierung mit RLP44:GFP fehlte, was darauf hindeutet, dass es nicht direkt mit RLP44 assoziiert. Das dritte untersuchte Gen ist RECEPTOR-LIKE-PROTEIN 46 (RLP46), ein Rezeptor-like Protein, das im gesamten Pflanzenreich einen hohen Grad an genetischer Konservierung aufweist. Die höchste RLP46-Expression wurde in reifem Wurzelgewebe gemessen, mit starker Hochregulierung der Expression bei Exposition gegenüber dem Elicitor elf18, was darauf hindeutet, dass RLP46 eine Rolle bei der angeborenen Immunantwort der Pflanze spielt. Das CRISPR/Cas9-System wurde verwendet, um eine rlp46-Mutantenlinie zu erzeugen, die auf biotische und abiotische Stressphänotypen getestet wurde. *rlp46* zeigte zunächst einen möglichen NaCl-Resistenz-Phänotyp, aber Wiederholungen des Experiments ergaben widersprüchliche Ergebnisse. Es gab jedoch einen subtilen, aber konsistenten Phänotyp der Resistenz gegen durch Auslöser induzierte Wachstumshemmung in der rlp46-Linie. Co-Immunpräzipitation und Western Blot zeigten Hinweise auf eine Assoziation zwischen RLP46 und SUPPRESSOR-OF-BIR 1 (SOBIR1), was einen starken Hinweis darauf liefert, wie RLP46 mit dem Signalnetzwerk der pflanzlichen Immunantwort interagieren könnte. Diese Arbeit beschreibt die erfolgreiche Charakterisierung dieser drei Proteine, und bildet eine fundierte Basis für weitere Forschung.

Introduction

The ability to interact with its surroundings is a function critical for any living organism, and one that has been a constant evolutionary driving force throughout the history of life. The practical results of this necessity can be seen all around. It is found on a macro scale in the many examples of complex sensory organs possessed by animals, and on a micro scale in the myriad collections of different sensory proteins deployed by cells. An example of the latter can be found in the rich and diverse families of leucine-rich repeat receptor-like kinases (LRR-RLK's) and receptor-like proteins (RLP's). These two related families are comprised of membrane bound proteins possessing both cytoplasmic domains, such as the kinase domains of the LRR-RLK's, and extracellular domains, such as leucine-rich repeats (Shiu and Bleecker, 2001). In fact, LRR-RLK's get their name from these repeating leucine-rich extracellular domains, domains that are often found in RLP's as well (Wang et al., 2008). These extracellular domains are highly variable, and allow for the perception and binding of different ligands, which results in conformational changes in the receptor protein often promoting heterodimerization and, in the case of RLK's, kinase domain activation (Hohmann et al., 2017; Santiago et al., 2013). This in turn allows for the propagation of external signals or stimuli into the signaling network of the cell, which often leads to immediate protein dependent responses and transcriptional changes (He et al., 2018; Hohmann et al., 2017). Two LRR-RLK's that illustrate this well are the proteins BRASSINOSTEROID-INSENSITIVE 1 (BRI1) and PHYTOSULFOKINE-RECEPTOR 1 (PSKR1). BRI1 is an excellent example of external perception of a ligand leading directly to transcriptional changes in the cell. In this case the perception of a brassinosteroid (BR) ligand, such as Brassinolide (BL), leads to BRI1's heterodimerization with BRI1-ASSOCIATED-KINASE 1 (BAK1), which activates BRI1's kinase domain causing phosphorylation of BRI1-SUPPRESSOR 1 (BSU1), subsequent degradation of BRASSINOSTEROID-INSENSITIVE 2 (BIN2), and ultimate translocation of the transcription factor BRASSINAZOLE-RESISTANT 1 (BZR1) to the nucleus (Li and Chory, 1997; Nam and Li, 2002; Li et al., 2002; Li and Nam, 2002; Wang et al., 2002; Yin et al., 2002). This portion of the BR signaling pathway, which leads to cellular responses by

directly causing transcriptional changes (Chaiwanon and Wang, 2015; Sun et al., 2010; Yu et al., 2011), can be contrasted with that of PSKR1, where part of the signaling response operates independent of transcriptional alterations. Here the perception of another ligand, in this case Phytosulfokine (PSK), causes heterodimerization of PSKR1 with BAK1 (Sauter, 2015; Amano et al., 2007; Matsubayashi et al., 2002, 2006; Wang et al., 2015a), and the formation of a membrane complex with the H+-ATPases AHA1 and AHA2 as well as the protein CYCLIC-NUCLEOTIDE-GATED-CHANNEL 17 (CNGC17), which is itself activated by the cGMP generated downstream of the complex. The influx of cations into the cell in conjunction with the acidification of the apoplast that results from the creation of this complex leads to an elongation of the cell (Ladwig et al., 2015), and is an example of a cellular response that is not directly reliant on transcriptional changes. These 2 examples, BRI1 and PSKR1, are just 2 from the over 200 currently identified LRR-RLK's in *Arabidopsis thaliana* (Shiu and Bleecker, 2001, 2003), and as such it is no surprise that the field of plant signaling proteins is one that has experienced rapid growth in the past few decades. With the advent of DNA sequencing and genome comparison it has become increasingly clear that evolution has provided plants with an amazingly large and diverse assortment of sensor and receptor proteins (Shiu and Bleecker, 2003). These sensors and receptors are critical to the plant cell's ability to perceive its environment and respond accordingly (Hohmann et al., 2017). Whether it's facilitating the perception of brassinosteroids and phytosulfokines, detecting pathogens, responding to environmental stimuli, perceiving critical nutrients, or monitoring the internal cellular environment, these diverse protein families provide the communication infrastructure that allows a plant cell to coordinate all of its disparate parts. Understandably, the pace of identification of these genes far outstrips their characterization, as a single genomic analysis can yield dozens if not hundreds of new potential genes of interest while the characterization of a single gene routinely last years. The result of this mismatch in pacing is a vast sea of potentially interesting but as yet uncharacterized genes. This thesis attempts to plumb the depths of a small corner of this ocean by reporting the initial characterization of three previously unstudied genes of interest. The experiments outlined in the following three chapters cover three distinct genes from the model organism *Arabidopsis thaliana* that are loosely tied

together by their apparent links, either directly or indirectly, with cell wall signaling. The first reported upon is what seems to be a potential preproprotein with probable links to Phytosulfokine singling, the second is a F-Box/RNI Like family gene identified in a forward genetic screen, and the third is a receptor like protein with a high degree of genetic conservation throughout the plant kingdom. Over the course of the experiments outlined below an initial characterization emerges for each of the three, one that can serve as a solid foundation for future research.

Chapter 1

Introduction

Chapter one pertains to the initial observations of the previously uncharacterized protein PHYTOSULFOKINE LIKE 1 (PSKL1) (AT2G22942). Ever since the discovery of Phytosulfokines (PSKs) in *Asparagus officinalis L*. by Matsubayashi and Sakagami (1996), PSK's have shown themselves to be a critical component of the plant cell signaling network, with links to cell elongation and immune response (Igarashi et al., 2012; Ladwig et al., 2015; Sauter, 2015; Amano et al., 2007; Matsubayashi et al., 2006; Kutschmar et al., 2009). They were originally discovered when they were revealed to be the key active ingredient responsible for allowing the plant cell culture proliferation at lower cell densities observed in conditioned media (Matsubayashi and Sakagami, 1996). Subsequent studies went on to determine that phytosulfokines are critical for plant cell culture trans-differentiation into treachery elements and that the active element is a five amino acid long peptide with the sequence YIYTQ with sulfation of the two tyrosine residues (Matsubayashi and Sakagami, 1996). The active PSK pentapeptide is the product of posttranslational modifications of the larger PSK preproprotein (Yang et al., 2001; Lorbiecke and Sauter, 2002). These preproproteins are derived from gene families found across all higher plants (Sauter, 2015). In the model organism *Arabidopsis thaliana,* the PSK gene family contains 6 genes with varying expression and distribution patterns (Lorbiecke and Sauter, 2002; Sauter, 2015), all of which contain the PSK YIYTQ motif with the exception of PSK6 which has a YIYTH motif. PSK6 appears to be only marginally expressed however, if at all, as evidenced by the RNA-Seq data available (Klepikova et al., 2016), data which is further supported by older experiments showing an absence of cDNA's and Expressed Sequence Tags (EST's) (Lorbiecke and Sauter, 2002). After translation, the PSK preproprotein undergoes sulfation in the trans-Golgi network by the enzyme TYROSYLPROTEIN-SULFOTRANSFERASE (TPST), which is localized there (Komori et al., 2009). After being modified, PSK is subsequently exported to the apoplast (Lorbiecke and Sauter, 2002; Komori et al., 2009). In the apoplast, PSK is cleaved by the subtilase protein AtSBT1.1 (Srivastava et al., 2008),

though there is a lack of certainty whether other enzymes contribute to the production of the final mature peptide. Now a mature peptide in the apoplast, PSK is perceived by leucine-rich repeat receptor-like kinases (LRR-RLK's), which in *A. thaliana* are the LRR-RLK's PHYTOSULFOKINE-RECEPTOR 1 and PHYTOSULFOKINE-RECEPTOR 2 (PSKR1 and PSKR2) which are located at the plasma membrane (Matsubayashi et al., 2002, 2006)(. PSK interacts with PSKR1 and PSKR2 by binding to the island domains of the LRR regions of the proteins (Matsubayashi et al., 2002). This perception of the PSK ligand by PSKR1 and PSKR2 begins the PSK signaling cascades which are responsible for a number of plant responses involving both growth (through cell elongation) and pathogen defense (Igarashi et al., 2012; Ladwig et al., 2015; Sauter, 2015; Amano et al., 2007; Matsubayashi et al., 2006). In the case of PSKR1, perception of PSK promotes the formation of a protein complex with BRI1-ASSOCIATED-KINASE 1 (BAK1) and the plasma membrane-localized H+-ATPases AHA1 and AHA2, leading to the downstream generation of cGMP and the consequent activation of CYCLIC-NUCLEOTIDE-GATED-CHANNEL 17 (CNGC17), which is also present in the complex (Ladwig et al., 2015). This leads to an influx of cations into the cell and acidification of the apoplast, resulting in cell elongation (Ladwig et al., 2015). This process is very similar to the Brassinosteroid (BR) signal pathway with Brassinolide (BL) and the LRR-RLK BRASSINOSTEROID-INSENSITIVE 1 (BRI1), which also interacts with BAK1 and AHA1, resulting in cell wall acidification and elongation (Caesar et al., 2011). As such, it seems likely that there is a degree of crosstalk occurring between these two pathways, and recent studies have indeed identified at least one protein facilitating this exchange of information, a protein by the name of RECEPTOR-LIKE-PROTEIN 44 (RLP44) (Holzwart et al., 2018). RLP44 seems to serve as a scaffold for the interactions of LRR-RLK's such as BRI1, BAK1, and PSKR1 (Holzwart et al., 2018), as well as conveying information about the state of the plant cell wall into the plant signaling network (Wolf et al., 2014; Holzwart, 2018). In addition to this, RLP44 determines vascular cell fate in a PSK dependent manner (Holzwart et al., 2018). The exact nature of RLP44's interaction with PSK signaling is not entirely known, though is seems to involve PSK signaling in the procambial cells, where both RLP44 and PSK are expressed (Brady et al., 2007). From this uncertainty, the protein PSKL1 emerges as a

potential player. This uncharacterized protein was first identified by microarray data from the *rlp44-3* null mutant which showed it to be upregulated (unpublished data), suggesting a link between the two. Analysis of PSKL1's structure reveals 2 of the YIYTQ PSK motifs found in PSK genes, but no recognition site for cleavage by AtSBT1.1 which previous work has shown to have high target specificity (Srivastava et al., 2008; Berardini et al., 2015). As such, PKL1's role is not clear, as it could be cleaved by an unidentified enzyme into the PSK pentapeptide, or it could also conceivably act as some sort of negative regulatory element, such as a competitive inhibitor for the LRR-RLK island domains or of the proteases tasked with processing other PSK preproproteins. The research presented here aims to first characterize PSKL1 by looking for phenotypes in *PSKL1* knockout and overexpression lines in the *A. thaliana* model organism, and then to look for possible interactions with RLP44 by assessing *pskl1,rlp44* double mutant lines. To this end, experiments were performed to screen for phenotypes involving root length, hypocotyl length, abiotic stress response, and vascular cell fate, as these are already known to be impacted by RLP44 and PSK signaling (Kutschmar et al., 2009; Holzwart et al., 2018; Wolf et al., 2014; Stührwohldt et al., 2011; Sauter, 2015).

Results

Initial confirmation of T-DNA *pskl1* mutant line homozygosity proves successful

After confirmation of the homozygosity of the two T-DNA lines obtained for *PSKL1* (SALK 203857C and SALK 058177C), sequencing was used to determine the T-DNA insertion sites. By use of sanger sequencing it was determined that the *pskl1* SALK *Arabidopsis thaliana* line number 203857C (hereafter referred to as *pskl1-203*) had an insertion after the 155th base pair of the *PSKL1* gDNA (starting from ATG) (TAIR Accession Sequence: 5019476919), placing it upstream of the two putative PSK motifs and in the first intron (See figure 1), while SALK *Arabidopsis thaliana* line number 058177C (hereafter referred to as *pskl1-058*) had an insertion event after the 716th base pair of the gDNA (starting from ATG) (TAIR Accession Sequence: 5019476919), placing it just downstream of the PSK motifs (See figure 1). Subsequent sequencing of the *pskl1-058* line showed that the insertion of the T-DNA into the gene had in fact also led to the loss of 17 base pairs downstream of the insertion site.

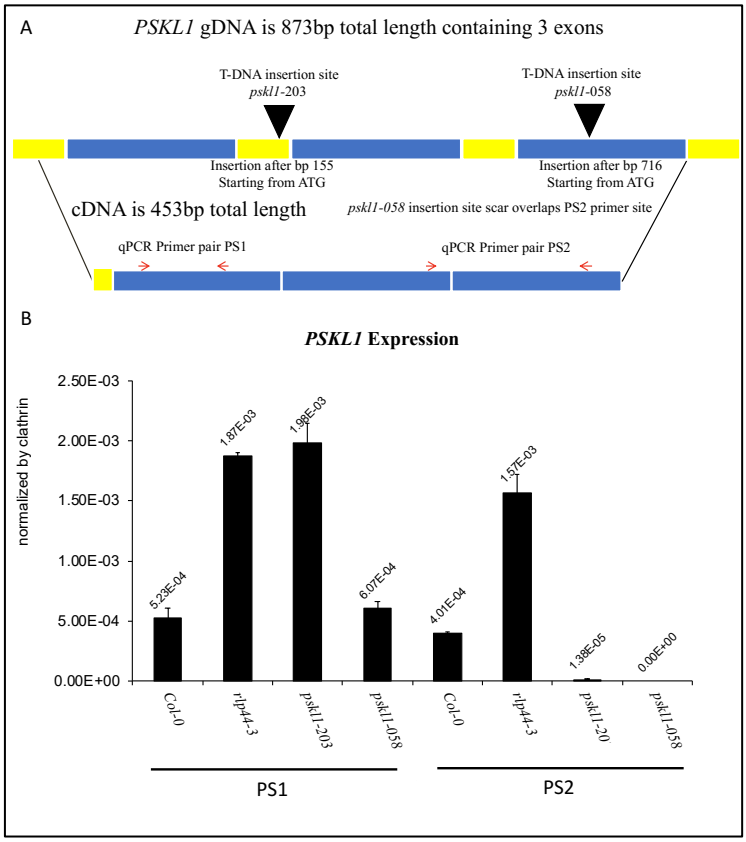

Figure 1: **A**. Diagram showing points of T-DNA insertion for the two SALK lines as determined by sanger sequencing. Sites of RT-qPCR primer pairs (PS1 and PS2) also shown. Insertion site scar of *pskl1-058* disrupts PS2 primer annealing site (primer sequences can be found in appendix 1). **B**. RT-qPCR data from bulk seedling cDNA. *PSKL1* expression is extremely low across all lines tested. Elevated expression in *rlp44-3* and *pskl1-203* (presumably a truncated transcript) and WT like expression in *pskl1-058* for PS1 data set. Elevated expression in *rlp44-3* line, reduced expression in *pskl1-203* line (possibly explained by a basal level of transcription of the gene fragment) and zero expression in *pskl1-058* line (explained by insertion scar disrupting primer annealing site) in PS2 data. Error bars denote standard deviation.

In order to assess the impact of these T-DNA insertions on the expression of the *PSKL1* gene, RT-qPCR was performed using two primer sets (hereafter referred to as PS1 and PS2) which were upstream and downstream of the *pskl1-203* insertion site, and upstream and overlapping with the stretch of DNA damaged by the *pskl1-058* insertion site (primers can be found in appendix 1). Col-0, *pskl1-203*, *pskl1-058*, and *rlp44-3* seedlings were harvested for RNA extraction and cDNA preparation, the *rlp44-3* line being included due to the previously reported elevation in *PSKL1* expression observed in it (unpublished data). Analysis of the RT-qPCR data revealed several interesting results. First and foremost of these is that expression of the *PSKL1* gene is extremely low across all lines, including wildtype. While it is possible that expression is more elevated during a different developmental stage of the plant, the data shown here indicates that seedlings have low expression of the *PSKL1* gene. The elevation in *PSKL1* expression reported previously in the *rlp44-3* genetic background (unpublished data) was confirmed. The *pskl1-203* line PS1 data showed elevated expression of what presumably was a truncated transcript not containing any PSK motifs, while the PS2 data showed reduced expression. The presence of some cDNA containing the PS2 sequence in the *pskl1-203* line, despite the presence of a T-DNA insertion upstream of it, can potentially be explained by a basal level of transcription of the gene fragment still occurring despite the presence of the T-DNA insert. The theoretical low-level production of this gene fragment transcript containing the DNA sequence for the PS2 transcript would then be weakly detected by the RT-qPCR assay. The results for *pskl1-058* show roughly wildtype expression levels in the PS1 data, despite the disruption of the third exon by the T-DNA insertion site which is located downstream of the annealing site for the primers (see figure 1), and no expression in the PS2 data, which makes sense due to the insertion scar disrupting the sequence where the primer would anneal (see figure 1), giving a potential false negative. This RT-qPCR data, taken together with the sequencing results, confirmed that the mutant lines *pskl1-203* and *pskl1-058* contain homozygous mutations affecting the *PSKL1* gene.

Initial observations of *pskl1* mutants finds potential root length phenotype

With the T-DNA lines confirmed, side by side growth comparisons were performed to look for phenotypic differences in rosette, hypocotyl length, and root length. Plants were germinated and grown on Phyto-Agar plates for 10 days and then transferred to soil and allowed to grow for 14 days before imaging.

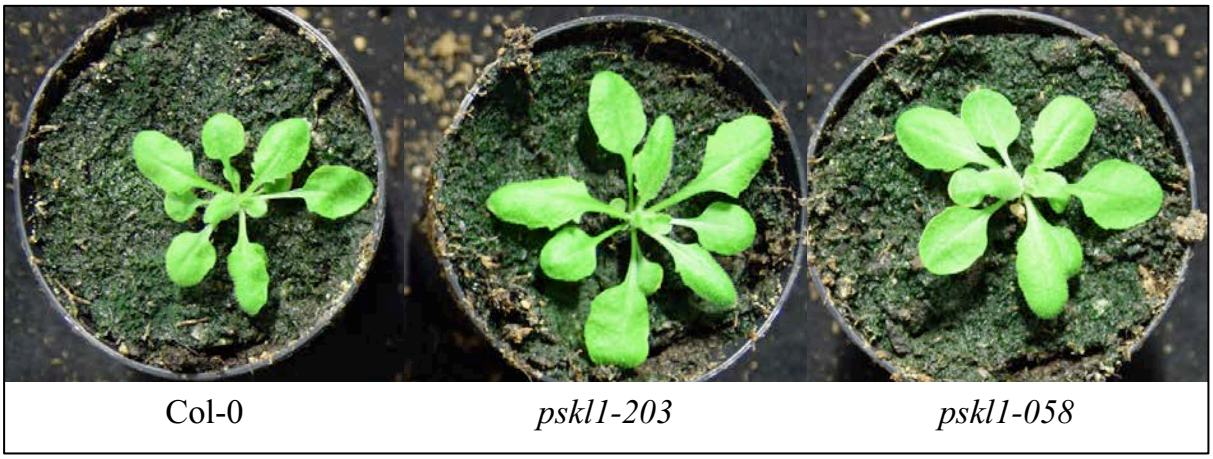

Figure 2: A. thaliana rosettes grown in parallel under controlled long day growth conditions. No obvious phenotypic differences between *pskl1* mutants and WT were observed. Images taken 24 DAG. Plants germinated on Phyto-Agar plates and allowed to grow for 10 days, then transferred to soil and allowed to grow for 14 days before imaging.

Observations of rosettes grown in controlled long day conditions did not reveal any obvious phenotypes. This was also the case when measuring hypocotyl lengths of etiolated seedlings 4 days after germination, which likewise showed no significant difference between the *pskl1* mutants and WT.

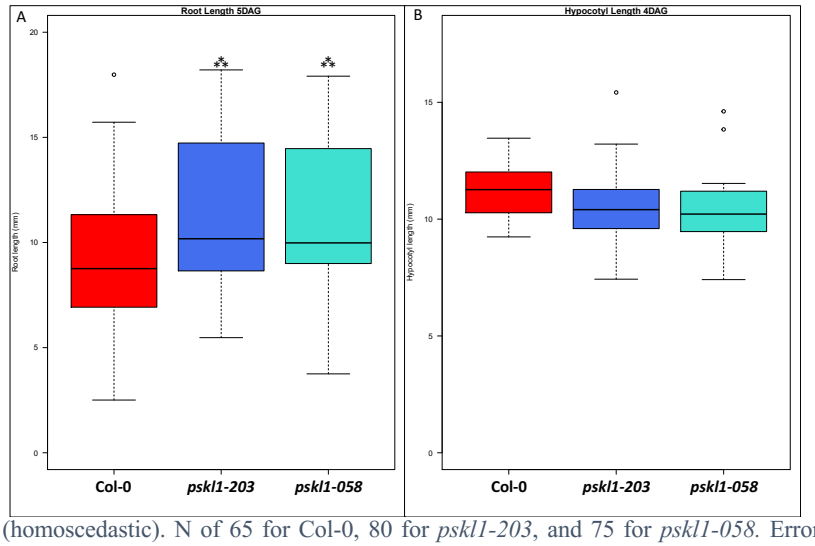

Figure 3: **A**. Boxplot of seedling root length 5 days after germination. Data combined from 2 iterations of experiment. Both *pskl1* mutants showed a small but significant increase in root length compared to WT (0.0003 and 0.0001 p values respectively). Student T-Test (homoscedastic). N of 65 for Col-0, 80 for *pskl1-203*, and 75 for *pskl1-058*. Error bars denote standard deviation. **B**. Boxplot of hypocotyl length in etiolated seedlings 4 days after germination. Data combined from 2 iterations of experiment. No significant difference was observed between mutant lines and WT. N of 17 for Col-0, 30 for *pskl1-203*, and 29 for *pskl1-058*. Error bars denote standard deviation.

Interestingly, analysis of 5 day old seedling root length did show a phenotype of a small but significant increase in root length for the *pskl1* mutants as compared to WT. With no observed phenotypic differences in rosette or hypocotyl length, and with a potential phenotype for root length, the mutants were next tested for abiotic stress induced root length phenotypes. Plants were grown on Phyto agar plates containing either mannitol, sucrose, or NaCl at various concentrations, which served as a source of abiotic stress. 5 Day old seedling root lengths were then compared.

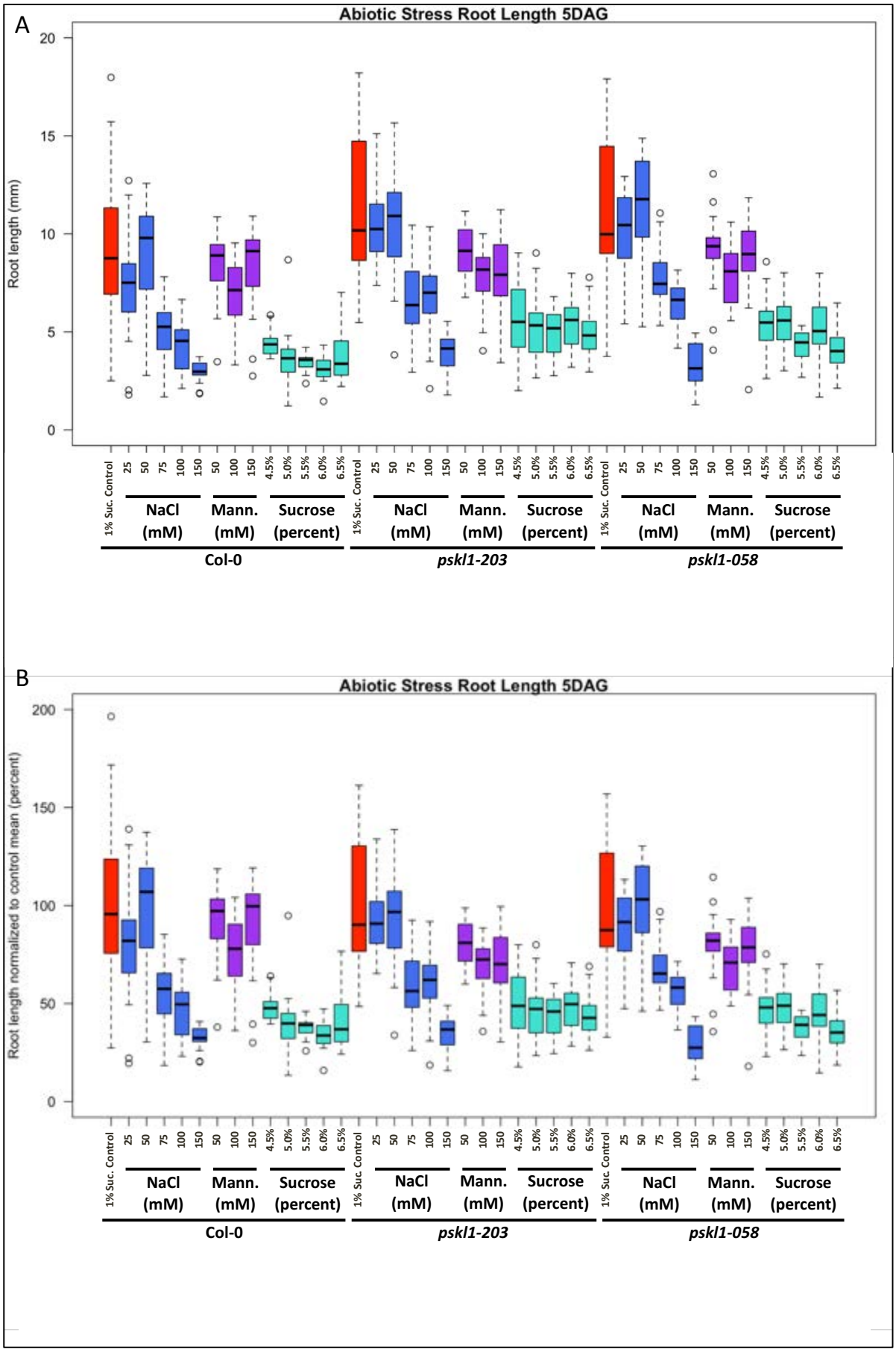
A
Abiotic Stress Root Length 5DAG
Root length (mm)
0
5
10
15
20
1% Suc. Control
25
50
75
100
150
50
100
150
4.5%
5.0%
5.5%
6.0%
6.5%
NaCl (mM)
Mann. (mM)
Sucrose (percent)
Col-0
pskl1-203
pskl1-058
B
Abiotic Stress Root Length 5DAG
Root length normalized to control mean (percent)
0
50
100
150
200

Figure 4: **A**. Boxplot of seedling root length 5 days after germination. Plants grown on Phyto-Agar plates containing abiotic stressors. Small increase in *pskl1* mutant root lengths still apparent, however large variability in samples undermines result. N of 65, 26, 21, 23, 18, 17, 18, 26, 18, 22, 23, 15, 23, 21, 80, 29, 30, 29, 28, 29, 28, 29, 29, 33, 29, 15, 29, 26, 75, 28, 28, 30, 28, 28, 30, 29, 30, 30, 29, 15, 29, 27 respectively. Data combined from 2 iterations of experiment. Error bars denote standard deviation. **B**. Same experimental data normalized to percent growth relative to the control treatment for the plant line. No immediately obvious *pskl1* mutant phenotypes for abiotic stress responses observed. Data combined from 2 iterations of experiment. Error bars denote standard deviation.

Upon completing the experiment, review of the data showed a great deal of variation in root length in the sample populations, however the trend of a small overall increase in *pskl1* mutant root length appeared to persist. Further analysis of the data after normalization led to the conclusion that there were no immediately obvious abiotic stress phenotypes for either of the *pskl1* mutant lines.

pskl1 mutants show phenotype of increased metaxylem cell number

The next set of experiments were designed to search for possible *pskl1* phenotypes related to PSK signaling, as well as test for a potential role for PSKL1 in the interaction between RLP44 and PSKR1 signaling (Holzwart et al., 2018). Analysis of Previous results had shown RLP44 to have an impact on metaxylem cell number in *A. thaliana* seedling roots (Holzwart et al., 2018). Therefore, metaxylem cell numbers were counted in 6 day old seedlings using basic fuchsine staining with fluorescent microscopy, paying close attention for the presence of metaxylem cells outside of the normally linear xylem axis.

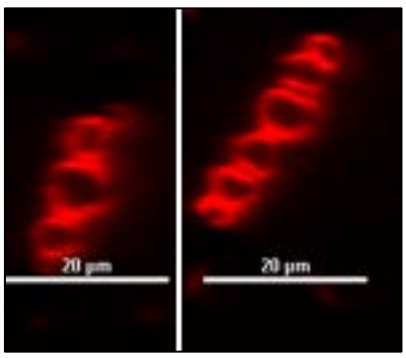

*Figure 5:*Fluorescent microscopy image showing basic fuchsine stained root metaxylem tissue of 6 day old Col-0 seedlings. Example on left shows 3 central metaxylem cells and 2 protoxylem cells (one on each end), while the example on the right shows 4 central metaxylem cells and 2 protoxylem cells (one on each end).

In addition, plants were grown on media with and without PSK, as the production of PSK's is a possible, though not certain, result of *PSKL1* expression.

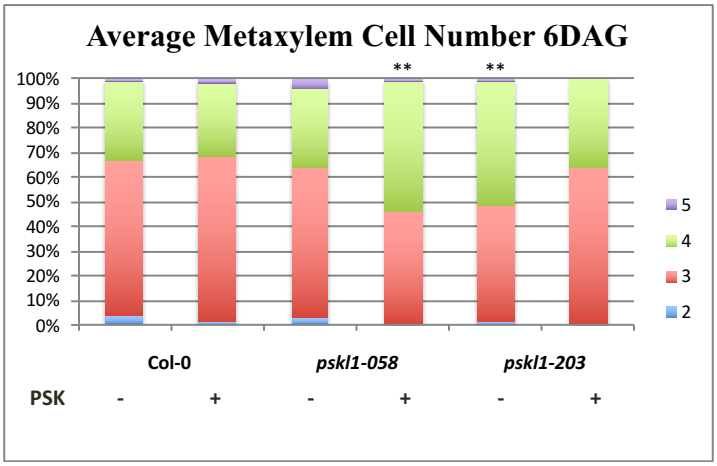

*Figure 6:*Graph showing percent breakdown of average metaxylem cell number in roots of 6 day old seedlings grown on Phyto Agar plates with or without PSK (1 µM). *pskl1-058* +PSK treatment showed a significant increase in average metaxylem cell number as compared to both Col-0 treatments (Homoscedastic Student T-Test p values of 0.001 and 0.003 respectively), while *pskl1-203* -PSK treatment showed a significant increase in average metaxylem cell number as compared to both Col-0 treatments (Homoscedastic Student T-Test p values of 0.004 and 0.012 respectively). Data combined from 6 iterations of experiment. N of 119, 99, 103, 88, 110, and 94 respectively.

Counting metaxylem cell numbers yielded some interesting results. The *pskl1* lines did not show an increased level of out of axis metaxylem cell events, but both lines did show a significant increase in the average number of metaxylem cells. Both lines showed a response to PSK treatment, which contrasted with the apparent PSK insensitivity of the Col-0 WT, but surprisingly the PSK response trend was inverted between the two lines (see figure 6). This could be the result of the presence of two functional PSK motifs in the *pskl1-058* line as opposed to the zero in the *pskl1-203* line (see figure 1), however experiments testing this hypothesis were not pursued. PSK effects on *pskl1* mutant root lengths were also measured.

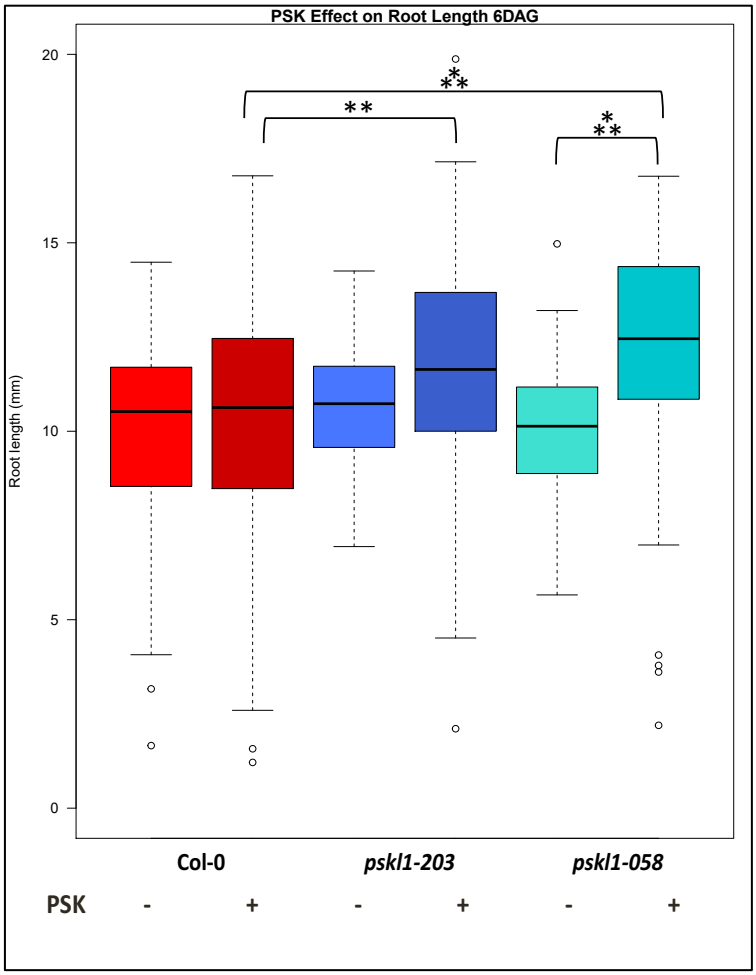

Figure 7: Boxplot showing root length for plantlets grown on Phyto-Agar plates either with or without PSK (1 µM) present in the media. *pskl1* mutant lines show a significant difference in their response to PSK treatment as compared to the WT control (p value of 0.002 and 6.1×10^{-6} respectively), however only *pskl1-058* showed a significant response to PSK (p value of 4.8×10^{-5}), which contradicts literary sources on Col-0 response (Kutschmar et al., 2009). Absence of a significant difference between all three PSK negative treatments undermines the previously observed phenotype of increased root length in the *pskl1* mutants, though this experiment's use of 6 DAG seedlings is a possible explanation. Statistical significance calculated using Tukey HSD test (see appendix 6 for complete results). N of 94, 93, 60, 77, 58, and 81 respectively. Data combined from 3 iterations of experiment. Error bars denote standard deviation.

The results from measuring root lengths showed a significant difference between the PSK response of the *pskl1* mutant lines when compared to WT, though only *pskl1-058* showed a significant difference from its own PSK negative sample group. It should be noted that the lack of a Col-0 response to PSK contradicts previous findings (Kutschmar et al., 2009), which undermines these results. Also, the absence of a significant difference between all three PSK negative treatments undermines the previously observed phenotype of increased root length in the *pskl1* mutants. It is possible of course that this phenotype is only present in 5 DAG seedlings, and therefore the sample group of 6 DAG seedlings used in this experiment does not exhibit it.

CRISPR/Cas9 successfully used to create new *pskl1* mutants

Since the 2 *pskl1* T-DNA mutant lines appeared to be giving conflicting results with regards to the newly identified metaxylem phenotype, it seemed prudent to generated new *pskl1*

mutants in order to confirm that the mutations in the *PSKL1* gene found in the T-DNA lines were in fact responsible for the observed mutant phenotype. Therefore, new mutant lines were generated using CRISPR/Cas9 with the goal of using them to further explore the role of PSKL1, the end result being the generation of 2 new mutant lines with different mutations in the *PSKL1* gene. Both mutations lead to premature stop codons that should result in a truncated protein, resulting in one mutant containing only one of the PSK motifs, and a second containing no PSK motifs (see figure 8). The first mutant line was given the name *Cpskl1-20* and the second the name *Cpskl1-62* and *Cpskl1-68* (two separately derived lines that ended up having the same mutation). Overexpression lines were also generated using the GreenGate system (see methods section), resulting in 3 p35S promotor driven $PSKL1_{OX}$ lines. These 3 lines were given the names $PSKL1_{OX}$*-27,* $PSKL1_{OX}$*-42,* and $PSKL1_{OX}$*-48.* These new lines were then confirmed with sequencing and RT-qPCR.

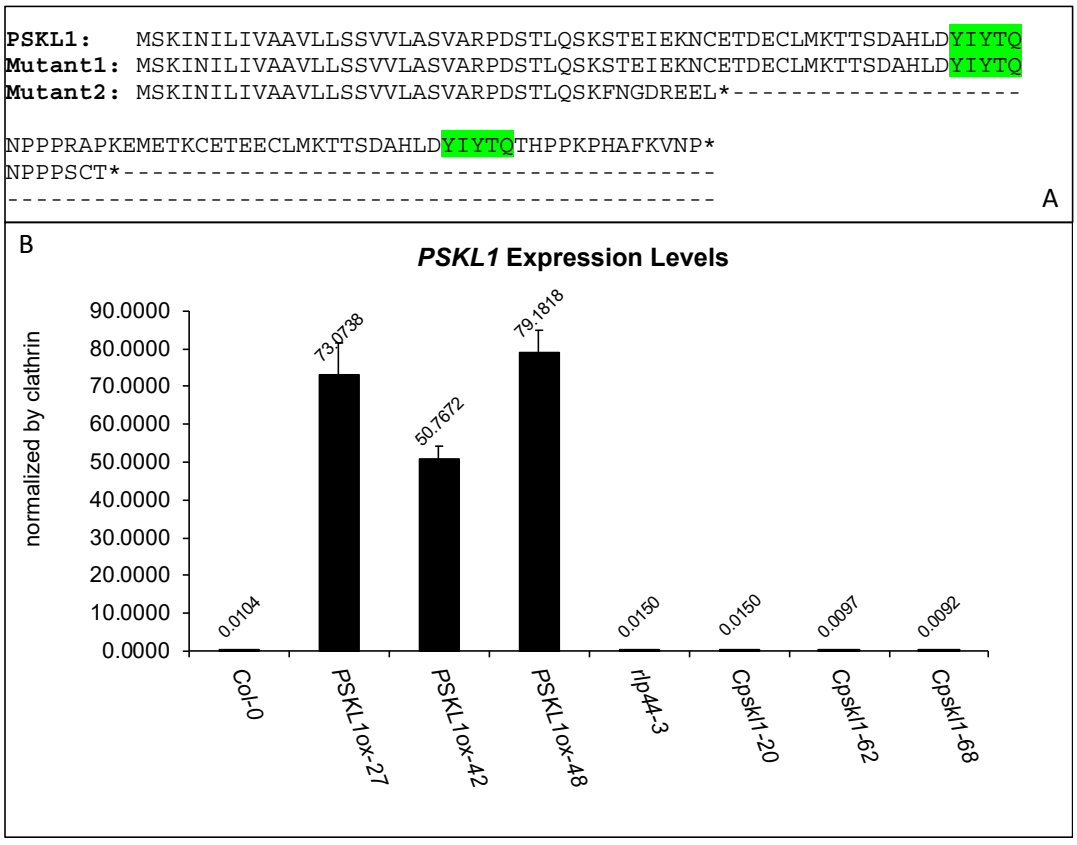

Figure 8: **A**. Comparison of protein sequences of both CRISPR/Cas9 derived *pskl1* mutants with that of WT. Putative PSK motifs highlighted in green. **B**. RT-qPCR data from bulk seedling cDNA showing *PSKL1* expression levels across newly generated mutant lines. Overexpression lines show extremely elevated *PSKL1* expression relative to WT, while the CRISPR *pskl1* mutants show expression levels similar to WT and *rlp44-3.* PS1 RT-qPCR primers used. Error bars denote standard deviation.

The RT-qPCR results showed high expression of *PSKL1* in the overexpression lines relative to WT, and expression levels similar to WT and *rlp44-3* in the CRISPR derived *pskl1* mutants. These results confirmed that the new *PSKL1* lines were now ready for use in experiments.

CRISPR generated *pskl1* mutants confirm increased metaxylem phenotype

The newly derived *PSKL1* lines were tested for root length phenotypes and for PSK responsiveness.

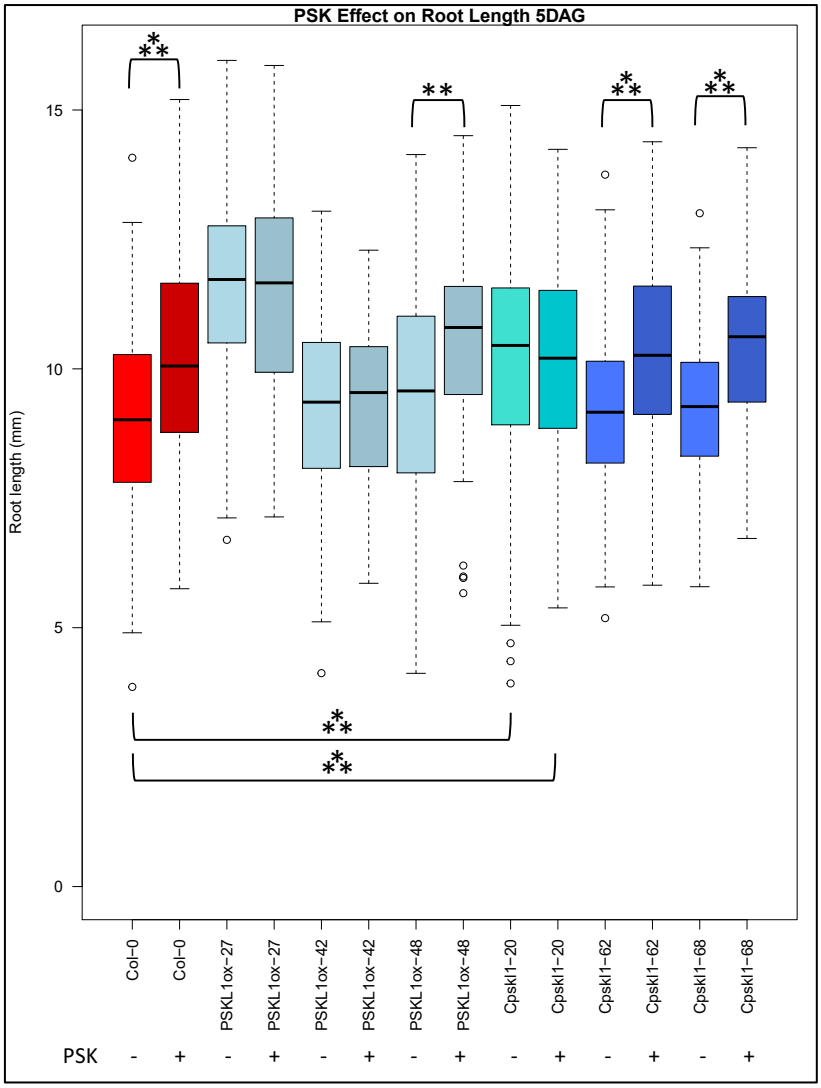

Figure 9: Boxplot showing average root length 5 days after germination. Col-0, *PSKL1$_{OX}$-48, Cpskl1-62,* and *Cpskl1-68* showed significant responses to exogenous PSK (1 µM) treatment (T-Test (homoscedastic) p value of $1.20x10^{-4}$, $3.60x10^{-3}$, $1.59x10^{-4}$, and $3.96x10^{-6}$ respectively). Both the *Cpskl1-20* PSK positive and negative sample groups differed significantly from the Col-0 PSK negative treatment (T-Test p value of $6.24x10^{-6}$ and $2.66x10^{-4}$ respectively). The *PSKL1$_{OX}$* lines showed differing phenotypes of exogenous PSK resistance and root length, suggesting that other factors besides *PSKL1* expression were probably at work. The two zero PSK motif lines (*Cpskl1-62* and *Cpskl1-68*) behaved similar to WT, and the single PSK motif line (*Cpskl1-20*) showed PSK resistance and increased root length. Data combined from 3 iterations of experiment. N of 121, 54, 137, 49, 98, 33, 133, 54, 105, 48, 115, 55, 112, and 50 respectively. Error bars denote standard deviation.

The results of these experiments testing PSK's effects on root length showed the expected Col-0 response of a statistically significant increase in root length (Kutschmar et al., 2009), a result the zero PSK motif mutants *Cpskl1-62* and *Cpskl1-*

68 also shared. Interestingly, the 1 PSK motif mutant *Cpskl1-20* showed resistance to PSK treatment, and still possessed the increased root growth phenotype seen in the T-DNA mutants, a result that could possibly be explained by a still functional remaining PSK motif. The *PSKL1* overexpression line results were very mixed, with line *PSKL1$_{OX}$-27* showing increased root length and PSK resistance, line *PSKL1$_{OX}$-42* showing no increase in root length and PSK resistance, and line *PSKL1$_{OX}$-48* showing no increase in root length and PSK responsiveness. Since the RT-qPCR results suggest that the PSKL1 transcripts should be in extreme excess in all 3 overexpression lines as compared to WT, the conflicting results suggest that some other unknown factor might be responsible for the observed discrepancies between lines. That said, testing PSK's effects on metaxylem cell number in 6 day old seedlings did yield interesting results. All lines with the exception of *Cpskl1-20, PSKL1$_{OX}$-42,* and *PSKL1$_{OX}$-48* showed a statistically significant response to PSK treatment (while not found significant by homoscedastic student T-Test, *PSKL1$_{OX}$-48* did seem to have a subtle response to PSK treatment), which was in contrast to the apparent PSK insensitivity of the Col-0 WT control. The results from the *PSKL1$_{OX}$* lines were not consistent, with differences in average metaxylem cell number observed between the lines for both exogenous PSK positive and negative treatments. Interestingly, many lines did show a significant divergence from the WT samples receiving the same treatment, however, since the RT-qPCR results indicated that all 3 *PSKL1$_{OX}$* lines have *PSKL1* transcripts in excess, the lack of a consistent phenotype across all the *PSKL1$_{OX}$* lines suggests that *PSKL1* expression levels might not be responsible for the observed results in these experiments. Analysis of the of the CRISPR generated *pskl1* lines yielded more consistent results. All lines, with the exception of *Cpskl1-20* showed a response to PSK treatment. Also, the increased average metaxylem cell number and return to wildtype levels with exogenous PSK treatment seen in the zero PSK motif *pskl1-203* mutant was replicated in the zero PSK motif mutants *Cpskl1-62* and *Cpskl1-68*. The double PSK motif mutant *pskl1-058*'s trend of WT average metaxylem cell number in PSK negative treatments, and increased average metaxylem cell number when treated with exogenous PSK, was paralleled by the single PSK motif mutant *Cpskl1-20*, though it started with a higher average metaxylem cell number in the PSK negative treatments than the *pskl1-058* line. When compared directly with the Col-0 WT samples, all of the

CRISPR/Cas9 derived *pskl1* lines showed a significant increase in average metaxylem cell number in the PSK negative treatments. This phenotype was once again rescued upon exogenous PSK treatment for the zero PSK motif mutant lines, and generated or exacerbated in the double/single PSK motif mutant lines.

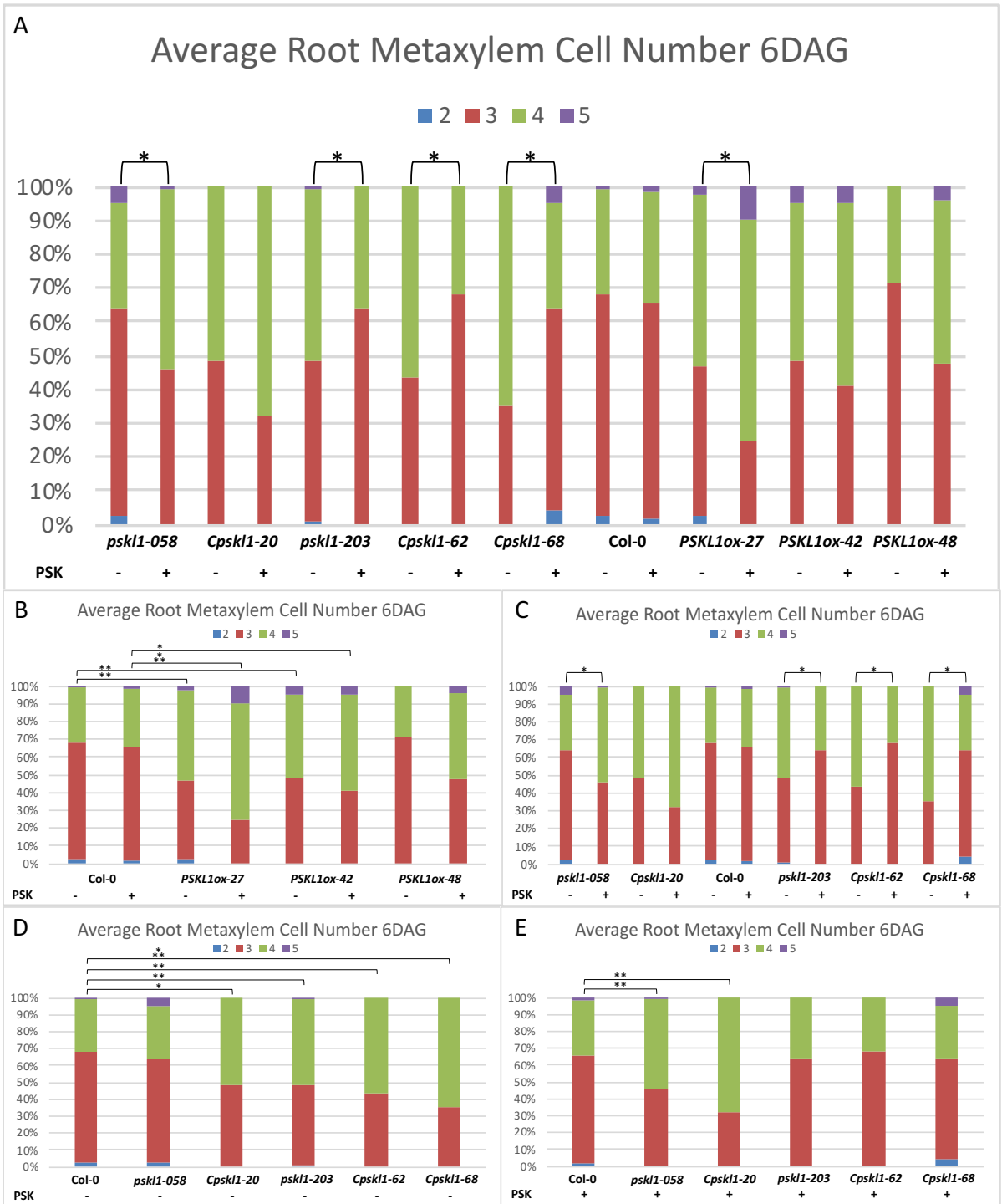

Figure 10: Data combined from 8 iterations of experiment for *pskl1-058*, *pskl1-203*, and Col-0 lines, and 2 iterations for all other lines. See Table 1 for all n values and average metaxylem percent breakdowns for each line. All graphs show percent breakdown of average metaxylem cell number in roots of 6 day old seedlings grown on Phyto Agar plates with or without exogenous PSK (1 µM) treatment. **A**. *Cpskl1-20* and *PSKL1$_{OX}$-42* showed WT PSK insensitivity, while all other lines showed significant responses to PSK treatment, except *PSKL1$_{OX}$-48* who's response fell short of statistical significance (Student T-Test (homoscedastic) p values of 0.036, 0.045, 0.049, 0.048, and 0.049 respectively). **B**. *PSKL1$_{OX}$* lines showed mixed phenotypes and PSK responses, while *PSKL1$_{OX}$-27 and PSKL1$_{OX}$-42* showed a significant difference

from the WT control on PSK negative media (Student T-Test (homoscedastic) p values of 0.011 and 0.007 respectively), and lines *PSKL1$_{OX}$-27 and PSKL1$_{OX}$-42* showed a significant difference from the WT control on PSK positive media (Student T-Test (homoscedastic) p values of 2.14×10^{-4} and 0.024 respectively). The lack of a consistent phenotype from the *PSKL1$_{OX}$* lines suggests that alterative factors might be responsible besides PSKL1 over expression. **C**. All *pskl1* lines showed a significant response to exogenous PSK treatment, except *Cpskl1-20* who's response fell short of statistical significance (Student T-Test (homoscedastic) p values of 0.036, 0.045, 0.049, and 0.048 respectively), which contrasted with the PSK insensitivity of the Col-0 control samples. All zero PSK motif mutants (*pskl1-203, Cpskl1-62, and Cpskl1-68*) showed a similar phenotype of increased average metaxylem cell number which was rescued back to WT levels by exogenous PSK treatment. The double/single PSK motif mutant lines (*pskl1-058* and *Cpskl1-20*) seemed to show a similar trend of increased average metaxylem cell number when grown with exogenous PSK, but with the *Cpskl1-20* line having a higher starting average number of metaxylem cells. **D**. All lines showed a significant increase in the average root metaxylem cell number with the exception of line *pskl1-058* (Student T-Test (homoscedastic) p values of 0.019, 1.56×10^{-3}, 2.57×10^{-3}, and 6.56×10^{-5} respectively) when compared to WT controls. **E**. The double/single PSK motif lines (*pskl1-058* and *Cpskl1-20*) showed a significant increase in the average root metaxylem cell number as compared to WT (Student T-Test (homoscedastic) p value of 5.06×10^{-3} and 7.34×10^{-3} respectively), while the zero PSK motif mutant lines (*pskl1-203, Cpskl1-62, and Cpskl1-68*) were rescued back to WT levels by exogenous PSK treatment.

Percent Average Root Metaxylem Cell Number 6DAG

Line	n	PSK	2	3	4	5
pskl1-058	110	-	2.7	60.9	31.8	4.5
pskl1-058	94	+	0.0	45.7	53.2	1.1
Cpskl1-20	43	-	0.0	48.8	51.2	0.0
Cpskl1-20	22	+	0.0	31.8	68.2	0.0
pskl1-203	103	-	1.0	47.6	50.5	1.0
pskl1-203	88	+	0.0	63.6	36.4	0.0
Cpskl1-62	46	-	0.0	43.5	56.5	0.0
Cpskl1-62	25	+	0.0	68.0	32.0	0.0
Cpskl1-68	48	-	0.0	35.4	64.6	0.0
Cpskl1-68	22	+	4.5	59.1	31.8	4.5
Col-0	157	-	2.5	65.6	31.2	0.6
Col-0	119	+	1.7	63.9	32.8	1.7
PSKL1ox-27	45	-	2.2	44.4	51.1	2.2
PSKL1ox-27	20	+	0.0	25.0	65.0	10.0
PSKL1ox-42	39	-	0.0	48.7	46.2	5.1
PSKL1ox-42	22	+	0.0	40.9	54.5	4.5
PSKL1ox-48	35	-	0.0	71.4	28.6	0.0
PSKL1ox-48	25	+	0.0	48.0	48.0	4.0

Table 1: Table containing average metaxylem cell numbers for data used in figure 10. Data combined from 8 iterations of experiment for *pskl1-058*, *pskl1-203*, and Col-0 lines, and 2 iterations for all other lines. Exogenous PSK treatment, n values, and percent breakdown of average metaxylem cell numbers shown.

Reviewing all the data, these very interesting results hints at some sort of dual role for the PSKL1 peptide, since the rescue by exogenous PSK treatment would suggest PSKL1 could act as a PSK source, while the inverse phenotype shown by the double/single PSK motif mutants hints at a different, potentially even regulatory role for the PSKL1 protein.

Experiment with *rlp44,pskl1* double mutant suggests *PSKL1* is epistatic to *RLP44*

Since the elevated expression of *PSKL1* in the *rlp44-3* mutant line (unpublished data) suggests some sort of interaction between *PSKL1* and *RLP44*, *rlp44-3* and *Cpskl1-68* were crossed to create an *rlp44,pskl1* double mutant. This newly derived line was first compared side by side with *rlp44-3*, *Cpskl1-68*, and Col-0 controls to look for any additive phenotypes in the plant rosettes.

Figure 11: A. thaliana rosettes grown in parallel under controlled long day growth conditions. No obvious phenotypic differences between any of the lines were observed. Images taken 25 DAG. Plants germinated on Phyto-Agar plates and allowed to grow for 3 days, then transferred to soil and allowed to grow for 22 days before imaging

Analysis of the rosettes of the 4 lines did not yield any obvious phenotypes. The *rlp44,pskl1* double mutant line was then tested for phenotypes in the average number of root metaxylem cells. As before, 6 day old seedlings were stained with basic fuchsine and the number of root metaxylem cells counted.

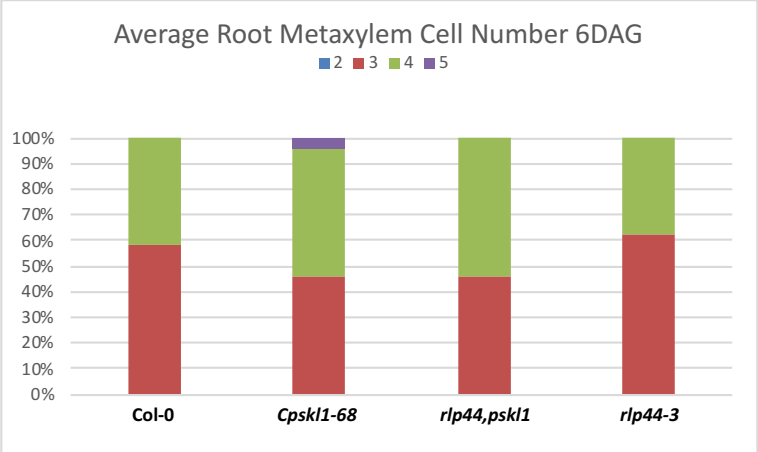

Figure 12: Graph showing percent breakdown of average metaxylem cell number in roots of 6 day old seedlings grown on Phyto Agar plates. *Cpskl1-68* seemed to show an increase in average root metaxylem cell numbers compared to WT (consistent with previous experiments), while *rlp44-3* showed WT metaxylem cell numbers. The *rlp44,pskl1* double mutant seemed to emulate the *Cpskl1-68* trend of increased average root metaxylem cell numbers, suggesting that *PSKL1* is epistatic to *RLP44*. Observations weren't statistically significant using Student T-Test (homoscedastic). This is likely the result of the small sample size of this experiment. Data collected from 1 experimental iteration. N of 24, 24, 24, and 24. See Table 2 for all n values and average metaxylem percent breakdowns for each line.

The experiment seemed to show that the *rlp44-3* mutant had average root metaxylem cell numbers similar to WT, in contrast to the established literature (Holzwart et al., 2018), while the *Cpskl1-68* and *rlp44,pskl1* mutants seemed to show a small increase in average root metaxylem cell numbers compared to WT, though it should be noted that with the small sample size of this experiment, these observations weren't statistically significant using a Homoscedastic Student T-Test and should be considered preliminary.

Table 2: Table containing average metaxylem cell number for data used in figure 12. Data collected from 1 experimental iteration. N values and percent breakdown of average metaxylem cell numbers shown.

Percent Average Root Metaxylem Cell Number 6DAG

Line	n	2	3	4	5
Col-0	24	0	58.3	41.7	0
Cpskl1-68	24	0	45.8	50	4.2
rlp44,pskl1	24	0	45.8	54.2	0
rlp44-3	24	0	62	38	0

Taking this data into consideration with the previous results, the experiment does seem to suggest that *PSKL1* is epistatic to *RLP44*, though given cursory nature of the experiment and the deviation of the *rlp44-3* result from the published literature (Holzwart et al., 2018), these results should not be viewed as conclusive.

Discussion

While many of the experiments performed using PSKL1 knockout and overexpression mutants to assess hypocotyl length, root length, and abiotic stress response yielded inconclusive or mixed results, there was one trend that consistently emerged, that of PSKL1 playing a role in the determination of metaxylem cell number. Across the experiments performed with the T-DNA and CRISPR derived *pskl1* mutants, the *pskl1* lines containing no PSK motifs consistently had a phenotype of higher average metaxylem cell numbers than the WT controls, and this mutant phenotype was also consistently rescued back to WT by exogenous application of PSK. This is similar to the trend for *rlp44-3* (Holzwart et al., 2018), which when taken into consideration with the RT-qPCR results showing elevated *PSKL1* expression in the *rlp44-3* mutant background (unpublished data), argues for PSKL1 playing a role in RLP44's PSK dependent regulation of vascular cell fate. These results become more interesting and nuanced when reviewing the trends for the other *pskl1* mutant lines. The T-DNA mutant line *pskl1-058* showed the opposite trend to that of the zero PSK motif *pskl1* mutants, with WT metaxylem cell numbers that were significantly increased by exogenous PSK treatment. This could potentially be explained by the location of the T-DNA insertion at the very tail end of gene. Sequencing shows that both PSK motifs are unaffected in the mutant, and furthermore, the RT-qPCR data shows WT levels of *PSKL1* transcripts in the *pskl1-058* line. It is therefore quite possible that the modified PSKL1 transcript is still functional enough to result in WT metaxylem cell numbers. The response to exogenous PSK treatment is harder to explain, but it is conceivable that the location of the T-DNA insertion disrupts a regulatory region or recognition site in 3'UTR of the mature transcript or at the tail end of the putative preproprotein. This hypothetically could interact with the signal cascade caused by the perception of exogenous PSK, leading to the observed phenotype. This line of reasoning could also then explain the phenotype observed in the *Cpskl1-20* mutant line. The presence of the 1 remaining PSK motif could theoretically cause the average metaxylem cell number to fall between that of the 2 PSK motif WT and the zero PSK motif mutants, while the absence of the hypothetical regulatory element in the C terminal end or 3'UTR would cause the same trend of increased metaxylem cell number

upon exogenous PSK treatment seen in the *pskl1-058* mutant line. This is of course a completely speculative line of reasoning as at this time it is not even clear whether PSKL1 is processed into mature PSK pentapeptides or if it functions in some other capacity. In this regard it was unfortunate that analysis of the *PSKL1ox* mutants failed to elucidate the role of PSKL1 more, as a consistent trend from overexpression lines could have provided more insight into the role of PSKL1. While the RT-qPCR data showed *PSKL1* expression levels vastly in excess of the WT controls, the phenotypic manifestations of the lines were not consistent. While all 3 lines seemed to respond to exogenous PSK treatment with at least some increase in the number of metaxylem cells, a result similar to the observations for *pskl1-058* and *Cpskl1-20, PSKL1ox-42* put this trend in doubt by being borderline resistant to exogenous PSK. This combined with the varying levels of metaxylem cell number on PSK free media makes it difficult to draw any strong conclusions from experiments using the *PSKL1ox* lines. This lack of consistent results was true for many of the other experiments of this study, such as with the effects of PSKL1 on root length. Several of the experiments failed to show an increase in root length for Col-0 plants grown on PSK containing media, immediately making the results suspect due to their divergence with the established literature on the topic (Kutschmar et al., 2009), while others showed variations within the same *PSKL1* mutant lines between experiments. As far as testing for direct interactions between RLP44 and PSKL1, the preliminary experiments with the *rlp44,pskl1* double mutant line seemed to show PSKL1 to be epistatic to RLP44 in affecting vascular cell identity. It should of course be noted again that these results are preliminary and that the seemingly WT average root metaxylem cell numbers in the *rlp44-3* mutants deviates from previously reported results (Holzwart et al., 2018). With regards to possible future research, the repetition of the metaxylem experiments with the *rlp44,pskl1* double mutant would be a logical place to begin, as this would help to better characterize the apparent interaction between the two genes. In addition to that, *PSKL1* rescue lines would help confirm PSKL1's role in determining vascular cell fate, and Co-immunoprecipitation of PSKL1 coupled with mass-spectroscopy could be used to begin the search for possible interaction partners. That being said, and taking all of the experiments above into consideration, an initial portrait of PSKL1 does emerge. *PSKL1* appears to be a gene with very low-level or time specific

expression levels that does nonetheless affects vascular cell identity, most likely through some sort of interaction with RLP44. Whether it accomplishes this by being a source for mature PSK pentapeptides or through other means remains to be discovered by future work.

Chapter 2

Introduction

In chapter 2 we shift the focus of our inquiry directly to RLP44. RLP44 was first discovered in a forward genetic screen using Ethyl methanesulfonate (EMS) on a transgenic *A. thaliana* line ectopically expressing PECTIN-METHYLESTERASE-INHIBITOR (PMEI). PMEIox causes modifications to the plant cell wall which result in the activation of the BR signaling pathway and a distinctive root-waving phenotype. A forward genetic screen of a *PMEIox A. thaliana* line using EMS generated several suppressors of the PMEIox phenotype, and the responsible mutations were subsequently identified to be present in either the *BRI1* or *RLP44* genes (Wolf et al., 2012, 2014). BR signaling is usually activated by the binding of BRI1 with a ligand, such as BL, which promotes heterodimerization with BAK1 (Nam and Li, 2002; Li et al., 2002) and subsequently results in negative regulation of BRASSINOSTEROID-INSENSITIVE 2 (BIN2) (Li and Nam, 2002). This negative regulation of BIN2 prevents it from phosphorylating BRASSINAZOLE-RESISTANT 1 (BZR1) and BRI1-EMS-SUPPRESSOR 1 (BES1)/BZR2, which in turn allows them to translocate to the nuclease where they function as transcription factors (Wang et al., 2002; Yin et al., 2002; Chaiwanon and Wang, 2015; Sun et al., 2010; Yu et al., 2011). As such it was not immediately clear at the time how modifications to cell wall pectin would activate BR signaling. Subsequent experiments answered this question by showing that the other PMEIox phenotype suppressing mutant gene identified, *RLP44*, interacts with pectate (Holzwart, 2018) and is responsible for conveying this information about the state of the cell wall to the BR signaling pathway. It was also subsequently determined that RLP44 forms a complex with BRI1 and BAK1, and that it functions in facilitating crosstalk between the BR and PSK signaling pathways (Wolf et al., 2014; Holzwart et al., 2018). It was also observed that the overexpression of RLP44 creates a distinctive phenotype very similar to BRI1 overexpression, that of elongated petioles and narrow leaf blades. Interestingly, the *RLP44ox* line does not exhibit the BL hypersensitivity displayed by the *BRI1ox* line (Wolf et al., 2014), indicating that RLP44 is not a direct part of the BR signaling cascade. This

could possibly be explained by RLP44 acting as a scaffold for bringing BRI1 and BAK1 together, a function that would not be dramatically altered by an overabundance of BL ligands (Holzwart et al., 2018). With this in mind, another forward genetic screen using EMS was performed, this time in the *RLP44ox* genetic background. This screen resulted in a number of potential *RLP44ox* suppressor mutants. The putative suppressor lines were tested for BL and PPZ (a compound that inhibits the BR signaling pathway)(Hartwig et al., 2012) insensitivity or hypersensitivity, as mutations effecting the BR signaling pathway were of less interest (Garnelo Gómez, 2017) due to the role of BR signaling in the manifestation of the RLP44ox phenotype having already been established (Wolf et al., 2014; Holzwart et al., 2018). After this process, 4 putative suppressor lines showing no BR signaling hypersensitivity or insensitivity remained. It is at this point that the work of this study began. Using these 4 putative suppressor lines, this study hoped to first identify the gene mutations responsible for the observed suppression of the RLP44ox phenotype, confirm them through the use of targeted mutation using the CRISPR/Cas9 system, and then test them for interactions with RLP44. This experimental pipeline would then ideally lead to the identification of a RLP44 interaction partner acting independent of the BR signaling pathway or a factor modifying the cell wall in such a way as to affect RLP44's interaction with it. This pipeline proved successful, as the results outlined below will show. Two candidate mutations were identified, though interestingly the two affected proteins turned out to most likely be involved in the ubiquitination pathway as opposed to the other options outlined above. One was a predicted F-Box protein and the other a predicted Ubiquitin-protein ligase (UPL), meaning that both should be involved in the substrate specificity of the E3 ubiquitin ligase pathway, the F-Box protein as a component of the SCF complex and the UPL as an E3 ubiquitin ligase (Bai et al., 1996; Pickart, 2001; Zheng and Shabek, 2017). Since E3 ubiquitin ligases facilitate the transfer of ubiquitin from the E2 ubiquitin-conjugating enzyme to the correct ubiquitination target (Pickart, 2001; Zheng and Shabek, 2017), and as protein turnover is a known component of plant cell wall signaling (Bu et al., 2009; Stone, 2014), one can see how these two candidate genes could impact the RLP44ox phenotype.

Results

Candidate genes responsible for RLP44$_{OX}$ suppression identified

Already having *A. thaliana RLP44:RFP$_{OX}$* genetic background EMS mutant lines showing suppression of the RLP44:RFP$_{OX}$ phenotype (see figure 13), as outlined in the introduction of this chapter, the first step was to identify where in the genomes of the EMS mutant lines the responsible suppressing gene or genes might be located.

Figure 13: Comparison of 24 day old *A. thaliana* rosettes from RLP44$_{OX}$, Col-0, and EMS derived RRE lines. *RLP44:RFP$_{OX}$* mutant phenotype of elongated petioles and narrow leaf blades clearly visible. RRE lines have same genetic background as RLP44$_{OX}$ line shown.

Bulked Segregant Analysis (BSA) was performed on 2 of the EMS mutant lines (RRE 24.1 and RRE 38.6) with the hopes of finding the chromosome region that contained the responsible mutation.

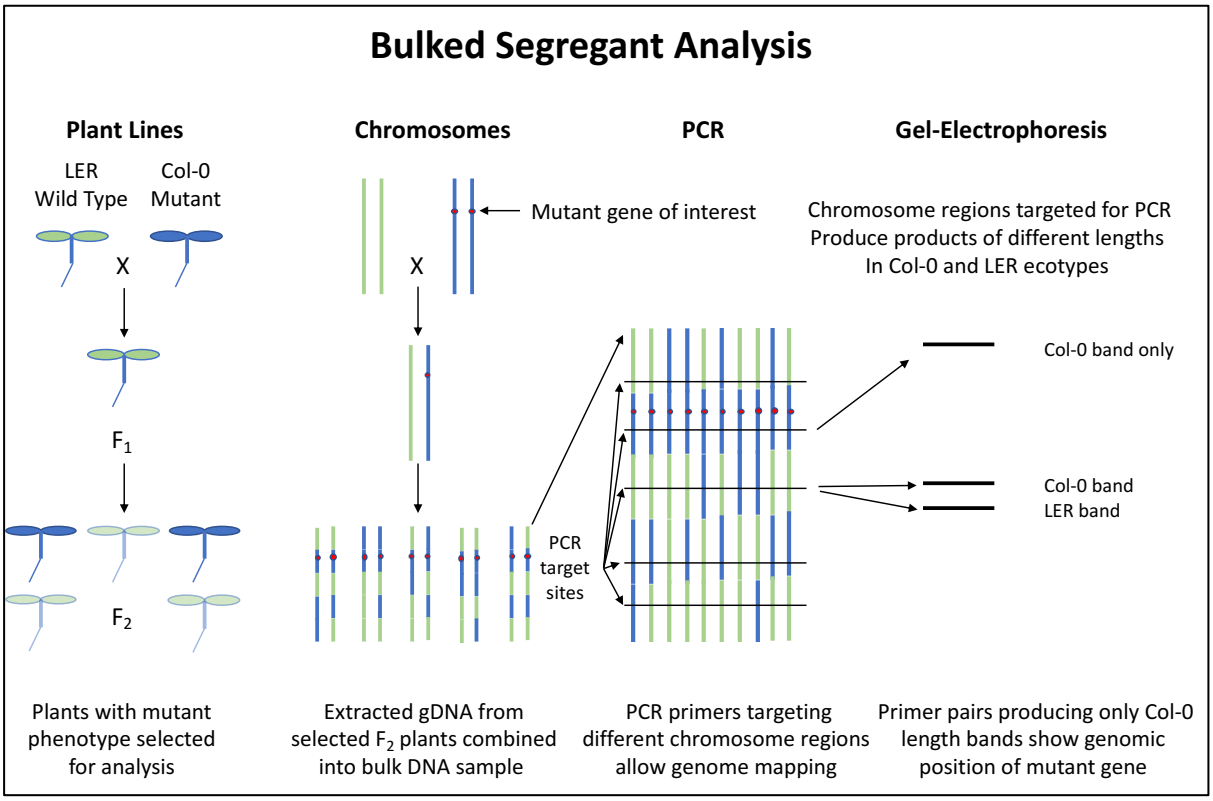

Figure 14: Diagram outlining Bulked Segregant Analysis (BSA) experimental procedure and analysis.

F2 seeds from previously performed crosses of *RRE 24.1* and Landsberg (Ler), as well as *RRE 38.6* and Ler, were grown and analyzed for the segregating phenotype of suppression of the RLP44:RFP$_{OX}$ phenotype. Tissue and seeds were harvested from Plants identified as having this suppression phenotype and gDNA was extracted for BSA. The BSA PCR results of pooled gDNA were analyzed via agarose gel electrophoresis to look for genomic regions only comprised of Col-0 DNA, as this would be a strong indication that this stretch of the genome houses the responsible mutation.

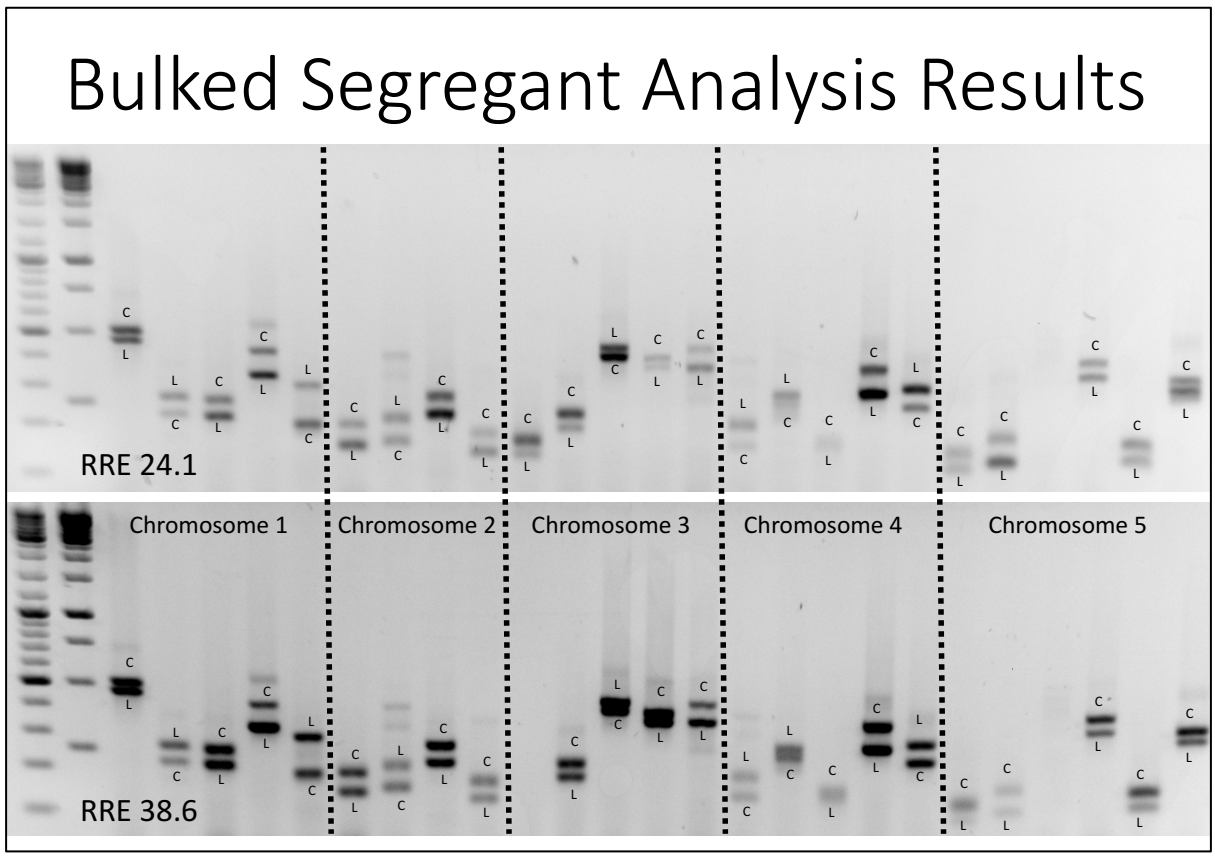

Figure 15: BSA analysis of EMS derived lines RRE 24.1 and RRE 38.6. 25 primer pairs used (BSA primers 1-25 from left to right, see appendix 1). C stands for bands from the Col-0 genetic background and L stands for bands from the Landsberg genetic background. While some bands seemed to be enriched for Col-0, the results were not conclusive enough to definitively locate the mutant genes responsible for the suppression of the RLP44ox phenotype. That said, the results for the RRE 38.6 line show stronger Col-0 bands on chromosome 5, suggesting the mutation might be located there.

Unfortunately, the BSA experiment did not yield a definitive answer as to the genomic location or locations of the responsible EMS mutation or mutations. While some areas of the genome did seem enriched for Col-0 DNA, such as in chromosome 5, it was not strong enough to be definitive. That being said, it did suggest that the responsible mutation in the RRE 38.6 line could be located on chromosome 5. As a result of this uncertainty however, a new plan was pursued to identify the responsible mutation. Previously performed Next Generation Sequencing (NGS) data had been collected from several of the lines derived from the original EMS mutant screen (Garnelo Gómez, 2017), and analysis of the NGS data had identified several mutations (see table 3) to be present in the RRE lines, all of which were located on chromosome 5 in lines RRE 24.1 and RRE 38.6, supporting the BSA data.

Table 3: Table showing list of NGS detected mutations in RRE lines that were deemed to be of potential interest (Garnelo Gómez, 2017).

NGS Detected Mutations in RRE Lines					
Line:	**Gene ID:**	**Gene:**	**Mutation:**	**Gene Location:**	**Amino acid Effect:**
RRE 9.2	AT3G04490	Exportin-4 protein	C-T	Intron	-
RRE 9.2	AT3G05280	Yip1 family protein	C-T	Exon	R to R
RRE 9.2	AT3G14010	CID4	G-A	Exon	A to T
RRE 11.1	AT5G05690	CPD	G-A	Exon	K to K
RRE 11.1	AT5G09890	Protein kinase	G-A	Exon	K to K
RRE 24.3	AT5G02880	UPL4 Ub-prot ligase	G-A	Exon	G to E
RRE 24.3	AT5G02910	F-box/RNI like	G-A	Exon	E to K
RRE 24.3	AT5G04170	EF-hand family protein	C-T	Exon	S to S
RRE 38.6	AT5G04630	CYP77A9	C-T	Exon	L to F
RRE 38.6	AT5G07050	UMAMIT9	G-A	Exon	G to S
RRE 38.6	AT5G13580	ABCG6	C-T	Exon	R to C
RRE 38.6	AT5G13920	GRF zinc finger / Zinc knuckle protein	G-A	Exon	G to D
RRE 38.6	AT5G16210	HEAT repeat-containing protein	G-A	Exon	R to R

These identified mutations were then analyzed to determine which were the best candidates to pursue. This was done by selecting for mutations present in exons or very near to splice sites within introns. Candidates with synonymous or silent mutations were ruled out as well as intron mutations not near the splice site. This analysis yielded several candidate genes, though the RRE 11.1 line was not pursued as both mutations appeared synonymous in addition to the fact that the CPD gene impacts Brassinosteroid signaling (Szekeres et al., 1996) which is already known to suppress the RLP44:RFP$_{OX}$ phenotype (Wolf et al., 2014) and was therefore not of interest in this study. The GRF zinc finger gene (AT5G13920) was also excluded as the NGS detected mutation could not be confirmed by Sanger sequencing. This process yielded 6 candidate genes spread across 3 of the RRE EMS derived lines (see Table 4).

Mutant lines for candidate genes generated

With this data, the next step was to generate knockout mutant lines of these genes in the *RLP44:RFP$_{OX}$* genetic background using CRISPR/Cas9 and test for phenotypic suppression.

Table 4: Table showing CRISPR/Cas9 generated mutant lines. Targeted gene, nature of mutation, effect of mutation, and associated RRE line shown. gDNA refers to TAIR Accession Sequences 4010723200, 4515110747, 3707920, 4515110841, 1005037771, and 1005038049 respectively (Berardini et al., 2015).

CRISPR/Cas9 Generated Mutant Lines

Associated RRE Line:	Gene:	Mutation:	Mutation Effect:
RRE 9.2	CID4	A deleted gDNA 1302 starting from ATG	Frameshift leading to premature stop codon
RRE 24.1	UPL4	32 bases deleted after gDNA 2338 starting from ATG	Frameshift leading to premature stop codon
RRE 24.1	Fbox/RNI Like	T deleted gDNA 69 starting from ATG	Frameshift leading to premature stop codon
RRE 38.6	UMAMIT9	A insert after gDNA 1429 starting from ATG	Frameshift leading to premature stop codon
RRE 38.6	CYP77A9	A insert after gDNA 970 starting from ATG	Frameshift leading to premature stop codon
RRE 38.6	ABCG6	T insert after gDNA 750 starting from ATG	Frameshift leading to premature stop codon

After the mutant lines were generated and confirmed homozygous, the Cas9 genes were segregated out of the lines. This was important as the CRISPR/Cas9 cassette used had a p35S promotor in it which frequently led to false positive results due to silencing of the p35S driven *RLP44:RFP$_{OX}$* gene.

CRISPR mutants for line RRE 24.1 appear to show phenotypic suppression

With mutant lines successfully generated, the next step was to test for suppression of the RLP44:RFP$_{OX}$ phenotype and to compare it with the original EMS screen suppression lines.

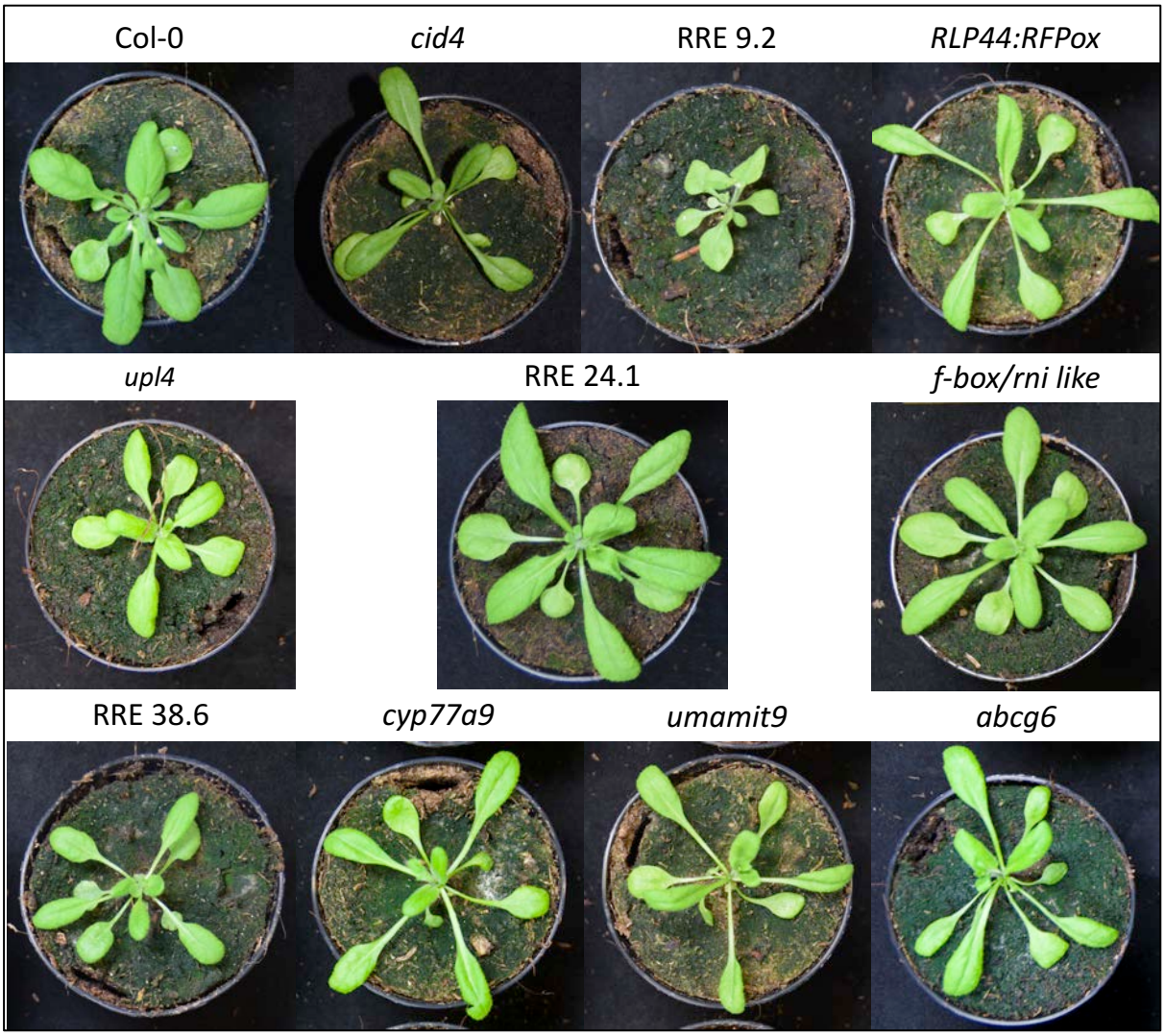

Figure 16: Comparison of 24 day old *A. thaliana* rosettes. *RLP44:RFP$_{OX}$* mutant phenotype of elongated petioles and narrow leaf blades clearly visible. Visual comparison suggests that only the mutant lines made in consultation with the RRE 24.1 NGS data (*upl4* and *f-box/rni like*) show suppression of the *RLP44:RFP$_{OX}$* mutant phenotype. Plants grown in parallel, geminated on Phyto-agar plates, then transferred to soil and grown in controlled long day conditions.

To do this, mutant and control lines were grown in parallel under controlled conditions to allow for effective head to head comparison. The *RLP44:RFP$_{OX}$* phenotype was clearly visible in the *RLP44:RFP$_{OX}$* control samples and was suppressed to varying degrees in the RRE controls. RRE 24.1 Seemed to be the closest to WT while RRE 9.2 seemed to replace the *RLP44:RFP$_{OX}$* phenotype with a mild dwarf phenotype and RRE 38.6 seemed to be a partial suppression of the *RLP44:RFP$_{OX}$* phenotype. The *cid4* mutant line seemed to still possess the *RLP44:RFP$_{OX}$* phenotype, ruling it out as a candidate gene, and possibly indicating that the suppression of the *RLP44:RFP$_{OX}$* phenotype seen in RRE 9.2 is the result of multiple damaging mutations causing mild dwarfism rather than a mutation of a protein that interacts directly or indirectly with RLP44. All 3 of the RRE 38.6 associated

mutant lines (*cyp77a9, umamit9,* and *abcg6*) did not show suppression of the *RLP44:RFP$_{OX}$* phenotype, ruling them out as candidate genes. The lack of *RLP44:RFP$_{OX}$* phenotypic suppression in the mutant lines and the seemingly partial *RLP44:RFP$_{OX}$* phenotype suppression in the RRE 38.6 line suggest that either the NGS data failed to find the responsible mutation, or that perhaps RRE 38.6 was a false positive result from the EMS screen. In contrast to the other mutant lines, both of the RRE 24.1 associated mutant lines (*upl4* and *f-box/rni like*) seemed to show suppression of the *RLP44:RFP$_{OX}$* phenotype. This is problematic as well due to the fact that the chances of having 2 EMS derived *RLP44:RFP$_{OX}$* phenotype suppressing mutations in the same line, while not impossible, is extremely unlikely. That being said, both *upl4* and *f-box/rni like* did consistently show *RLP44:RFP$_{OX}$* phenotypic suppression during several iterations of the experiment.

Fluorescent microscopy rules out gene silencing as explanation

Given the frequent occurrence of *RLP44:RFP* gene silencing, and consequent false positive for *RLP44:RFP$_{OX}$* phenotypic suppression, observed during the generation of the CRISPR/Cas9 derived mutant lines, the *RLP44:RFP* overexpression needed to be confirmed in the candidate lines. Fortunately, the RFP tag of the overexpressed RLP44 protein made this a straightforward task.

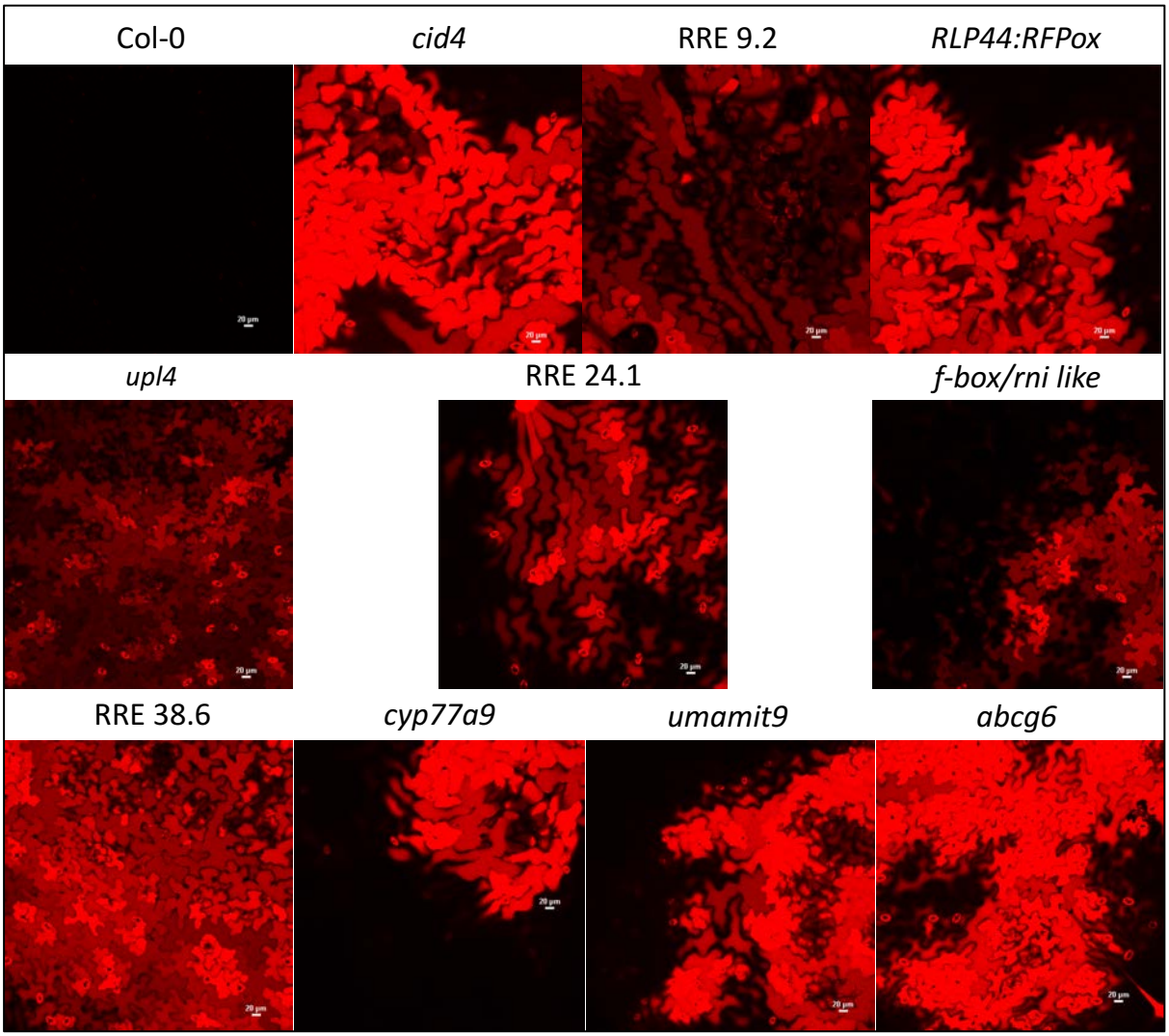

Figure 17: Fluorescent microscopy images of *A. thaliana* leaf disks from 26 day old CRISPR derived mutant plants with *RLP44:RFP*$_{OX}$ genetic background as well as image of Col-0 negative control. RFP channel shown. All lines with the exception of Col-0 showed RLP44:RFP expression levels similar to that of the *RLP44:RFPox* positive control, suggesting that gene silencing is not the cause of the observed suppression of the *RLP44:RFP*$_{OX}$ phenotype in the *f-box/rni like*, and *upl4* mutant lines. Leaf disks collected from plants in figure 16.

Fluorescent microscopy of leaf disks from *upl4* and *f-box/rni like* mutant plants consistently showed RFP fluorescence to a degree similar to the *RLP44:RFP*$_{OX}$ controls, ruling out gene silencing as an explanation for the observed *RLP44:RFP*$_{OX}$ phenotypic suppression. Taken together, this made a strong case that one or both of the RRE 24.1 associated mutant lines (*upl4* and *f-box/rni like*) is a direct or indirect interaction partner of RLP44.

Allelism test supports *f-box/rni like* as RLP44ox phenotype suppressor

In order to further support the role of *f-box/rni like* as a suppressor of the RLP44ox phenotype, an allelism test was performed. The *f-box/rni like* T-DNA line (SALK 01956) was acquired, and after being confirmed homozygous, crossed with the CRISPR *f-box/rni like* mutant, which as stated earlier has a *RLP44:RFP$_{OX}$* genetic background, meaning that the F1 plants would be heterozygous for the RLP44 overexpression gene and therefore should exhibit the *RLP44:RFP$_{OX}$* phenotype. The F1 plants from this cross were then examined for continued suppression of the RLP44ox phenotype, as this would suggest that the *f-box/rni like* mutation is in fact responsible for the observed phenotypic suppression due to the fact that any other mutation would be heterozygous in the F1 generation which would lead to expression of the RLP44ox phenotype since previous research had determined the unidentified EMS suppressing mutations to be recessive (Garnelo Gómez, 2017).

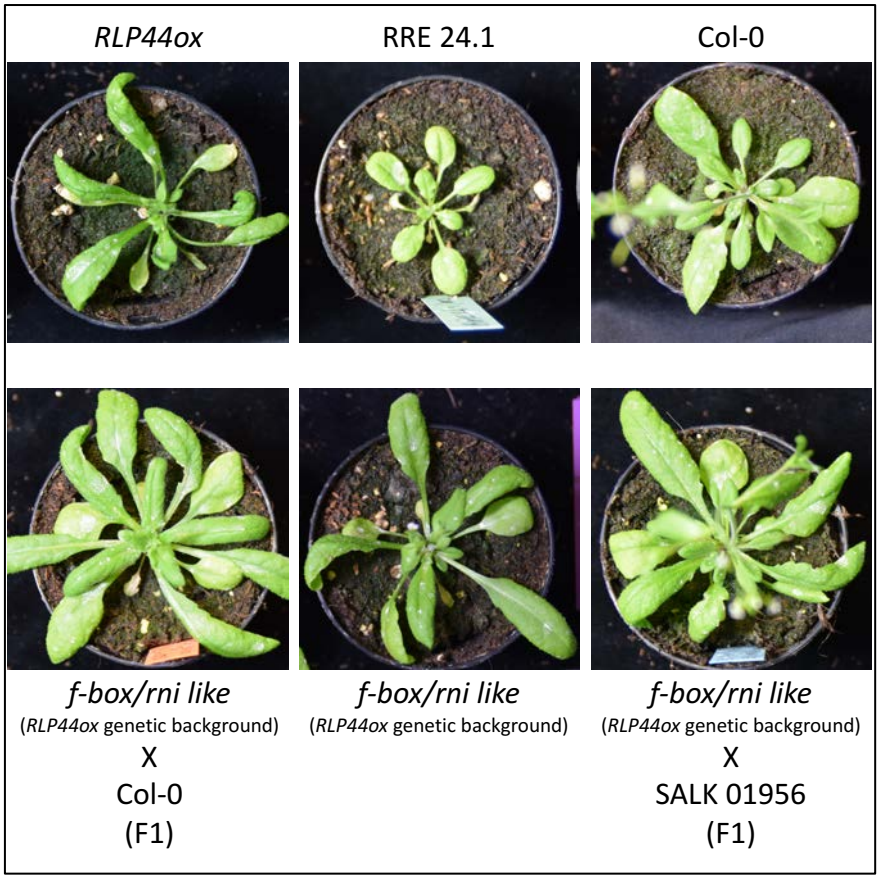

Figure 18: Comparison of 29 day old *A. thaliana* rosettes. *RLP44:RFP$_{OX}$* mutant phenotype of elongated petioles and narrow leaf blades clearly visible in *RLP44:RFP$_{OX}$* control. CRISPR *f-box/rni like* T-DNA cross F1's maintain suppression of the RLP44ox phenotype, supporting the role of *f-box/rni like* as the causative mutation, but CRISPR *f-box/rni like* Col-0 negative control cross also shows suppression of the RLP44ox phenotype in the F1 generation undermining result. All lines are either homozygous or heterozygous for the *RLP44:RFPox* transgene except the Col-0 WT control.

The results of the allelism test proved to be positive but suspect. The CRISPR *f-box/rni like* T-DNA cross F1 plants did maintain their suppression of the RLP44ox phenotype, supporting the role of *f-box/rni like* as the

causative mutation, but the negative control of CRISPR *f-box/rni like* crossed with Col-0 also showed suppression of the RLP44ox phenotype in the F1 generation, which undermined the results. One potential explanation was that crossing had led to the silencing of the *RLP44:RFPox* gene, however fluorescent microscopy eliminated this possibility as RFP fluorescence was still observed. There is of course also the possibility that the *f-box/rni like* mutation is in fact dominant, but this seems unlikely given the extreme disruption of the gene in this CRISPR derived mutant. Therefore, in summation the allelism test supports the case for the *f-box/rni like* mutation being responsible for the observed suppression of the RLP44ox phenotype but the lack of a satisfactory explanation for the suppression observed in the negative control throws these results into doubt.

F-Box/RNI Like appears to be expressed in the cytosol

With *F-Box/RNI Like* appearing to be the strongest candidate for the responsible suppressing gene, its predicted expression pattern was assessed using BAR eFP Browser. The limited data available on BAR eFP Browser for *F-Box/RNI Like* predicted that it is widely expressed throughout the plant, such as in the root, leaves, and petioles (Klepikova et al., 2016), which means it would theoretically be present in the correct plant tissues to interact with RLP44 signaling and facilitate the RLP44ox mutant phenotype. Therefore, in order to further explore the role of the *F-Box/RNI Like* gene, a *F-Box/RNI Like:RFP$_{OX}$, RLP44:GFP$_{OX}$* transgenic line was created.

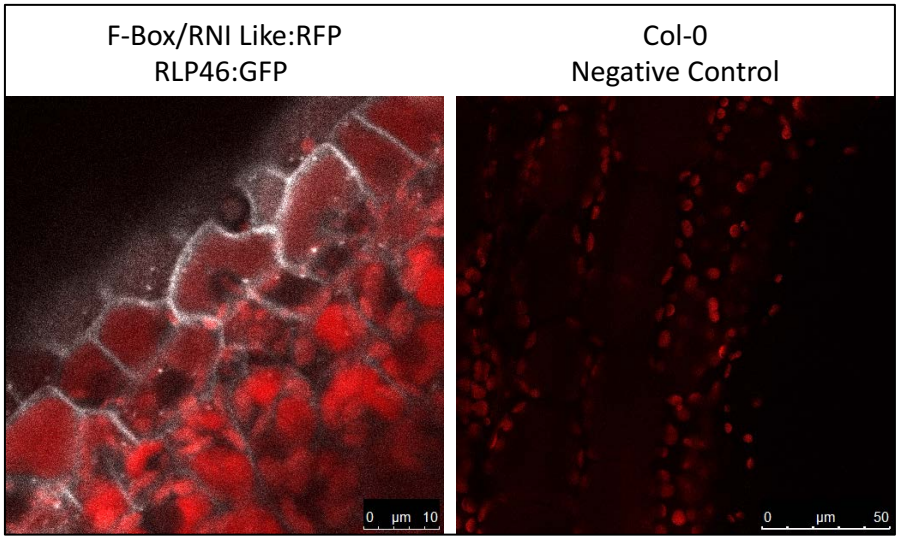

Figure 19: Fluorescent microscopy images of area adjacent to apical meristem in 4 day old seedlings expressing *F-Box/RNI Like:RFP$_{OX}$* in a *RLP44:GFP$_{OX}$* genetic background as well as image of Col-0 negative control. RFP channel shown in red, GFP in white. F-Box/RNI Like:RFP protein seemed to be expressed in the cytosol as well as possibly in the vacuole

Analysis of the line at the seedling stage 4 days after germination via fluorescent microscopy yielded some interesting results. The F-Box/RNI Like:RFP protein seemed to be localized to the cytosol (which would make sense for what is predicted to be a F-Box protein) (Bai et al., 1996; Zheng and Shabek, 2017; Kuroda et al., 2012; Berardini et al., 2015) as well as possibly in the vacuole, though this was probably sequestered free RFP. Looking at GFP and RFP fluorescence simultaneously, there was no apparent co-localization of fluorescence, suggesting that any interaction is not direct. It should be noted that while RFP fluorescence is a strong indicator of the presence of the F-Box/RNI Like protein in this line, it is possible that the F-Box/RNI Like protein was quickly degraded leaving behind only the RFP. Since we did not directly test for the presence of the F-Box/RNI Like protein in this study, this prospect can't be ruled out. Interestingly, the RFP fluorescence was strongest near the shoot apical meristem, and absent in the root. This is strange as the promotor driving the *F-Box/RNI Like:RFP* expression in this line is a UBQ10 (Ubiquitin-10) promotor and therefore should be expressed throughout the entire plant.

Discussion

Reflecting on the experiments performed over the course of the RLP44ox suppression screen we are confronted with mixed results. The absence of an identified causative gene for the lines RRE 9.2 and RRE 38.6 is unfortunate. Whether this was the result of a failure in analyzing the NGS data, the initial selection of candidate genes, or the original phenotyping of the putative suppressor mutant is not completely clear, though it does seem to point to problems with the phenotyping of lines, or an inconsistent presentation of phenotypes in different generations due to varying degrees of gene silencing. It is of course also possible that the suppression causing point mutation resulted in a still partially functional protein in the original RRE line, a condition that which would not have been replicated in the CRISPR derived mutant. Plant signaling networks often have a degree of redundancy and the loss of one signaling protein can prompt the up regulation or down regulation of other components to compensate (Lempe et al., 2013; El-Brolosy and Stainier, 2017). Additionally, proteins can continue to serve as scaffolds for larger complexes even if they themselves have lost all or part of their functionality (Kung and Jura, 2016; Gurevich and Gurevich, 2015). It is therefore conceivable that the original point mutations in the RRE lines, which resulted in changes to single amino acid residues, caused the suppression of the RLP44ox phenotype in a manner that the CRISPR derived mutants would not recapitulate, as all the CRISPR mutant confirmation lines created were most likely null mutants resulting from early stop codons. This hypothesis would in theory be possible to test, as single nucleotide base editors are becoming more wide spread. As such, a mutant line could be created containing the exact mutation reported by the NGS data, which would definitively prove if the detected point mutation was indeed responsible for the observed phenotypic suppression. Contrasting with the negative results of RRE 9.2 and RRE 38.6, RRE 24.1 had the problem of yielding two causative gene candidates, both of which are predicted to be involved in the E3 ubiquitin ligase pathway. CRISPR derived mutants for the *F-Box/RNI Like* and *UPL4* genes both seemed to recapitulate the suppression of the RLP44ox phenotype observed in the RRE 24.1 line. This is a problematic result given the fact that the odds of the occurrence of two EMS derived point mutations that suppress the RLP44ox

phenotype in the same individual genome is incredibly unlikely. In this regard, it is unfortunate that the *F-Box/RNI Like* allelism test yielded mixed results, as secondary confirmation would have been very useful in affirming the identity of at least one of the putative suppressor genes. That being said, while the likelihood of such a double mutation is extremely unlikely it is not impossible, and a similar argument can be made for how both these mutant proteins could cause the observed RLP44ox phenotypic suppression. Both F-Box/RNI Like and UPL4 will presumably be involved with the ubiquitination pathway, the former as a part of the SCF complex and the latter as a ubiquitin E3 ligase (Bai et al., 1996; Pickart, 2001; Zheng and Shabek, 2017). Since target specificity is so critical for these types of proteins in bringing E2 ubiquitin-conjugating enzyme into proximity with the correct target of ubiquitination (Zheng and Shabek, 2017), changes to single amino-acid residues, like those reported in the NGS data, could very easily cause them to lose their target specificity. Taking these results into consideration, 3 possibilities emerge. 1: Both genes are indeed responsible, and are operating in the same signaling pathway. 2: Both genes are responsible, and are operating in different signaling pathways. And 3: One or both of the suppressing lines is a false positive. If option one or two is indeed the case, then a rescue mutant of the CRISPR derived suppressor mutants should confirm the role of F-Box/RNI Like and UPL4. After this point, comparison of RNAseq data as well as looking for co-localization of fluorescent tagged proteins could provide a clearer answer as to whether F-Box/RNI Like and UPL4 function together or separately. In addition, Co-IP coupled with mass spectrometry would also be an excellent method to help identify the potential targets of F-Box/RNI Like and UPL4 and see if they do indeed fit into the web of RLP44 signaling. With this in mind, and looking at the preliminary data for the tagged F-Box/RNI Like:RFP lines, we arrive at a few interesting conclusions. While the lack of fluorescence in the roots of the seedlings assayed is curious given the use of a constitutive promotor in the line, we do observe RFP fluorescence in the cytosol as well as in the vacuole, though the latter could simply be sequestered cleaved RFP. We also don't seem to observe colocalization with RLP44:GFP, though this it perhaps not surprising given the latter's localization to the plasma membrane. Taking all of these results together then in consultation with the limitations of the data collected, this study does make a successful and strong case for the

roles of F-Box/RNI Like and UPL4 in helping facilitate the phenotypic expression of RLP44ox. While more work remains to be done to finally and conclusively confirm them, it is clear that they are without a doubt two strong candidate genes deserving of future research.

Chapter 3

Introduction

Chapter 3 outlines the initial characterizations of RECEPTOR-LIKE-PROTEIN 46 (RLP46). RLP's are a family of 57 genes in *A. thaliana*, and are similar to Receptor Like Kinases with regards to their localization to the plasma membrane and LRR extracellular domains. However, they differ in their lack of a functioning kinase domain (Shiu and Bleecker, 2001, 2003; Wang et al., 2008; Fritz-Laylin et al., 2005). RLP's have been shown to be important players in the network of signaling proteins found at the plasma membrane due to their interactions with extracellular compounds (such as ligands), RLK's, and other RLP's (He et al., 2018). A particularly well-known example of this is RECEPTOR-LIKE-PROTEIN 10 (RLP10) with is also known as CLAVATA 2, a protein that helps maintain the Stem Cell niche by perceiving CLE ligands and interacting with RLK's (Jeong et al., 1999; Fiers et al., 2005). Current studies continue to affirm the high importance of RLP's and often showcase their ability to interact with a variety of other proteins, sometimes simultaneously (He et al., 2018). The recent publication showing RLP44's interaction with both BAK1 and PSKR1 is an excellent example of this (Holzwart et al., 2018). RLP's are not solely linked to responding to developmental cues however, but have been shown to play a role in abiotic stress responses (Wu et al., 2016) as well as to be critical components of the plant immune system (Jamieson et al., 2018). This importance to plant immunity is shown by the innate immune response, where perception of a microbe-associated molecular pattern (MAMP) by pattern recognition receptors (PRR's) leads to activation of the plant's innate immune system (Tena et al., 2011). This immune response is characterized by a rapid release of reactive oxygen species, the aptly named ROS burst response, as well as further propagation of the signal, leading to modifications in the cell's gene expression patters, for example in the gene *FLG22-INDUCED RECEPTOR-LIKE KINASE 1* (*FRK1*) (Asai et al., 2002), and to further immune responses (Tena et al., 2011). This signaling requires a complex cross talk between receptor proteins, which is facilitated by the formation of heterodimers and protein complexes (He et al., 2018; Tena et al., 2011). Two proteins

involved in this immune related signal interplay are SUPPRESSOR-OF-BIR1 (SOBIR1) and BAK1 (Zhang et al., 2013; Liebrand et al., 2013; Burgh et al., 2019), which help convey the signals that are initiated by the binding of ligands to proteins like FLAGELLIN-SENSING 2 (FLS2) and EF-TU-RECEPTOR (EFR) (Zipfel et al., 2004, 2006). Taken together then, it is clear that RLP's help plant cells modulate their responses the both external and internal stimuli (Wang et al., 2008). Despite the increasingly clear importance of the RLP gene family, many of the genes remain uncharacterized, and *RLP46* is no exception. Notwithstanding this dearth of knowledge, there are a few things known about *RLP46* currently. It appears to be highly evolutionarily conserved (Augustin, 2015; Wang et al., 2008; Fritz-Laylin et al., 2005), to be expressed in mature xylem and procambium in seedlings as well as throughout the entire mature plate to a lesser extent (Klepikova et al., 2016), and it is strongly upregulated by the binding of EFR with the peptide ligand elf18 (Zipfel et al., 2006). Using these initial clues as a road map, this study aimed to perform an initial characterization of RLP46, looking for the possible connection to development hinted at by the evolutionarily conserved nature of the gene, for any possible role in abiotic stress responses, and for the possible link between RLP46 and plant immune responses suggested by the elevation of *RLP46* expression after elf18 perception.

Results

rlp46 mutant lines successfully generated using CRISPR/Cas9 system

The first step in the study of RLP46 was to generate a *rlp46* mutant line. This was done using CRISPR/Cas9. A Bi-allelic mutant was generated and the two mutations allowed to segregate into homozygous lines. The CRISPR/Cas9 cassette was then allowed to segregate out of the lines as well. The end result was two *rlp46* mutants derived from the same original bi-allelic line which were given the names *Crlp46-1* and *Crlp46-2*.

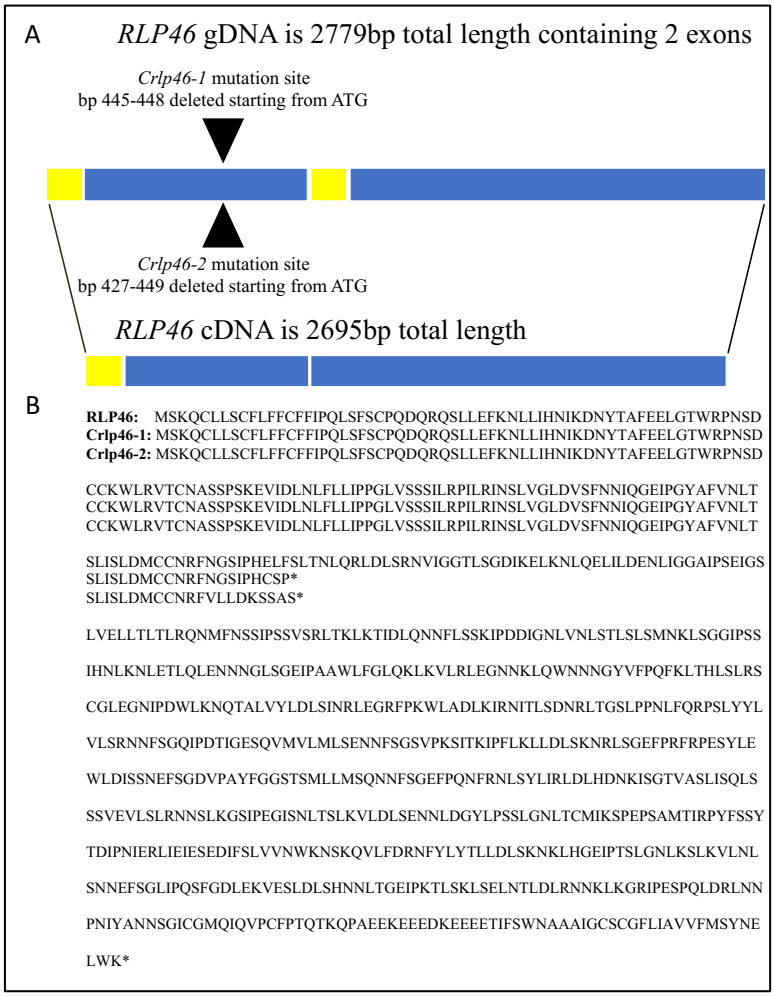

Figure 20: **A**. Diagram showing points of mutation in CRISPR derived lines as determined by sanger sequencing. gDNA refers to TAIR Accession Sequence 2137299. **B**. Comparison of RLP46 protein sequences of both CRISPR/Cas9 derived *rlp46* mutants with that of WT.

These two lines have homozygous deletions of 4 and 23 base pairs respectively (see figure 20) which cause frameshifts that lead to premature stop codons which should result in extremely truncated RLP46 proteins. Given the extremely truncated nature of the RLP46 protein in the two *rlp46* mutants, it seemed likely that these lines would function as null mutants, though of course there are instances of truncated receptor proteins behaving as dominant-negative mutations, such as in the case of the *ERECTA* gene (Shpak

et al., 2003). However, given the termination of the RLP46 protein well within its predicted LRR domains (Berardini et al., 2015) this seemed unlikely.

No obvious *rlp46* growth phenotype observed

With two *rlp46* mutants generated, the next step was to look for any obvious growth phenotypes.

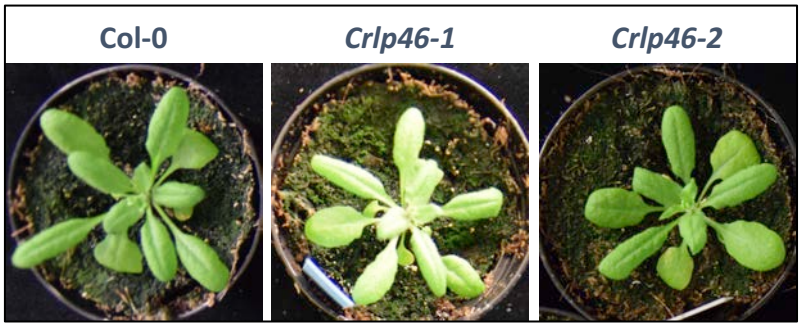

Figure 21: Comparison of Col-0 and *rlp46 A. thaliana* rosettes. Images taken 26 days after germination. No obvious growth phenotypes observed in *rlp46* mutants compared to Col-0 WT.

Head to head comparison of *rlp46* mutant plants with Col-0 WT plants did not reveal any obvious growth phenotypes. Plants were then tested for any possible drought tolerance phenotype, as there was existing data suggesting a role for RLP46 in plant stress responses (Klepikova et al., 2016). Col-0 and C*rlp46-1* were grown in single pots under short day conditions (to prevent bolting) until 24 days after germination, after which watering was discontinued. 38 days after germination, plants were top watered with 10 mL each to assess their ability to recover from the initial drought stress. After this, the plants were given no water until the end of the experiment at 42 days after germination to test for any phenotypic differences in stress induced drought tolerance.

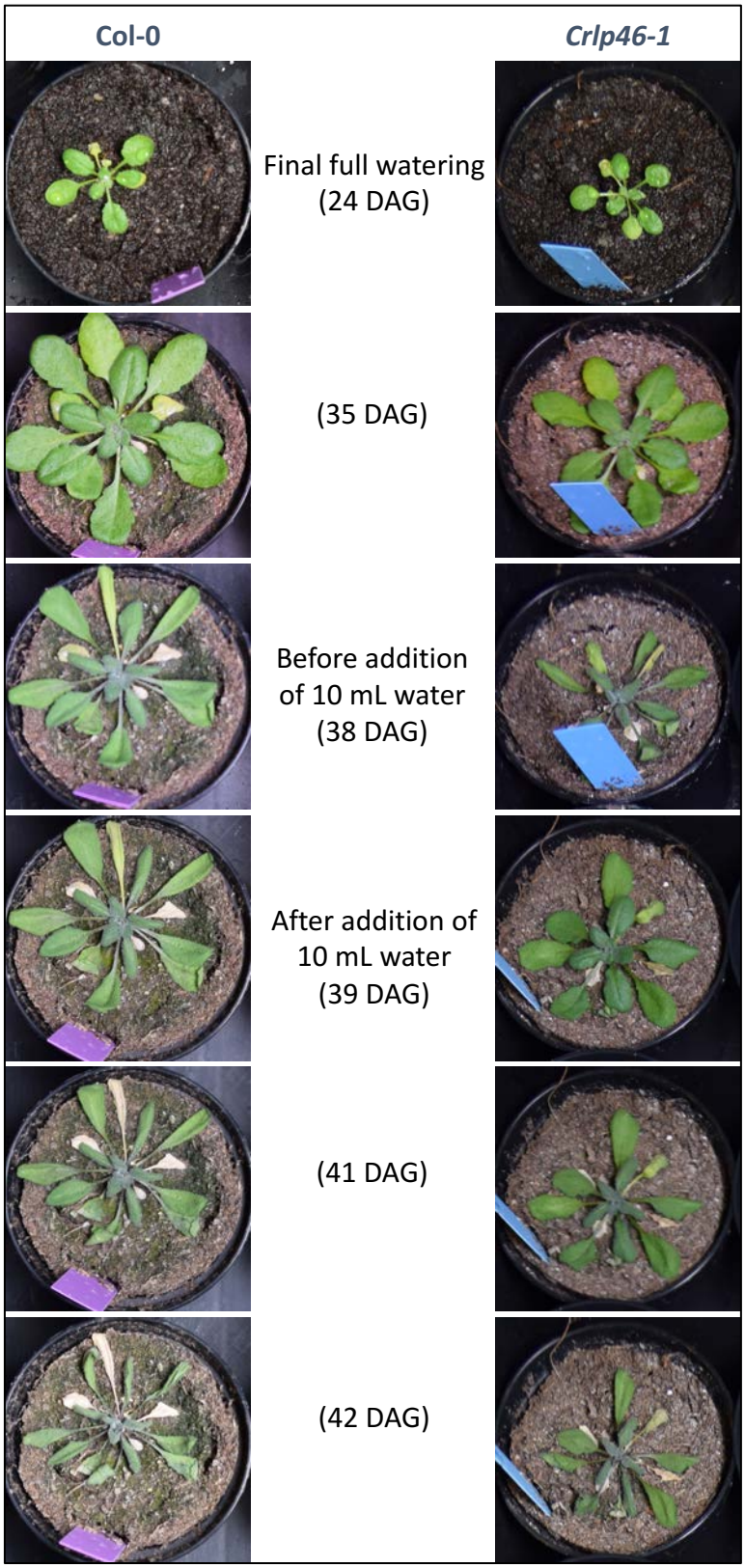

Figure 22: Comparison of Col-0 and C*rlp46-1 A. thaliana* rosettes under drought conditions. No apparent phenotypic difference between *Crlp46-1* and Col-0 WT control. Watering discontinued at 24 DAG. Plants top watered 38 DAG with 10 mL each to assess their ability to recover from the initial drought stress. Plants given no additional water until the end of the experiment at 42 DAG to test for any phenotypic differences in stress induced drought tolerance Plants germinated on Phyto-agar plates and transferred to soil 7 DAG. Plants grown in short day conditions to prevent bolting.

Analysis of the drought tolerance experiment did not show any divergent phenotypes for the C*rlp46-1* mutant line in either innate tolerance, degree of recovery, or stress induced tolerance. With no obvious rosette phenotypes observed, and since the available data on BAR eFP Browser suggested elevated expression of RLP46 in the root as well as a possible role for RLP46 in stress response (Klepikova et al., 2016), root length was next tested for mutant phenotypes.

Possible NaCl stress resistance phenotype observed

For the next experiment, plants were grown on Phyto-Agar plates containing various stress inducing compounds and their root lengths measured.

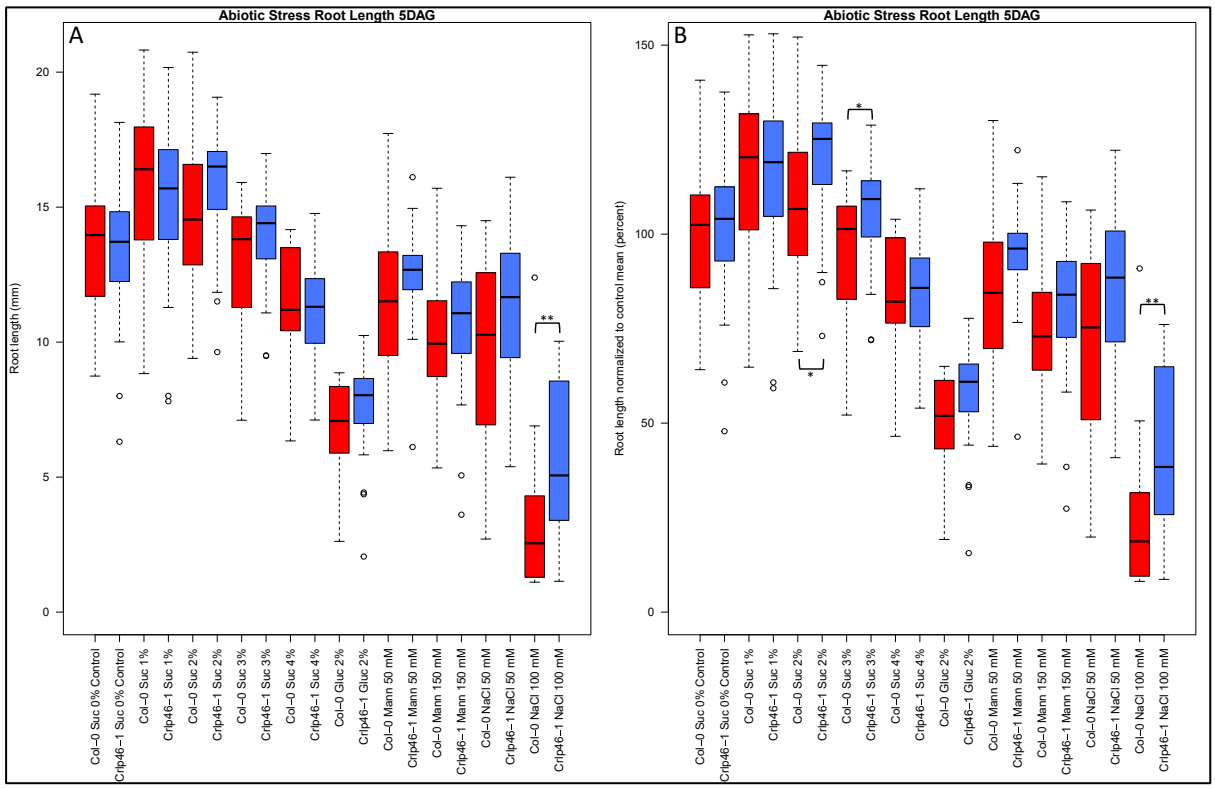

Figure 23: **A**. Boxplot of seedling root length 5 days after germination. Plants grown on Phyto-Agar plates containing abiotic stressors. *Crlp46-1* appears to have little to no variation from the Col-0 WT for the 0% sucrose control and the 1% sucrose treatment groups, suggesting no root length phenotype under non-stress conditions. There seems to be a significant difference in response to the 100 mM NaCl treatment, with the *Crlp46-1* seeming to show resistance compared to Col-0 WT (Student T-Test (homoscedastic) P value of 9.48×10^{-3}). There also appears to be a trend of increased growth at higher concentrations of sucrose compared to the Col-0 WT. **B**. Same experimental data normalized to percent growth relative to the control treatment for the plant line. There seems to be a significant difference in response to the 100 mM NaCl treatment, with *Crlp46-1* seeming to show resistance compared to Col-0 WT (homoscedastic Student T-Test P value of 6.22×10^{-3}). The trend of increased growth at higher concentrations of sucrose compared to the Col-0 WT is also significant (homoscedastic Student T-Test P values of 0.012 for the 2% sucrose treatment and 0.020 for the 3% sucrose treatment). N of 18, 25, 28, 27, 28, 29, 27, 27, 29, 26, 22, 27, 22, 26, 24, 27, 18, 24, 19, and 23. Data from single iteration of experiment. Error bars denote standard deviation.

Analysis of the results of the abiotic stressor experiment appeared to show that *Crlp46-1* had little to no variation from the Col-0 WT for the 0% sucrose control and the 1% sucrose treatment groups, suggesting that there is no *Crlp46-1* root length phenotype under non-stress conditions. There were however 2 treatments that showed possible *Crlp46-1* phenotypic trends. The first and clearest was the possible trend of increased NaCl resistance, which was significant at the higher 100 mM concentration level (Student T-Test

(homoscedastic) P value of $9.48x10^{-3}$), while the second was a potential trend of increased growth at higher concentrations of sucrose. Normalization of the data further supported the initial conclusions of the experiment. The NaCl resistance phenotype was more pronounced, and the increased growth compared to the Col-0 WT in response to higher concentrations of sucrose became significant for the 2% and 3% sample groups. Due to these promising initial results, it was determined that the NaCl resistance phenotype should be better characterize, therefore a similar abiotic stress experiment was performed using more gradations of NaCl concentrations.

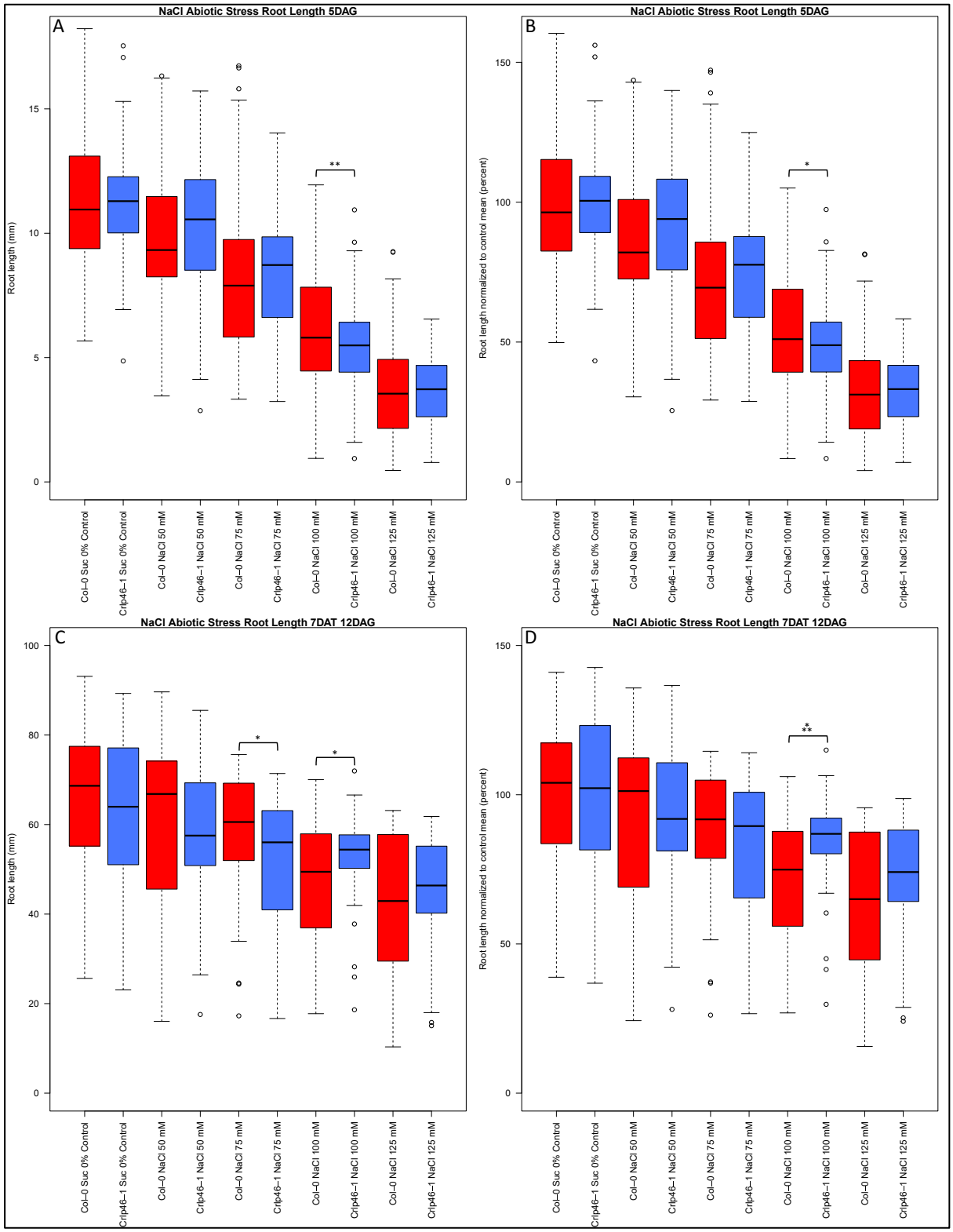

Figure 24: **A**. Boxplot of seedling root length 5 days after germination. Plants grown on Phyto-Agar plates containing abiotic stressors. The NaCl resistance phenotype seen in the previous experiment seemed to have reversed, with a Student T-Test (homoscedastic) p value of 5.08×10^{-3} (see figure 23). N of 134, 138, 100, 167, 132, 138, 124, 150, 120, and 130.

Error bars denote standard deviation. Data from 2 iterations of experiment. **B**. Boxplot of normalized seedling root length data 5 days after germination. Plants grown on Phyto-Agar plates containing abiotic stressors. The reversed NaCl resistance phenotype had reduced significance in the normalized data (homoscedastic Student T-Test p value of 0.011). The 50 mM group was borderline insignificant for the original trend (homoscedastic Student T-Test p value of 0.066) N of 134, 138, 100, 167, 132, 138, 124, 150, 120, and 130. Error bars denote standard deviation. Data from 2 iterations of experiment. **C**. Boxplot of seedling root length 7 days after seedling transfer and 12 days after germination. Plants grown on Phyto-Agar plates and then transferred by toothpick to plates containing abiotic stressors. *Crlp46-1* seemed to be less resistant to NaCl at the 75 mM concentration (homoscedastic Student T-Test p value of 0.017) and more resistant at the 100 mM NaCl concentration (homoscedastic Student T-Test p value of 0.011). N of 57, 60, 52, 60, 54, 55, 52, 57, 52, and 58 respectively. Error bars denote standard deviation. Data from 2 iterations of experiment. **D**. Boxplot of normalized seedling root length data collected 7 days after seedling transfer and 12 days after germination. Plants grown on Phyto-Agar plates and then transferred by toothpick to plates containing abiotic stressors. After normalization, only the increased NaCl resistance in *Crlp46-1* at 100 mM remained significant (homoscedastic Student T-Test p value of 2.06×10^{-4}), supporting the original observation of an increased NaCl resistance phenotype in the *Crlp46-1* line. N of 57, 60, 52, 60, 54, 55, 52, 57, 52, and 58 respectively. Error bars denote standard deviation. Data from 2 iterations of experiment.

Plants were once again germinated on Phyto-agar plates and root length measured 5 days after germination. In this case seeds were dispersed over the plates rather than places by tooth pick. This was done in order to prevent them from becoming buried in the media as this might adversely affect their growth or germination. This experiment was performed in 2 iterations. The results from this second round of abiotic stress experiments greatly undermined those the previous experiment, as in this iteration the original trend of increased NaCl stress resistance seemed to reverse its self in the 100 mM concentration treatment sample, while still appearing to remain at lower NaCl concentrations. Normalization of the data did not drastically impact the results either. The significance of the 100 mM NaCl treatment group result was reduced to a p value of 0.011 (homoscedastic Student T-Test) and the 50 mM group became borderline insignificant (homoscedastic Student T-Test p value of 0.066). These conflicting results raised serious questions about the original observation, so in order to control for other unaccounted for variables, such as the possibility that the abiotic stress was impacting the germination of the seeds differently, or that the placement method of the seeds had an impact, the root length experiment was repeated with the modification that all plants were germinated on control treatment plates and then transferred to the stressor containing plates at 5 days after germination. These plants were then allowed to grow for 7 days before their root lengths were measured. Analysis of the results collected across 2 iterations of this version of the experiment gave the seemingly conflicting results of an apparent increase in *Crlp46-1* sensitivity to NaCl at lower concentrations coupled with an increase in NaCl resistance at higher concentrations. This was very odd as this contrasted with the results seen in the previous experiment where the

seedlings were not transferred (see figure 24). This trend of increased *Crlp46-1* sensitivity to NaCl at 50 mM followed by increased resistance at the higher NaCl concentrations of 100 mM and 125 mM continued to persist after normalization of the data. *Crlp46-1* showed significantly increased resistance in the 100 mM treatment group with a p value of 2.06×10^{-4} (homoscedastic Student T-Test), however the results from the other abiotic stress experiments mean these results must be viewed with a degree of skepticism. They do however point to a possible role for RLP46 in NaCl abiotic stress responses, an exciting possibility that should certainly be pursued in future studies.

Elicitor response suggest RLP46 plays a role in plant immunity

Since the publicly available data shows elevated *RLP46* expression in *A. thaliana* plants exposed to the elicitor elf18 (Zipfel et al., 2006), *rlp46* mutants were tested for phenotypes in plant immune response. To this end, the *rlp46* mutant lines were tested for phenotypes in the plant ROS burst immune response. The *A. thaliana* lines Col-0, *Crlp46-1*, *Crlp46-2*, *pskr1-3* (a mutant line with elevated immune responses) (Igarashi et al., 2012), and *bak1-5,bkk1-1* (a mutant line with elicitor insensitivity) (Roux et al., 2011) were used in the first round of the experiment. Leaf disks were collected from the youngest fully mature leaves of plants 20-40 days after germination and elicitor induced ROS burst measured using a plate reader, with sample wells showing no ROS burst response being excluded from the final average (with the exception of *bak1-5,bkk1-1 samples*).

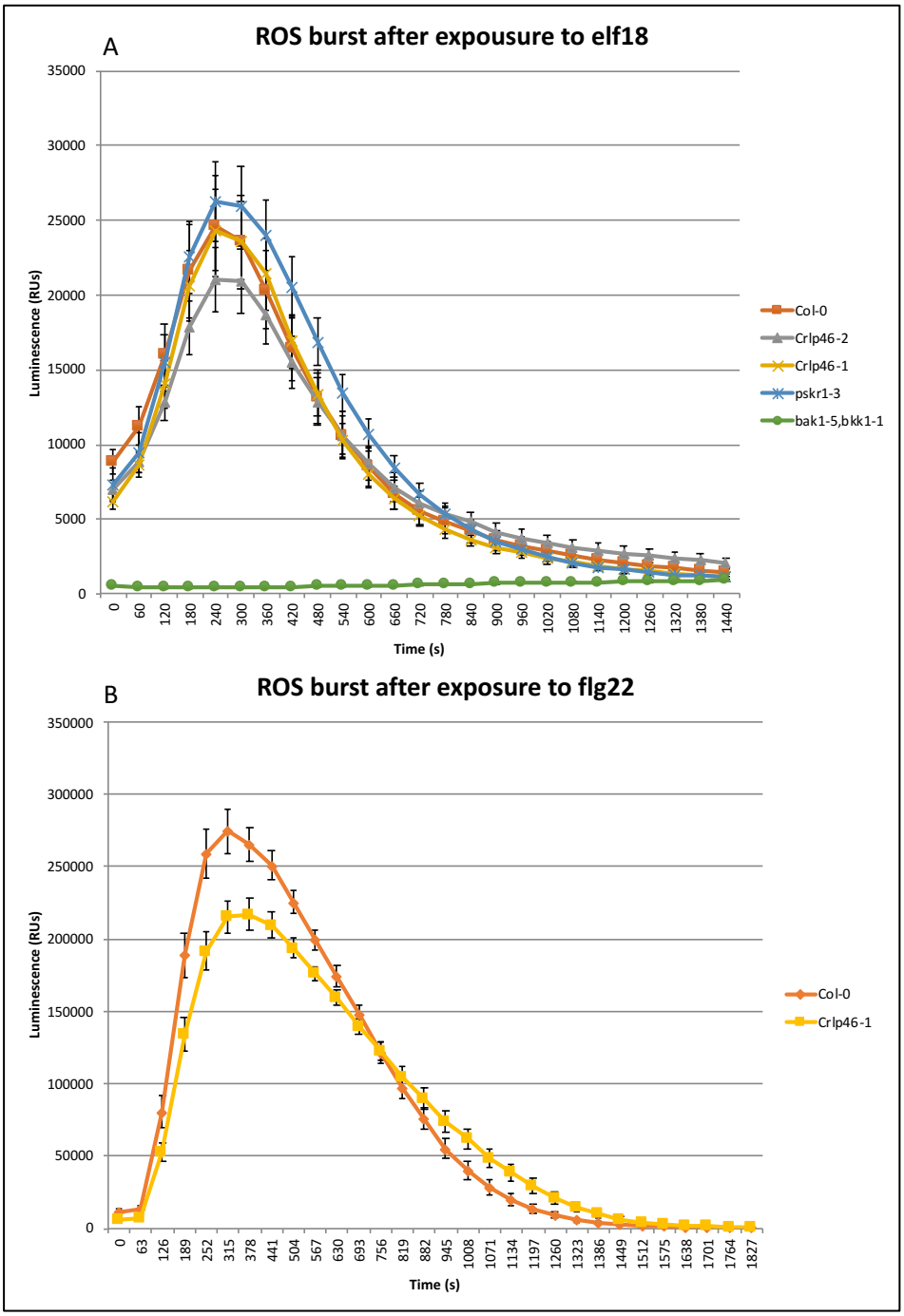

Figure 25: **A**. Graph showing average elf18 induced ROS burst for leaf disk sample groups as detected by plate reader using chemiluminescence. Results from sample wells showing no ROS burst response not included with exception of *bak1-5,bkk1-1* samples. There appeared to be no significant deviation from the Col-0 WT in either the timing or the magnitude of the elf18 induced ROS burst responses. Error bars denote standard error. N of 45, 57, 55, 35, and 20 for Col-0, *Crlp46-2, Crlp46-1, pskr1-3,* and *bak1-5,bkk1-1* respectively. Data from 2 iterations of experiment. **B**. Graph showing average flg22 induced ROS burst for leaf disk sample groups as detected by plate reader using chemiluminescence. Results from sample wells showing no ROS burst response not included. There appeared to be no significant deviation from the Col-0 WT in either the timing or the magnitude of the flg22 induced ROS burst response. Error bars denote standard error. N of 29 and 26 for Col-0 and *Crlp46-1* respectively. Data from 1 iteration of experiment.

Analysis of the results showed no phenotype in the timing or magnitude of the ROS bust in any of the lines, with the exception of the *bak1-5,bkk1-1* negative control. This suggests that RLP46 is not involved with the ROS burst immune response. This experiment was repeated using Col-0 and *Crlp46-1* with the elicitor flg22. This variation of the experiment also showed no conclusive differences in the ROS burst phenotype between *Crlp46-1* and the Col-0 WT. The results of these two experiments make a strong case that RLP46 is not involved in the ROS burst pathway or that its role is redundant. *Crlp46-1* was next tested for mutant phenotypes in elicitor induced transcriptional changes. The plant lines Col-0 and *Crlp46-1* were germinated on Phyto-Agar plates and transferred to liquid media at 5 days after germination, where they were then exposed to elf18 for 1 hour before being frozen in liquid nitrogen and used for RNA extraction. RT-qPCR was then performed to assess the changes in expression levels of the plant immune response associated genes *FRK1* and *NHL10* (Asai et al., 2002; Segonzac et al., 2014) (for primer list see appendix 1).

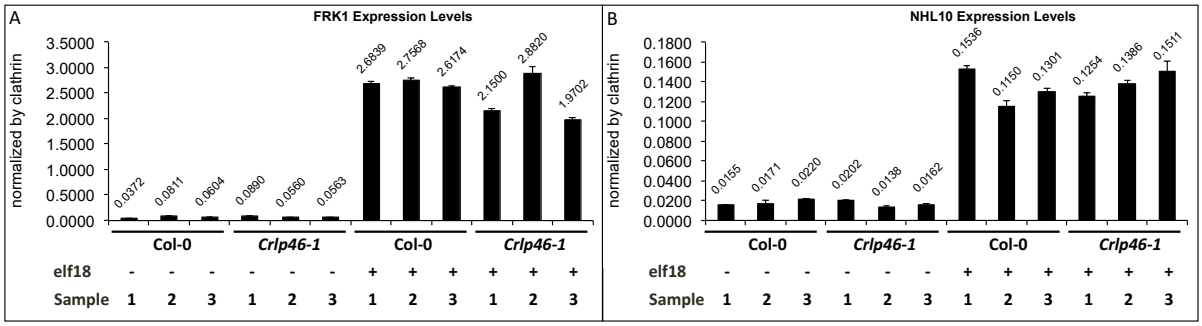

Figure 26: **A**. RT-qPCR data from bulk seedling cDNA. Plants exposed to elicitor containing liquid media for 1 hour before RNA extraction. All samples showed increased *FRK1* expression upon exposure to elf18 elicitor. *Crlp46-1* line seemed to have roughly WT levels of *FRK1* expression in both the control and elf18 treated groups. All sample groups contained 3 biological replicates. Error bars denote standard deviation. **B**. RT-qPCR data from same bulk seedling cDNA. All samples showed increased *NHL10* expression upon exposure to elicitor. *Crlp46-1* line seemed to have roughly WT levels of *NHL10* expression in both the control and elf18 treated groups. All sample groups contained 3 biological replicates. Error bars denote standard deviation.

Analysis of the experimental results clearly showed increased expression in *FRK1* and *NHL10* after exposure to the elicitor elf18, but the *rlp46* mutation did not seem to have any effect on the observed expression levels. Therefore, having ruled out rapid immune response phenotypes, the *Crlp46-1* mutant line was tested for phenotypes in elicitor induced growth inhibition (Gómez-Gómez and Boller, 2000; Zipfel et al., 2006; Igarashi et al., 2012). For the first iteration of this set of experiments elicitor induced growth inhibition of plants grown on Phyto-agar plates was tested. In addition, lateral root number was also recorded

as the available data on BAR eFP Browser predicted RLP46 expression in the root (Klepikova et al., 2016).

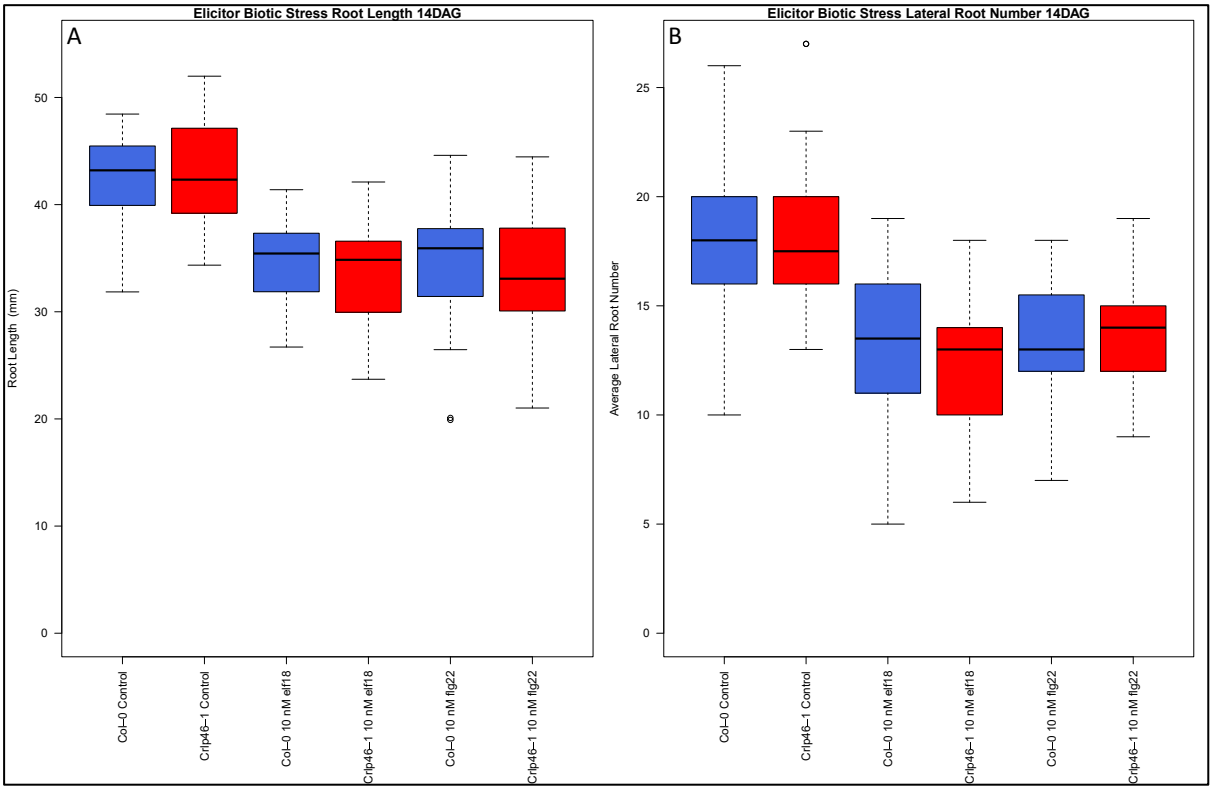

Figure 27: **A**. Boxplot of seedling root length 14 days after germination. Plants grown on Phyto-Agar plates containing elicitors. Both *Crlp46-1* and Col-0 WT control showed mild growth reduction on elicitor containing plates. There did not seem to be any significant deviation in phenotype between the two lines. N of 26, 29, 29, 33, 33, and 34 respectively. Data from 3 iterations of experiment. **B**. Boxplot of seedling lateral root number 14 days after germination from same experiment. Both *Crlp46-1* and Col-0 WT control showed mild reduction of lateral root number on elicitor containing plates, however this was simply a result of shorter average root lengths, as the ratio of lateral roots per unit of root length was unchanged (see table 5). There did not seem to be any significant deviation in phenotype between the two lines. N of 38, 42, 42, 43, 43, and 44 respectively. Data from 3 iterations of experiment.

Analysis of plant root growth inhibition on Phyto-agar plates containing elicitors did not yield any obvious phenotypes. It should also be noted that the observed growth inhibition seemed very mild for the amount of elicitor present in the media (Igarashi et al., 2012), suggesting that Phyto-agar plates might not be an effective means for delivering the elicitor induced biotic stress to the plants. Analyzing the lateral roots portion of the results did not show any significant variation between the *Crlp46-1* mutant line and the Col-0 WT control for the elf18, or the flg22 treatments either. Furthermore, comparing the ratios of lateral roots per millimeter of root showed that there was in fact very little variation across all of the plant lines and treatment groups.

Table 5: Table showing average root length, lateral root number, sample number, and lateral root per millimeter ratio of experimental data from Phyto-agar plate elicitor experiments (see figure 27). Data from 3 iterations of experiment.

Line:	Elicitor Treatment:	Average root length (mm):	Root Length Sample Number (n):	Average Lateral Root Number:	Lateral Root Sample Number (n):	Average Lateral Root Per mm Root Length:
Col-0	Control	42.7	26	17.6	38	0.41
Crlp46-1	Control	43.1	29	18.1	42	0.42
Col-0	10 nM elf18	34.8	29	13.4	42	0.38
Crlp46-1	10 nM elf18	33.4	33	12.2	43	0.36
Col-0	10 nM flg22	34.5	33	13.3	43	0.39
Crlp46-1	10 nM flg22	32.9	34	13.5	44	0.41

Given these results, and the apparent ineffectiveness of using Phyto-agar plates to administer elicitor induced stress, the next set of experiments exposed the plants to elicitors via liquid media. Plants were germinated on Phyto-Agar plates and then individual plants were transferred to liquid media containing wells of 48 well plates 4 days after germination. After 10 days of growth in liquid media (14 days after germination), fresh weights were measured.

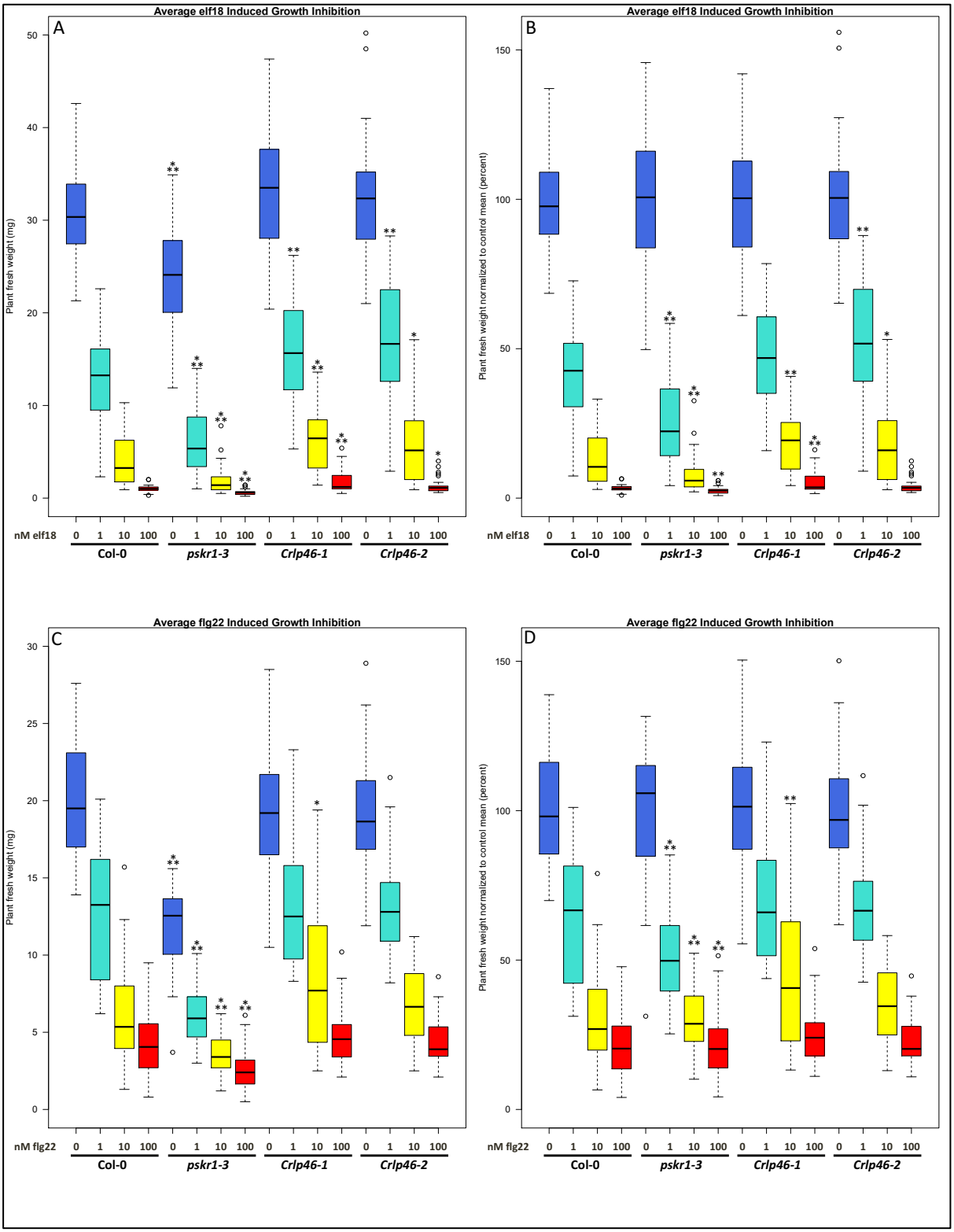

Figure 28: **A**. Boxplot of average plant fresh weight after 10 days in liquid media and 14 days after germination. All lines showed expected growth inhibition in response to elf18 elicitor containing growth media, with the *pskr1-3* positive control mutant showing the expected hyper sensitivity (Igarashi et al., 2012). Both *rlp46* mutant lines seemed to show significant

resistance to elicitor induced growth inhibition. Stars denote significant divergence from the Col-0 WT with the same elicitor treatment. N and P values shown in table 6. Data from 4 iterations of experiment. **B**. Data from section A normalized to 0 nM control treatment of same plant line. Both *rlp46* mutant lines seemed to show significant resistance to elicitor induced growth inhibition. Stars denote significant divergence from the Col-0 WT with the same elicitor treatment. N and P values shown in table 6. **C**. Boxplot of average plant fresh weight after 10 days in liquid media and 14 days after germination. All lines showed expected growth inhibition in response to flg22 elicitor containing growth media, with the *pskr1-3* positive control mutant showing the expected hyper sensitivity (Igarashi et al., 2012). Only the 10 nM C*rlp46-1* samples seemed to show significant resistance to flg22 elicitor induced growth inhibition. Stars denote significant divergence from the Col-0 WT with the same elicitor treatment. N and P values shown in table 7. Data from 4 iterations of experiment. **D**. Data from section C normalized to 0 nM control treatment of same plant line. Only the 10 nM C*rlp46-1* samples seemed to show significant resistance to flg22 elicitor induced growth inhibition. Stars denote significant divergence from the Col-0 WT with the same elicitor treatment. N and P values shown in table 7. Data from 4 iterations of experiment.

The experiments with liquid media containing elicitors proved to be much more effective at causing growth inhibition in the samples. All lines showed the expected response to elf18 elicitor containing media of reduced growth, and the *pskr1-3* mutant showed the expected hypersensitivity to elicitor exposure (Igarashi et al., 2012). Interestingly, both *rlp46* mutants seemed to show significant resistance to elicitor induced growth inhibition, supporting the hypothesis that RLP46 has a role in the plant immune response. Normalization of the data reduced the strength of the *rlp46* elf18 elicitor resistance results, however there did still seem to be a significant trend across the two *rlp46* mutant lines.

Table 6: Table showing average fresh weight, growth normalized to 0 nM control, sample number, and homoscedastic Student T-Test p values for significance between line and Col-0 control with same elf18 treatment for both fresh weight and normalized data used in figure 28 sections A and B. Data from 4 iterations of experiment.

Line:	elf18 Treatment (nM):	Average Fresh Weight (mg):	Normalized Growth (percent):	Sample Number (n):	T-Test p Value Fresh Weight:	T-Test p Value Normalized Growth:
Col-0	0	31.08	100	48	1	1
pskr1-3	0	23.94	100	48	8.17E-09	1
Crlp46-1	0	33.38	100	48	0.055	1
Crlp46-2	0	32.20	100	48	0.322	1
Col-0	1	12.92	41.6	48	1	1
pskr1-3	1	6.26	26.1	48	1.45E-11	2.76E-06
Crlp46-1	1	15.96	47.8	48	0.005	0.061
Crlp46-2	1	16.64	51.7	48	0.002	0.006
Col-0	10	3.99	12.8	48	1	1
pskr1-3	10	1.86	7.8	48	1.52E-06	6.86E-04
Crlp46-1	10	6.12	18.3	48	1.82E-04	1.61E-03
Crlp46-2	10	5.67	17.6	48	0.0106	0.020
Col-0	100	1.04	3.4	48	1	1
pskr1-3	100	0.63	2.6	48	2.26E-09	1.84E-03
Crlp46-1	100	1.78	5.3	48	4.77E-05	2.61E-04
Crlp46-2	100	1.25	3.9	48	0.0710	0.142

Having tentative evidence for *rlp46* resistance to elf18 induced growth inhibition, the lines were then tested for resistance to the elicitor flg22, as this would elucidate whether the observed *rlp46* response was elf18 specific. The expected plant response to flg22 elicitor containing media of reduced growth was observed again, as well as the *pskr1-3* mutant's expected hypersensitivity to elicitor exposure (Igarashi et al., 2012). Interestingly, the *rlp46* mutants appeared to not deviate as strongly from their Col-0 WT control treatment counterparts, with the exception of the *Crlp46-1* 10 nM treatment group, seeming to indicated that the *rlp46* mutant response in more strongly induced by elf18 than flg22. Normalization of the data yielded the same results but did strengthen the significance of the *Crlp46-1* 10 nM treatment group resistance phenotype.

Table 7: Table showing average fresh weight, growth normalized to 0 nM control, sample number, and homoscedastic Student T-Test p values for significance between line and Col-0 control with same flg22 treatment for both fresh weight and normalized data used in figure 28 sections C and D. Data from 4 iterations of experiment.

Line:	flg22 Treatment (nM):	Average Fresh Weight (mg):	Normalized Growth (percent):	Sample Number (n):	T-Test p Value Fresh Weight:	T-Test p Value Normalized Growth:
Col-0	0	19.88	100	48	1	1
pskr1-3	0	11.86	100	48	9.38E-15	1
Crlp46-1	0	18.95	100	48	0.391	1
Crlp46-2	0	19.25	100	48	0.509	1
Col-0	1	12.72	64.0	48	1	1
pskr1-3	1	6.06	51.1	48	3.16E-12	0.006
Crlp46-1	1	13.10	69.1	48	0.697	0.303
Crlp46-2	1	13.01	67.6	48	0.756	0.439
Col-0	10	6.17	31.0	48	1	1
pskr1-3	10	3.61	30.4	48	6.08E-05	0.857
Crlp46-1	10	8.57	45.2	48	0.020	0.008
Crlp46-2	10	6.66	34.6	48	0.477	0.310
Col-0	100	4.26	21.4	48	1	1
pskr1-3	100	2.61	22.0	48	2.51E-04	0.819
Crlp46-1	100	4.82	25.4	48	0.265	0.122
Crlp46-2	100	4.33	22.5	48	0.875	0.642

These experiments seemed to show that the *rlp46* mutants have a mild but consistent resistance to elicitor induced growth inhibition (around 8 percent on average for the elf18 treatments). There was however a great deal of variability in the results data (not uncommon for growth inhibition experiments), so a new round of growth inhibition experiments was performed using a more robust experimental set up. As before, plants were germinated on Phyto-Agar plates, but then groups of 30 seedlings were placed in Erlenmeyer flasks containing 25 mL liquid media, grown in shaking growth chambers, and then growth inhibition assessed via dry mass of the bulked plantlets. This new set up mitigated, but did not eliminate the observed variability.

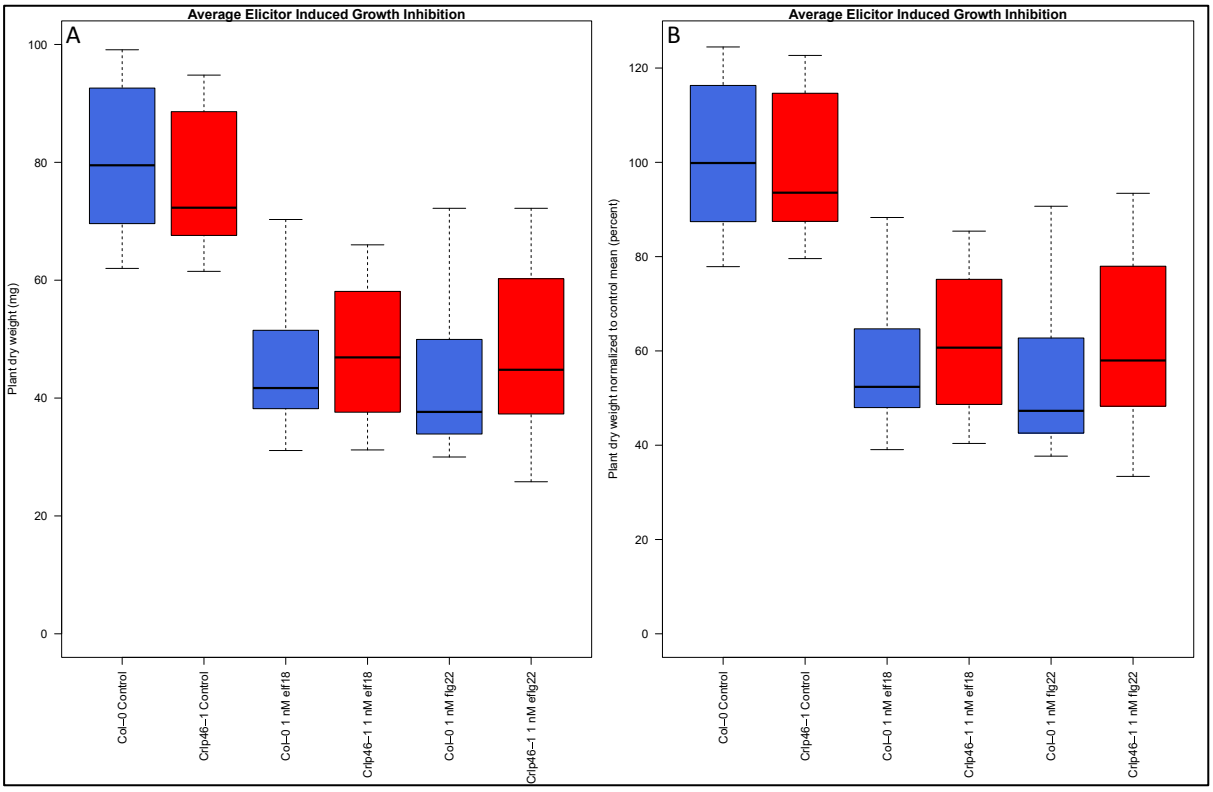

Figure 29: **A**. Boxplot of average plant dry weight after 7 days in liquid media and 11-12 days after germination. All lines showed expected the growth inhibition in response to elicitor containing growth media (Igarashi et al., 2012). C*rlp46-1* samples seemed to show mild resistance to elicitor induced growth inhibition as compared to the Col-0 WT samples. Stars denote significant divergence from the Col-0 WT with the same elicitor treatment. N of 13, 13, 13, 13, 8, and 8 respectively. Data from 3 iterations of experiment for elf18 samples and 2 iterations of experiment for flg22 samples. Exact values shown in table 8. **B**. Normalization of same data All lines showed the expected growth inhibition in response to elicitor containing growth media (Igarashi et al., 2012). C*rlp46-1* samples seemed to show mild resistance to elicitor induced growth inhibition as compared to the Col-0 WT samples. Stars denote significant divergence from the Col-0 WT with the same elicitor treatment. N of 13, 13, 13, 13, 8, and 8 respectively. Data from 3 iterations of experiment for elf18 samples and 2 iterations of experiment for flg22 samples. Exact values shown in table 8.

Analysis of the flask growth inhibition experiments supported the single plant experiment results, though interestingly in this iteration the *rlp46* elicitor resistance phenotype seemed to extend to flg22 as well. Normalization of the data further supported the trend of mild *rlp46* resistance to elicitor induced growth inhibition. The results also suggested that the *rlp46* elicitor resistance phenotype is not elf18 specific, but also applies to flg22 as well, with the C*rlp46-1* mutant showing on average a subtle resistance to both elf18 and flg22 of around 5% and 7% respectively across the course of all experiments.

Table 8: Table showing average dry weight, growth normalized to 0 nM control, plant per sample number, and n values for each treatment group. Data applies to flask growth inhibition experiments shown in figure 29. Data from 3 iterations of experiment for elf18 samples and 2 iterations of experiment for flg22 samples.

Line:	Elicitor Treatment:	Average Dry Weight (mg):	Normalized Growth (percent):	Plants Per Sample:	Sample Number (n):
Col-0	Control	79.6	100	30	13
Crlp46-1	Control	77.3	100	30	13
Col-0	1 nM elf18	45.8	57.6	30	13
Crlp46-1	1 nM elf18	48.3	62.5	30	13
Col-0	1 nM flg22	43.2	54.2	30	8
Crlp46-1	1 nM flg22	47.8	61.9	30	8

These results further support the idea that RLP46 could play a role in the propagation of elicitor induced plant immune responses, as evidenced by the phenotype of mild *rlp46* resistance to elicitor induced growth inhibition.

RLP46 is localized to the plasma membrane

The next step in the analysis of RLP46 was to create overexpression and fluorescently tagged lines in order to determine RLP46's localization and if there were any phenotypes associated with RLP46 overexpression. The GreenGate cloning system (Lampropoulos et al., 2013) was used to create a vector containing the *RLP46* gene fused with GFP driven by the UBQ10 promotor. This new plasmid was first tested through transient expression in *N. benthamiana* leaves and subsequent fluorescent microscopy of leaf disks.

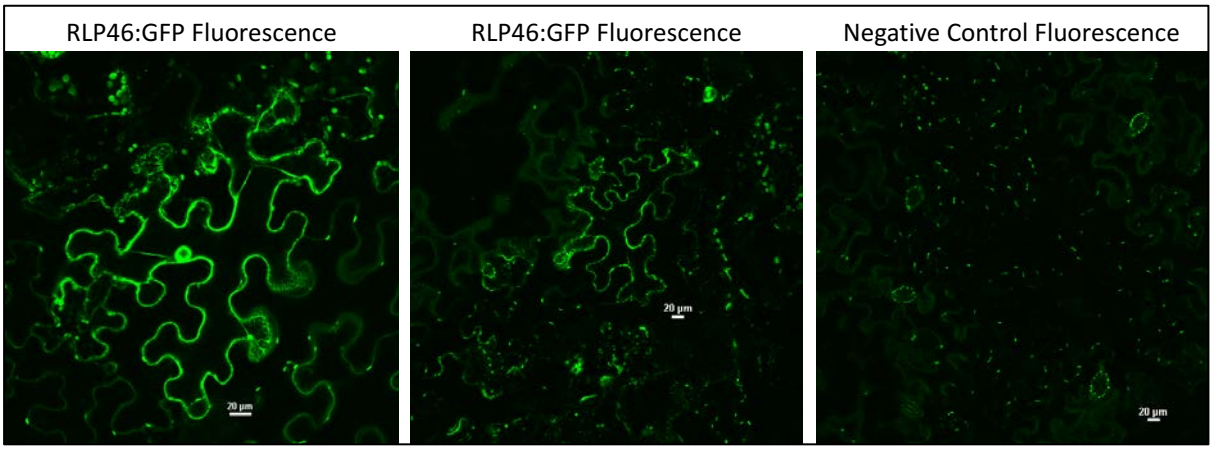

Figure 30: Fluorescent microscopy images showing RLP46:GFP fluorescence in leaf pavement cells transiently expressing the protein. RLP46:GFP appears to be localized to the plasma membrane of the cells examined. Untransformed negative control *N. benthamiana* leaf tissues cells shown for reference.

Fluorescent microscopy showed that the RLP46:GFP protein construct was being expressed successfully, and that it appeared to be localized to the plasma membrane of the *N. benthamiana* epidermal leaf tissue cells observed. Having confirmed the functionality of the *RLP46:GFP* plasmid vector, two transgenic *A. thaliana* lines were then generated. Both these lines contained the same DNA coding sequence for a GFP tagged RLP46 protein driven by the UBQ10 promotor, but differed in their genetic backgrounds, one being in the Col-0 background (hereafter referred to as *RLP46:GFP$_{OX}$-1*), and the other in the *Crlp46-1* genetic background (hereafter referred to as *RLP46:GFP$_{OX}$-2*). Fluorescent microscopy of the T1 plant that yielded the *RLP46:GFP$_{OX}$-2* line confirmed the expression of RLP46:GFP, which once again seemed to be localized to the plasma membrane. However overall expression levels seemed to be low for a UBQ10 constitutive promotor, though this could have been due to these leaves being from a T1 plant that had been exposed to selective media.

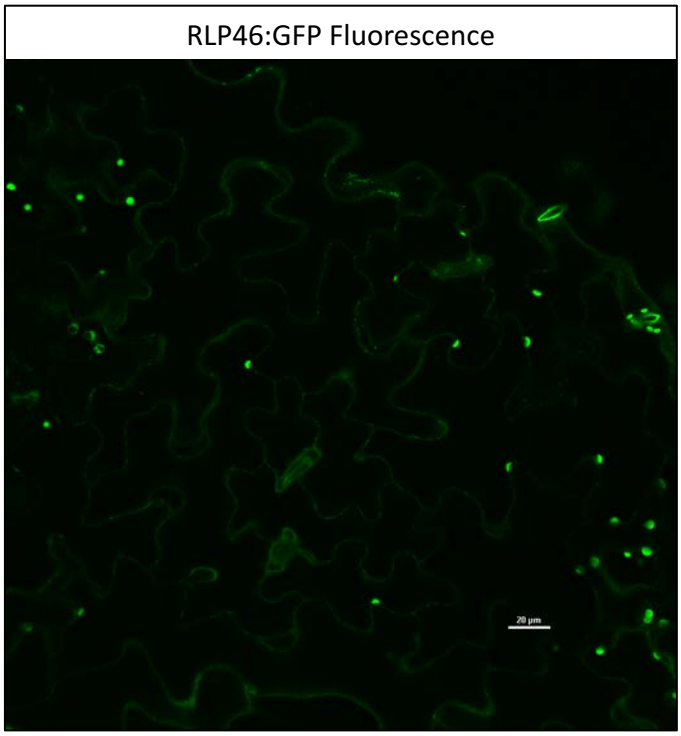

Figure 31: Fluorescent microscopy images showing RLP46:GFP fluorescence in leaf pavement cells of transformed *A. thaliana* T1 plant 27 days after germination. RLP46:GFP appeared to be localized to the plasma membrane of the cells examined. RLP46:GFP expression seemed low for a UBQ10 constitutive promotor but was still present. This could have been due to these leaves being from a T1 plant that had been exposed to selective media.

RLP46:GFPox does not strongly impact *FRK1* and *NHL10* gene expression levels

After confirmation of the presence of the gene through PCR, sequencing (primers can be found in appendix 1), and microscopy, *RLP46:GFP* expression levels were tested through RT-qPCR. This analysis was combined with a repeat of the experiment outlined in figure 26, where the impact of elicitors on the plant immune system related genes *FRK1* and *NHL10* were measured using RT-qPCR. As before, plantlets were germinated on Phyto-Agar plates and transferred to liquid media where they were then exposed to either elf18 or flg22 for 1 hour before being frozen in liquid nitrogen and used for RNA extraction. For this experiment, the plant lines Col-0, *Crlp46-1*, *RLP46:GFP*$_{OX}$*-1*, and *RLP46:GFP*$_{OX}$*-2* were tested for expression of *RLP46*, *FRK1*, and *NHL10* via RT-qPCR.

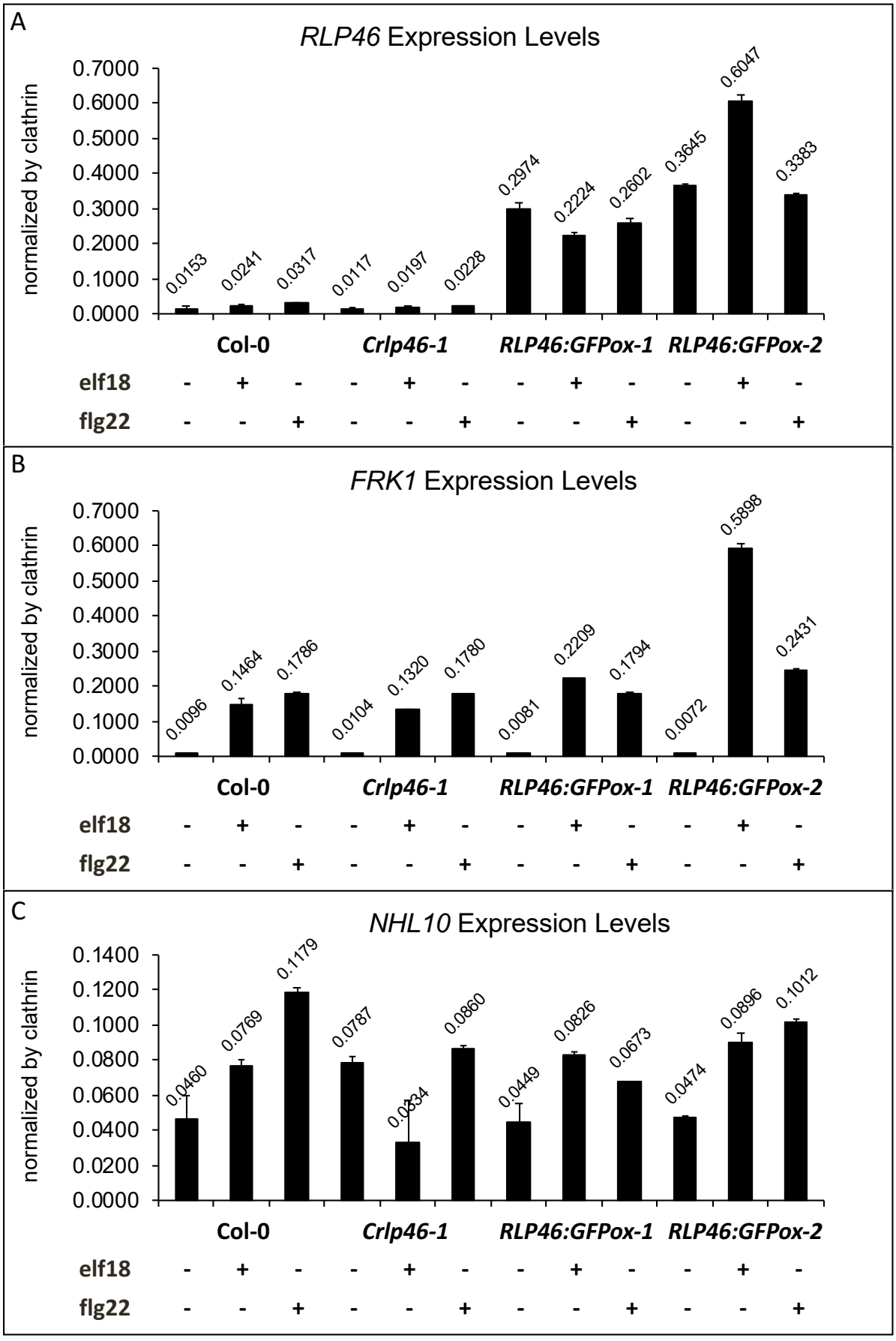
A
RLP46 Expression Levels
normalized by clathrin
0.7000
0.6000
0.5000
0.4000
0.3000
0.2000
0.1000
0.0000
0.0153
0.0241
0.0317
0.0117
0.0197
0.0228
0.2974
0.2224
0.2602
0.3645
0.6047
0.3383
Col-0
Crlp46-1
RLP46:GFPox-1
RLP46:GFPox-2
elf18 - + - - + - - + - - + -
flg22 - - + - - + - - + - - +
B
FRK1 Expression Levels
normalized by clathrin
0.7000
0.6000
0.5000
0.4000
0.3000
0.2000
0.1000
0.0000
0.0096
0.1464
0.1786
0.0104
0.1320
0.1780
0.0081
0.2209
0.1794
0.0072
0.5898
0.2431
Col-0
Crlp46-1
RLP46:GFPox-1
RLP46:GFPox-2
elf18 - + - - + - - + - - + -
flg22 - - + - - + - - + - - +
C
NHL10 Expression Levels
normalized by clathrin
0.1400
0.1200
0.1000
0.0800
0.0600
0.0400
0.0200
0.0000
0.0460
0.0769
0.1179
0.0787
0.0334
0.0860
0.0449
0.0826
0.0673
0.0474
0.0896
0.1012
Col-0
Crlp46-1
RLP46:GFPox-1
RLP46:GFPox-2
elf18 - + - - + - - + - - + -
flg22 - - + - - + - - + - - +

Figure 32: RT-qPCR data from bulk seedling cDNA. Plants exposed to elicitor containing liquid media for 1 hour before RNA extraction. Error bars denote standard deviation. **A**. Col-0 samples showed increased *RLP46* expression upon exposure to elicitors. *Crlp46-1* line also showed increased *RLP46* expression upon exposure to elicitors as well as basal expression of a presumably non-functional *rlp46* transcript. *RLP46:GFP$_{OX}$* lines showed elevated *RLP46:GFP* transcript levels and mixed responses to elicitor exposure. **B**. All samples showed increased *FRK1* expression upon exposure to elicitors. *Crlp46-1* line showed WT levels of *FRK1* expression across treatments. *RLP46:GFP$_{OX}$* lines showed elevated *FRK1* transcript levels in elf18 treatment samples, and *RLP46:GFP$_{OX}$-2* showed higher flg22 induced *FRK1* expression. **C**. All samples showed mildly increased *NHL10* expression upon exposure to elicitors except for *Crlp46-1* elf18 treatment sample. *Crlp46-1*showed above WT *NHL10* expression levels, which decrease upon elf18 exposure, and were below WT upon flg22 exposure. *RLP46:GFP$_{OX}$* lines showed WT *NHL10* expression levels that increased to slightly above WT levels upon elf18 exposure, and slightly below WT levels upon flg22 exposure.

Analysis of the *RLP46* expression data showed that *RLP46* expression seemed to be elevated by both elf18 exposure (supporting the literature on the topic) (Zipfel et al., 2006) as well as by flg22 exposure. The *Crlp46-1* line seemed to still have a degree of *rlp46* expression, presumably of a non-functional mutant *rlp46* transcript, and to also have expression levels elevated by exposure to elicitors. In addition, both *RLP46:GFP$_{OX}$* lines showed high expression of the *RLP46:GFP* transcript, though their responses to elicitor exposure were mixed. This is not necessarily a surprise as UBQ10 promotors were used in these lines, meaning that any promotor-controlled regulation of the WT *RLP46* gene would be diluted out by the overexpressing transgenic *RLP46* genes. Analysis of the plant immune response related gene *FRK1* yielded some very interesting results. All plant line controls showed a similar level of expression of the *FRK1* transcript. The *Crlp46-1* and *RLP46:GFP$_{OX}$* lines seemed to have a similar *FRK1* expression pattern as Col-0 for all treatments with the exception of the *RLP46:GFP$_{OX}$-2 elf18* treatment which showed higher expression levels. This is an interesting result, as it suggests that RLP46 could play a role in magnifying plant immune responses to elicitors, though of course the absence of a similar result in the *RLP46:GFP$_{OX}$-1 elf18* treatment casts doubt on this result. In contrast to the *FRK1* RT-qPCR data, the *NHL10* results were less clear. The Col-0 and *RLP46:GFP$_{OX}$* lines showed mild increases in *NHL10* expression upon exposure to elicitors, with all *RLP46:GFP$_{OX}$* line responses being the same as WT with the one exception of the *RLP46:GFP$_{OX}$-1* flg22 treatment sample. The *Crlp46-1* showed higher than WT *NHL10* expression in the control treatment, and lower than WT for the elicitor treatments. This result was in contrast to the data from the previous iteration of this experiment (see figure 26), and the *FRK1* data from the same experiment (see figure 32), causing this result to carry less weight. Taken together

then, these results seemed to suggest that RLP46 is not of central importance to the activation of immune defense related genes.

RLP46:GFP$_{OX}$ lines show increased NaCl sensitivity

The *RLP46$_{OX}$* lines were then tested for NaCl abiotic stress responses by repeating the previous NaCl stress experiments performed on the *rlp46* lines.

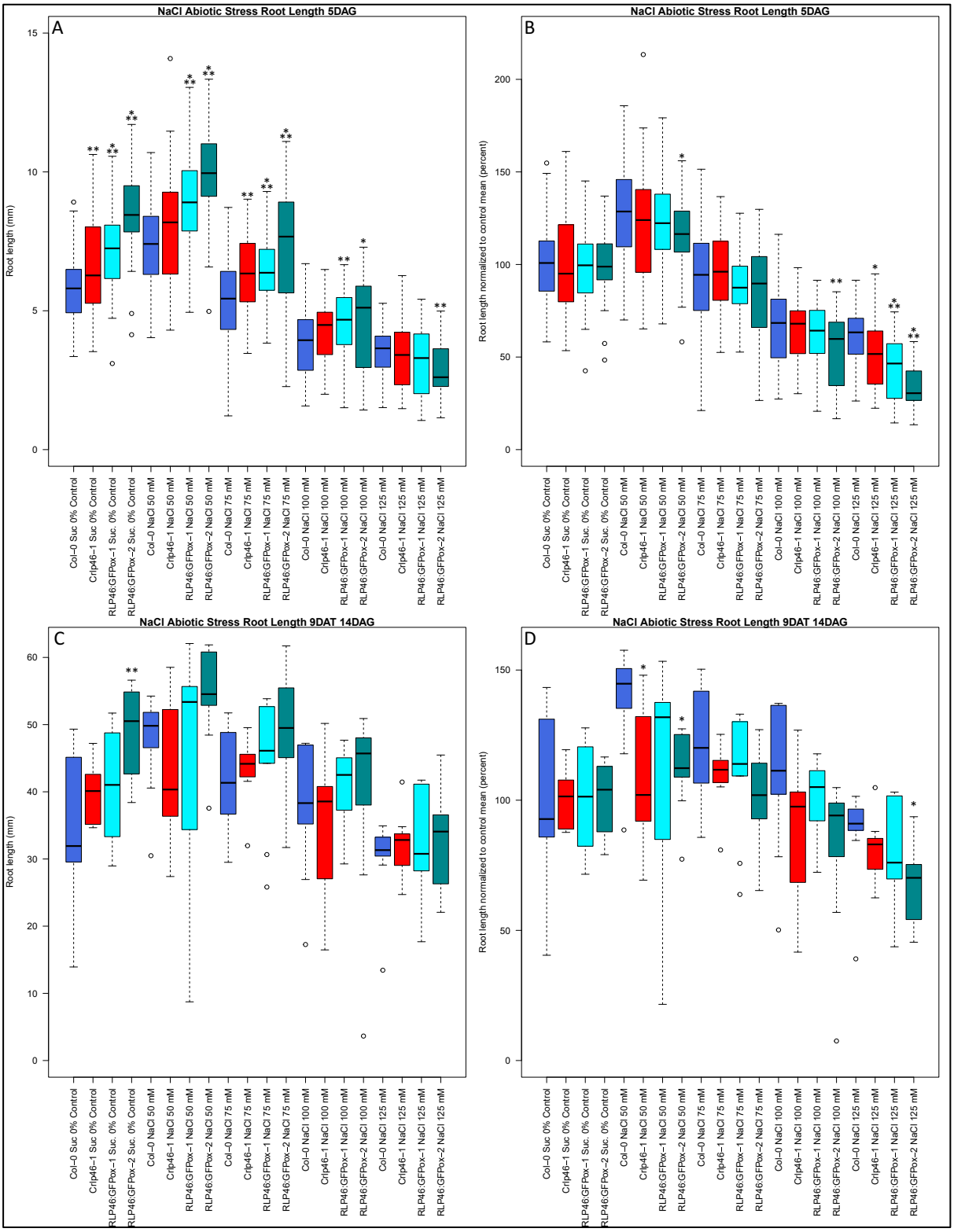

Figure 33: **A**. Boxplot of average plant root length 5 days after germination. Both *rlp46* and *RLP46$_{ox}$* mutants seemed to have higher overall growth rates compared to the Col-0 WT. This trend only reversed in the 125 mM NaCl treatment groups. Stars denote significant divergence from the Col-0 WT with the same NaCl treatment. N and P values shown in

table 9. Data from 1 iteration of experiment. **B**. Boxplot of normalized average plant root length 5 days after germination. Both *rlp46* and *RLP46$_{ox}$* mutants seemed to be more sensitive to NaCl stress at higher concentrations compared to the Col-0 WT, conflicting with earlier results for *Crlp46-1*. Stars denote significant divergence from the Col-0 WT with the same NaCl treatment. N and P values shown in table 9. Data from 1 iteration of experiment. **C**. Boxplot of seedling root length 9 days after seedling transfer and 12 days after germination. Plants grown on Phyto-Agar plates and then transferred by toothpick to plates containing abiotic stressors. Both *rlp46* and *RLP46$_{ox}$* mutants seemed to have higher overall growth rates compared to the Col-0 WT except perhaps for *Crlp46-1* at the 50 mM and 100 mM concentrations. Stars denote significant divergence from the Col-0 WT with the same NaCl treatment. Small sample size (n of 9) may explain lack of statistically significant divergence from WT for most lines. N and P values shown in table 10. Data from 1 iteration of experiment. **D**. Boxplot of normalized seedling root length 9 days after seedling transfer and 12 days after germination. Plants grown on Phyto-Agar plates and then transferred by toothpick to plates containing abiotic stressors. Both *rlp46* and *RLP46$_{ox}$* mutants seemed to show increased NaCl sensitivity across all treatments, conflicting with previous results. Stars denote significant divergence from the Col-0 WT with the same NaCl treatment. Small sample size (n of 9) may explain lack of statistically significant divergence from WT for most lines. N and P values shown in table 10. Data from 1 iteration of experiment.

Analysis of the results seemed to show that both *rlp46* and *RLP46$_{ox}$* mutants had significantly higher overall growth rates compared to the Col-0 WT controls except at the highest NaCl treatment concentration of 125 mM. This conflicted with earlier results for *rlp46* mutants. Normalization of the data showed no divergence in NaCl stress responses, with the possible exception of *RLP46:GFP$_{OX}$-2*, however at the 125 mM NaCl concentration all of the mutant lines showed increased sensitivity to NaCl stress compared to the Col-0 WT. This conflicted with the previous *Crlp46-1* results, throwing them into question.

Table 9: Table showing NaCl concentration, average root length, growth normalized to 0 mM control, sample number, and homoscedastic Student T-Test p values for significance between line and Col-0 control with same NaCl treatment for both root length and normalized data used in figures 33 sections A and B. Data from 1 iteration of experiment.

Line:	NaCl Concentration mM:	Root Length:	Normalized Growth (Percent):	Sample Number (n):	T-Test p Value Root Length:	T-Test p Value Normalized Growth:
Col-0	0	5.76	100	46	1	1
Crlp46-1	0	6.60	100	59	5.28E-03	1
RLP46:GFPox-1	0	7.28	100	60	2.30E-07	1
RLP46:GFPox-2	0	8.55	100	57	6.13E-17	1
Col-0	50	7.48	129.9	48	1	1
Crlp46-1	50	7.98	120.9	50	0.172	0.130
RLP46:GFPox-1	50	8.87	121.9	52	8.18E-05	0.132
RLP46:GFPox-2	50	10.02	117.1	44	3.33E-11	0.013
Col-0	75	5.41	93.9	39	1	1
Crlp46-1	75	6.32	95.8	51	5.59E-03	0.716
RLP46:GFPox-1	75	6.48	89.1	48	5.19E-04	0.319
RLP46:GFPox-2	75	7.35	85.9	42	2.47E-05	0.189
Col-0	100	3.84	66.7	39	1	1
Crlp46-1	100	4.22	64.0	34	0.203	0.563
RLP46:GFPox-1	100	4.60	63.2	44	4.38E-03	0.376
RLP46:GFPox-2	100	4.65	54.3	40	0.016	0.008
Col-0	125	3.56	61.8	43	1	1
Crlp46-1	125	3.50	53.1	44	0.824	0.028
RLP46:GFPox-1	125	3.23	44.4	48	0.177	7.10E-06
RLP46:GFPox-2	125	2.84	33.2	31	2.145E-03	4.92E-12

Analysis of the data from the seedling transfer portion of the experiments yielded some interesting results that seemed to contradict the results from the previous experiment. Both *rlp46* and *RLP46$_{ox}$* mutants seemed to have higher overall growth rates compared to the Col-0 WT except perhaps for *Crlp46-1* at the 50 mM and 100 mM concentrations. However, only the *RLP46:GFP$_{OX}$-2* control group diverged significantly from the Col-0 WT of the same treatment. This could be explained by the small sample size (n of 9) of this experiment.

Normalization of the data yielded the surprising results that both *rlp46* and *RLP46$_{ox}$* mutants seemed to show increased NaCl sensitivity across all treatments. This conflicted with previous results, though given the small sample size of this experiment (n of 9) perhaps this resulted from other unaccounted for factors.

Table 10: Table showing NaCl concentration, average root length, growth normalized to 0 mM control, sample number, and homoscedastic Student T-Test p values for significance between line and Col-0 control with same NaCl treatment for both root length and normalized data used in figure 33 sections C and D. Data from 1 iteration of experiment.

Line:	NaCl Concentration mM:	Root Length:	Normalized Growth (Percent):	Sample Number (n):	T-Test p Value Root Length:	T-Test p Value Normalized Growth:
Col-0	0	34.42	100	9	1	1
Crlp46-1	0	39.54	100	9	0.246	1
RLP46:GFPox-1	0	40.47	100	9	0.246	1
RLP46:GFPox-2	0	48.56	100	9	6.84E-03	1
Col-0	50	47.35	137.6	9	1	1
Crlp46-1	50	43.47	109.9	9	0.388	0.031
RLP46:GFPox-1	50	45.18	111.6	9	0.734	0.125
RLP46:GFPox-2	50	54.51	112.3	9	0.067	0.014
Col-0	75	41.84	121.5	9	1	1
Crlp46-1	75	43.37	109.7	9	0.622	0.185
RLP46:GFPox-1	75	44.79	110.7	9	0.498	0.348
RLP46:GFPox-2	75	49.15	101.2	9	0.084	0.053
Col-0	100	37.72	109.6	9	1	1
Crlp46-1	100	34.15	86.4	9	0.489	0.108
RLP46:GFPox-1	100	39.95	98.7	9	0.594	0.356
RLP46:GFPox-2	100	39.30	80.9	9	0.798	0.063
Col-0	125	29.93	87.0	9	1	1
Crlp46-1	125	31.86	80.6	9	0.484	0.405
RLP46:GFPox-1	125	32.81	81.1	9	0.443	0.550
RLP46:GFPox-2	125	33.44	68.9	9	0.308	0.041

RLP46:GFP$_{OX}$-1 also has mildly increased resistance to elicitor induced growth inhibition

To test if *RLP46ox* also has an impact on elicitor induced growth inhibition, elicitor experiments using flasks were repeated using the *RLP46:GFP$_{OX}$-1* line, with the one modification that 20 plants were placed in each flask as opposed to the 30 of previous iterations.

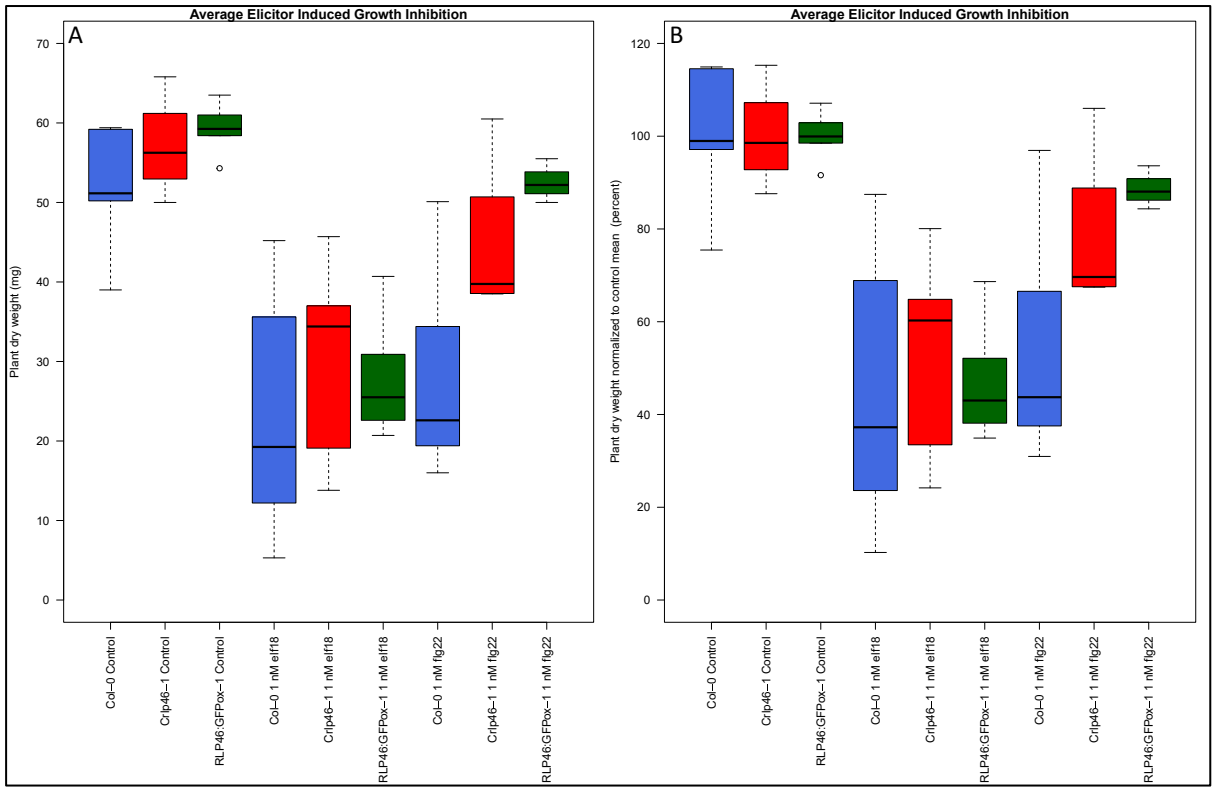

Figure 34: **A**. Boxplot of average plant dry weight after 7 days in liquid media and 12 days after germination. All lines showed expected growth inhibition in response to elicitor containing growth media (Igarashi et al., 2012). Both C*rlp46-1* and *RLP46:GFP$_{OX}$-1* samples seemed to show mild resistance to elicitor induced growth inhibition as compared to the Col-0 WT samples. N of 6, 4, 6, 6, 5, 5, 5,4, and 3 respectively. Exact values shown in table 11. Data from 2 iterations of experiment. **B**. Boxplot of normalized data from same experiments. Both C*rlp46-1* and *RLP46:GFP$_{OX}$-1* samples seemed to show mild resistance to elicitor induced growth inhibition as compared to the Col-0 WT samples, though the elf18 resistance was not as pronounced in the *RLP46:GFP$_{OX}$-1* samples. N of 6, 4, 6, 6, 5, 5, 5,4, and 3 respectively. Exact values shown in table 11. Data from 2 iterations of experiment.

Interestingly, both the *Crlp46-1* and *RLP46:GFP$_{OX}$-1* samples seemed to show mild resistance to elicitor induced growth inhibition as compared to the Col-0 WT samples, though the small sample size of these experimental iterations should be taken into consideration. Normalization of the data further supported the trend of mildly increased resistance to elicitor induced growth inhibition in both the *Crlp46-1* and *RLP46:GFP$_{OX}$-1*

samples as compared to the Col-0 WT controls. Interestingly, the elicitor resistance was not as strong in the *RLP46:GFP$_{OX}$-1* line for the elf18 treatment samples as compared to the flg22 treatment samples, perhaps hinting at a more specific interaction between RLP46 and elf18 as suggested by previous studies (Zipfel et al., 2006).

*Table 11:*Table showing sample treatment, average dry weight, normalized growth, number of plants per sample, and sample treatment n for figure 34. Data from 2 iterations of experiment.

Line:	Elicitor Treatment:	Average Dry Weight (mg):	Normalized Growth (percent):	Plants Per Sample:	Sample Number (n):
Col-0	Control	51.7	100	20	6
Crlp46-1	Control	57.1	100	20	4
RLP46:GFPox-1	Control	59.3	100	20	6
Col-0	1 nM elf18	22.8	44.1	20	6
Crlp46-1	1 nM elf18	30.0	52.6	20	5
RLP46:GFPox-1	1 nM elf18	28.1	47.4	20	5
Col-0	1 nM flg22	28.5	55.1	20	5
Crlp46-1	1 nM flg22	44.6	78.2	20	4
RLP46:GFPox-1	1 nM flg22	52.6	88.7	20	3

All in all, the results of the experiments with *RLP46:GFP$_{OX}$-1* and *RLP46:GFP$_{OX}$-2* undermined the previous NaCl resistance results and supported the elicitor resistance results, and while having the observed growth inhibition resistance trend of the overexpression mutant be similar to the phenotype of the putative null mutant is counter intuitive, it is not outside of the realm of possibility given the buffered nature of the plant immune signaling network (Hillmer et al., 2017) as well as the multifaceted interactions in signaling protein complexes.

Western Blot suggest RLP46 associates with SOBIR1

Given the experimental results suggesting that RLP46 interacts with the plant immune response, as well as its apparent localization to the plasma membrane, experiments testing for common Receptor Like Protein interaction partners were performed. SOBIR1 is known to interact with many receptor proteins involved with plant immune responses, making it an obvious candidate. BAK1 was also selected as it interacts with a number of receptor proteins

also involved with immune signaling, such as PSKR1 (Wang et al., 2015a; Zhang et al., 2013; Liebrand et al., 2013; Burgh et al., 2019). Fluorescent microscopy was used to confirm transient expression of the GFP fused protein constructs in *N. benthamiana* leaf disks, and then a protein extraction was performed on tissue from the same leaves used for the microscopy check.

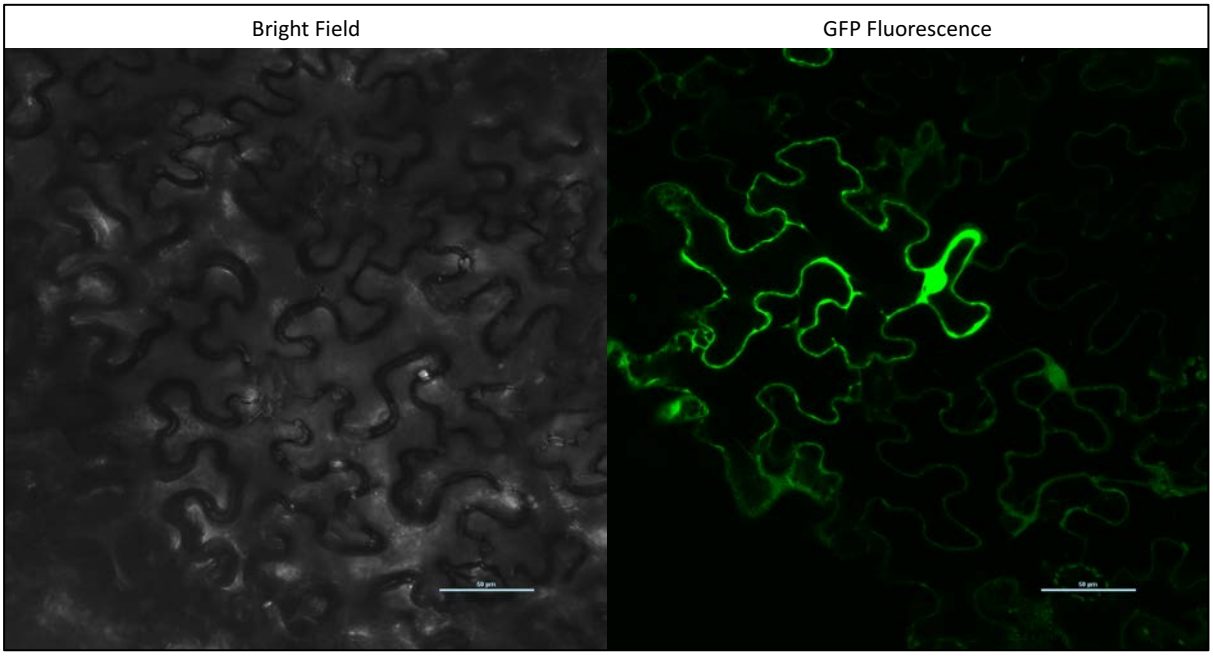

Figure 35: Fluorescent microscopy images showing RLP46:GFP fluorescence in *N. benthamiana* leaf pavement cells transiently expressing RLP46:GFP and SOBIR1:HAx3. Image shows GFP and bright field channels. RLP46:GFP appeared to be localized to the plasma membrane of the cells examined.

Co-Immunoprecipitation was then used to test for associations between RLP46 and SOBIR1 or BAK1 in transiently expressing *N. benthamiana* plants and the results assessed via PAGE and Western Blot. Two PAGE and Western Blots were performed using the products of the same Co-IP experiment.

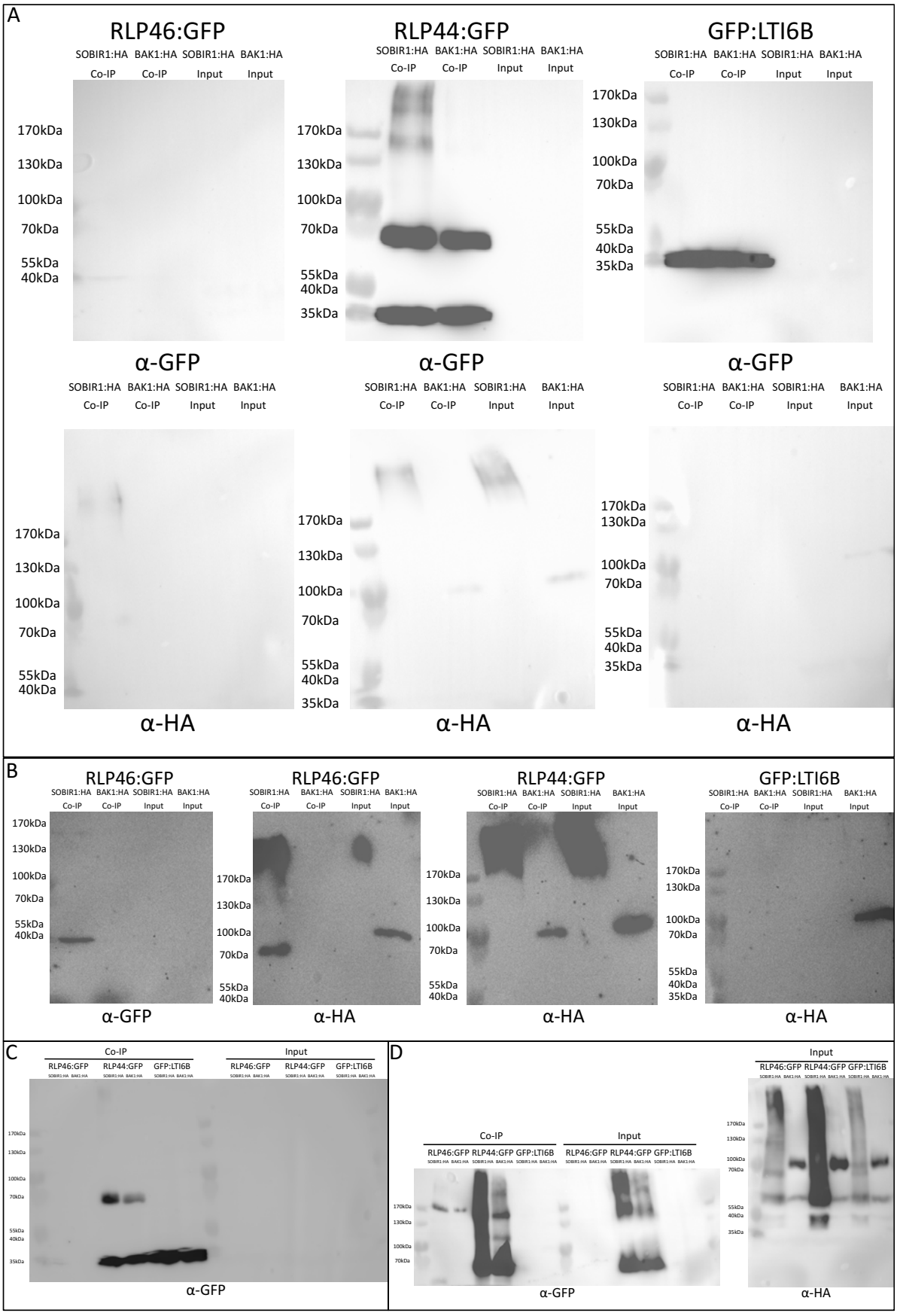
A
RLP46:GFP
RLP44:GFP
GFP:LTI6B
SOBIR1:HA BAK1:HA SOBIR1:HA BAK1:HA
Co-IP Co-IP Input Input
170kDa
130kDa
100kDa
70kDa
55kDa
40kDa
35kDa
α-GFP
α-HA
B
RLP46:GFP
RLP46:GFP
RLP44:GFP
GFP:LTI6B
α-GFP
α-HA
α-HA
α-HA
C
Co-IP
Input
RLP46:GFP RLP44:GFP GFP:LTI6B
α-GFP
D
Co-IP
Input
RLP46:GFP RLP44:GFP GFP:LTI6B
α-GFP
α-HA

Figure 36: **A**. Chemiluminescence image of Western Blot. Co-IP and input samples divided across 3 PAGE gels, transferred to membrane using Western Blot and then divided with scissors for incubation in either α-GFP or α-HA primary antibodies. Results for α-GFP blots showed strong bands in the RLP44 positive control and the LTI6B negative control in the CO-IP samples. The α-HA blot results showed the expected association between RLP44 and SOBIR1 or BAK1, the expected lack of association between LTI6B and SOBIR1 or BAK1, and seemed to suggest an association between RLP46 and SOBIR1. This was evidenced by the faint band around the expected size of ~74 KDa as well as the band present significantly above the 170 KDa ladder mark. Lack of bands in all input samples addressed in section D. Expected protein sizes found in table 12. Uncropped image can be found in appendix 2. **B**. Chemiluminescence image of same Western Blot from section A with longer imaging time. Co-IP and input samples divided across 3 PAGE gels, transferred to membrane using Western Blot and then divided with scissors for incubation in either α-GFP or α-HA primary antibodies. Results for α-GFP blots showed strong bands in the RLP44 positive control and the LTI6B negative control in the CO-IP samples. The α-HA blot results showed the expected association between RLP44 and SOBIR1 or BAK1, the expected lack of association between LTI6B and SOBIR1 or BAK1, and seemed to suggest an association between RLP46 and SOBIR1. This was evidenced by the faint band around the expected size of ~74 KDa as well as the band present significantly above the 170 KDa ladder mark. Lack of bands in all input samples addressed in section D. Expected protein sizes found in table 12. Uncropped image can be found in appendix 3. **C**. Chemiluminescence image of Western Blot incubated in α-GFP primary antibody. Results showed strong bands in the RLP44 positive control and the LTI6B negative control in the CO-IP samples but not in the Input samples. Presumably they were present but below the detection threshold of this assay. Band sizes were consistent with RLP44:GFP, GFP:LTI6B, and free GFP. Co-IP and input samples same as used for other sections. Expected protein sizes found in table 12. Uncropped image can be found in appendix 4. **D**. Chemiluminescence image of top half of Western Blot from section C incubated in α-GFP primary antibody as well was Western Blot with Input samples incubated with α-HA primary antibody. Results showed bands in the RLP44 Co-IP and Input positive control samples as well as in the RLP46 samples. It should be noted that the band in the RLP46 sample was higher on the gel then expected based on the size of the *RLP46* gene, though this is not unheard of as post translational modifications can affect migration on the gel (Shi et al., 2012). The α-HA results seemed to show the SOBIR1:HAx3 and the BAK1:HAx3 constructs to be present in all Input samples. Co-IP and input samples same as used for other sections. Expected protein sizes found in table 12. Uncropped image can be found in appendix 5.

Protein:	Expected Length:
RLP46	91 KDa
RLP44	30 KDa
GFP	27 KDa
SOBIR1	71 KDa
BAK1	74 KDa
3xHA	3 KDa
LTI6B	6 KDa

*Table 12:*Table showing expected KDa values based on literature for proteins appearing in figure 36 (Berardini et al., 2015).

Analysis of the Western Blots yielded some interesting conclusions. The results shown in figure 36 seemed to indicated that the collected *N. benthamiana* leaf samples were in fact transiently expressing the RLP46:GFP, RLP44:GFP. GFP:LTI6B, SOBIR1:HAx3, and BAK1:HAx3 proteins. This was evidenced by proteins of the roughly expected size being detected in the Western Blots (expected protein sizes can be found in table 12). Interestingly, there were bands present indicating proteins of much larger size than anticipated, though of course some proteins are known to migrate on gels differently than their size alone would predict (Shi et al., 2012; de Jong et al., 1978). It is interesting that this phenomenon seemed to mostly occur within the SOBIR1:HA samples with the one possible exception of the

RLP44:GFP with BAK1:HAx3 sample group, though it is definitely also possible that this was the result of sample bleeding into the neighboring lane. Analysis of the Western Blot from the second PAGE performed on the samples (see figure 36 section A) yielded some exciting preliminary results. Both the RLP44 and LTI6B positive and negative controls showed the expected results with regards to association with SOBIR1 and BAK1 while RLP46 appeared to associate with SOBIR1, as evidenced by the band around the expected size of ~74 KDa as well as the band present significantly above the 170 KDa ladder mark, a band also present in the RLP44 positive control. There appeared to be no band in the RLP46 with BAK1 sample, suggesting that these two proteins do not associate. It should be noted that the lack of bands in all of the input samples did undermine these results, but their detection in the second Western Blot performed on the same samples mitigated these doubts. Taken together then, the results of the Western Blots provided good preliminary evidence for the association between the RLP46 and SOBIR1 proteins, which supports the larger narrative of our results which suggests RLP46 plays a role in plant immune response.

Discussion

Upon reviewing the results of the experiments involving the previously uncharacterized protein RLP46, we are presented with a strong case for it having a role in plant immune response. While the results for abiotic stressors seemed to be inconclusive in the end, the evidence for RLP46 having a role in plant pathogen response was much more compelling. Building upon the starting point of upregulation in response to elf18 perception (Zipfel et al., 2006), several experiments showed a link between RLP46 and elicitor responses, seemingly with a subtle distinction between flg22 and elf18. This link seemed to not be related to the plant's initial rapid immune response, as assessment of the ROS burst experiments seemed to show that the loss of the RLP46 gene did not affect the timing or degree of the ROS burst response. This was shown by the trends of *rlp46* mutants remaining comparably similar to that of the Col-0 WT. It is of course possible that there is in fact a subtle effect on the ROS burst immune response, but that the sensitivity of the experimental assay was not high enough to detect it. That being said, it seems more likely that RLP46 could play a supporting role in the activation of immune pathways leading to secondary metabolite production and consequent reduced growth. This idea is buttressed by the apparently WT ROS burst pattern of the *pskr1-3* mutant line despite its widely reported hyperimmune response to elicitors (Igarashi et al., 2012). Furthermore, PSKR1 could serve as a good mirror example of an LRR-RLK with several functions whose loss increases the severity of the plant's growth inhibition response to elicitor treatment (Igarashi et al., 2012), while in contrast the loss of RLP46 seems to subtly reduce it. In the case of the *rlp46* mutants, there seemed to be little difference in the reduction of immune response between the elicitors flg22 and elf18, with both showing a reduction in growth inhibition ranging from roughly five to ten percent in different elicitor concentrations and experimental setups. Unfortunately, this subtilty probably also led to the lack of a detectable impact on *FRK1* and *NHL10* expression levels in the *rlp46* mutants. This lack of clarity was however partially mitigated by the experiments using the *RLP46:GFPox* lines. These experiments, though preliminary, seemed to show the *RLP46ox* line having an increased response to elf18 treatment, as evidenced by the increased expression of *FRK1* and to a lesser extent the

growth inhibition data, while seeming to have a response to flg22 that was similar to the *rlp46* mutant. This observation, if confirmed, could suggest that RLP46 does indeed possess a degree of specificity for elf18, either directly or through its interaction partners, while its impact on flg22 singling could theoretically derive from being a component of the larger plant elicitor immune response network. Additionally, the difference between the two responses could be further masked by the buffered nature of the plant immune signaling network reported in other studies (Hillmer et al., 2017). This would also create a possible explanation for the apparent contradiction in the experimental results shown by the RLP46ox lines in that the extra copies of RLP46 could disrupt the balance of an elicitor perception response membrane complex, but this disruption would be overcome in the case of elf18 exposure due to the higher number of receptors for that particular elicitor. The results from the Co-IP and Western Blot experiments in conjunction with the fluorescent microscopy of RLP46:GFP lend some credence to this hypothesis. We know from the microscopy results that RLP46 does indeed seem to be localized to the plasma membrane, as expected for a receptor like protein (Wang et al., 2008; Jamieson et al., 2018; Shiu and Bleecker, 2001, 2003), and a potential association partner in SOBIR1 was identified by the Co-IP results. The role of SOBIR1 as a potential association partner also fits nicely into the narrative of RLP46 being a component of the plant's immune responses to elicitor perception. This is due to SOBIR1's role in promoting a stronger immune response (Zhang et al., 2013; Liebrand et al., 2013; Burgh et al., 2019), the effectiveness of which could logically be impeded by the loss of an association partner, like perhaps RLP46. It should also be noted that the experiments performed in this study may not have been ideal for testing for RLP46 related phenotypes, as the currently available *RLP46* expression data shows it to be expressed mostly in mature vascular tissue (Klepikova et al., 2016). Since none of the experiments performed directly tested vascular immune response it is possible that the subtle *rlp46* phenotypes observed would have been much stronger had the plants been directly tested for immune responses to vascular pathogens. As such, future experiments could begin by testing the susceptibility of *rlp46* and *RLP46ox* mutants to vascular pathogens like *Fusarium* or *Xylella fastidiosa* (bacterial pathogens probably making more sense given RLP46's apparent link to efl18), and by using microscopy to

directly test the roots for phenotypes in elicitor induced ROS burst and Ca^{2+} flux. These experiments would go a long way to determining if RLP46 has a role in modulating vascular tissue specific immune responses and in explaining the subtlety of the *rlp46* immune phenotypes observed in this study. That being said, and viewing all of the results for RLP46 as a whole, we arrive at the interesting but by no means definitive conclusion that RLP46 is yet another of the many RLP's located at the plasma membrane which convey vital information about the external environment of the plant cell into the internal protein signaling network. With regards to its specific function, it seems to be involved with the plant's PAMP sensing innate immune system, and be more closely, but not exclusively, associated with the elf18 activated component of it. Furthermore, it appears to associate in some way with the immune response stimulating protein SOBIR1, though whether directly or as part of a larger complex is not known. In summation then, this study succeeded in an initial characterization of the RLP46 protein while also laying the groundwork for future studies investigating RLP46's role in plant innate immune response.

Discussion

Taken together, the analyses performed over the course of this thesis proved successful in providing an initial characterization of the three proteins of interest selected for study. PSKL1 was shown to have a role in determining metaxylem cell number, F-Box/RNI-Like to be somehow related to the expression of the RLP44ox phenotype, and RLP46 was shown to likely play a role in plant immune response. The results provide in this thesis combined with the scientific tools created to collect them, provide a clear starting point for future research on any of the three proteins studied, and while their exact roles in the plant cell remain unknown, the work in this thesis has established a scientific basecamp for future exploration. Taking a step back from the focus of this thesis to assess the state of the research field at large, it is clear that the plant cell wall and the complex web of signaling and communication it serves as a backdrop for remain an exciting and dynamic field of study. This ocean of scientific unknowns continues to reveal mysteries faster than the combined efforts of researchers can resolve them, and will no doubt serve as a wellspring of scientific knowledge for years to come. This thesis pushed against this vast unknown, adding one more paving stone to the road towards knowledge, and with any luck will serve as the foundation for many more stones to come.

Methods

Seed Sterilization Technique

Seeds of *A. thaliana* were placed in 1.5 mL or 2 mL Eppendorf tubes and mixed with between 0.5 mL and 1.5 mL of sterilization solution [70% EtOH, 0.05% Triton X100 (vol/vol)] depending on seed volume. After waiting (at least 40 seconds but ideally not longer than 5 minutes) the seeds were washed using a 99% EtOH solution and then dried in a sterile hood by either pipetting the mix of EtOH and seeds onto filter paper, or by pipetting off the excess EtOH and allowing the seeds to dry in the open tube.

Plant Cultivation Techniques

Medias used: ½ Murashige-Skooog (MS) media used with 0-0.9% Phyto-Agar, 0-6.5% Sucrose, 0-150 mM Mannitol, 0-2% Glucose, 0-150 mM NaCl, 0-1 µM PSK, 0-100 nM elf18, and 0-100 nM flg22. Media pH of 5.8 adjusted with HCl and KOH. Media then autoclaved and any necessary antibiotics added after as per experimental requirements.

Plant Growth: Square Greiner plates used to contain desired media, and seeds then sown on it under sterile conditions in sterile hood. Sterile seeds either taped out from 1.5 mL Eppendorf tubes onto plate or placed using sterile toothpick. Plates sealed with Millipore sterile surgical tape. Seeds then stratified for 2-3 days in dark at 4° C.

Plates containing seeds for experiments with light growth conditions then placed either horizontally or vertically, depending on media and experiment, in growth chambers or grow room with long day or short day conditions (16 hours light, 8 hours dark for long day and 8 hours light, 16 hours dark for short day, 100-150 µE light intensity in growth chamber and 5xPhilips Green power LED production module deep red/blue 120 LD [415 µmol/sec at distance of 40 cm] in grow rooms, 60-70% humidity, and 22-23° C).

Dark grown seedlings were placed in illuminated growth chamber for 6 hours and then wrapped in aluminum foil and returned to growth chamber.

Hygromycin B selection plates were placed horizontally in growth chamber, and covered with single sheet of paper for first 5 days and then uncovered after.

Seeds were also sown directly on soil when needed.
Plantlets transferred to soil earliest 5 days after germination, and then placed in long day or short day grow room (16 hours light, 8 hours dark for long day and 8 hours light, 16 hours dark for short day, 5xPhilips Green power LED production module deep red/blue 120 LD (415 μmol/sec at distance of 40 cm), 65% humidity, and 23° C) depending on experiment. Tray containing plant pots covered with clear plastic lid to maintain humidity for at least 1 day, but no longer than 7. Lid then removed. Plants watered as needed.
Plants for seedling transfer experiments sown as normal on Phyto-agar plates and stratified for 2-3 days in dark at 4° C. Plates then placed in long day growth chamber vertically and allowed to grow for 5 days. After 5 days, seedlings transferred one at a time using sterile toothpicks in sterile hood from germination plate to experiment plate containing abiotic stressors. Plates then resealed with Millipore sterile surgical tape and placed vertically back in growth chamber.

Plant Crossing

Plants for crosses grown until bolting stage. Inflorescence of female in cross allowed to mature to just prior to opening of flowers. Then, using forceps, axillary buds removed and all flowers that are too old or young in primary inflorescence also removed leaving 3 flowers of the proper age for crossing. Anthers, sepals, and petals then removed. Female flowers now ready for crossing. Then took anthers from mature flowers from male plant and used them to pollinate the flower of the female plant. Cross now performed. Silique allowed to mature and then F1 seeds collected.

Seed Harvest

Plants staked and bagged after bolting. Breathable plastic bag used and twisty tied at base. Plants moved to drying room after first siliques fully matured until plants fully dried and matured. Siliques then opened by kneading, then sieved and placed into paper storage packets.

gDNA Extraction

Tissue Homogenization by Hand: Plant material harvested and put in 1.5 mL Eppendorf tubes. 200 µL of gDNA extraction buffer added and them tissue ground by hand using small plastic pestle.

Tissue Homogenization by bead-mill: Plant material harvested and put in 2 mL Eppendorf tubes, then glass bead added and tubes frozen in liquid nitrogen. Tubes then placed in -80° C chilled bead-mill sample rack and homogenized using bead-mill (TissueLyser II, RETSCH, QIAGEN) with a setting of 30 Hz for 30 seconds.

gDNA Extraction: 200 µL of gDNA extraction buffer added to samples if not done already, and then samples centrifuged at max speed at room temperature for 10 minutes. 150 µL of supernatant transferred to new 1.5 mL Eppendorf Tube and then 150 µL Isopropanol added and then mixed. Sample centrifuged for 10 minutes at room temperature again. Supernatant removed, being careful not to disturb DNA pellet. 0.5-1.0 mL 70% EtOH added to wash pellet, and then sample centrifuged again for 10 minutes at room temperature. Supernatant removed being careful not to disturb DNA pellet. Pellet then allowed to airdry for 5 minutes or until dry. Then added 50 µL low TE buffer. Samples stored at 4° C.

gDNA Extraction Buffer: 150 mM Tris (pH 8), 250 mM NaCl, 25 mM EDTA, 0.5% SDS.

Low TE Buffer: 10 mM Tris HCl, 0.1 mM EDTA, pH 8.

RNA Extraction

RNA extractions performed using Universal RNA Purification Kit from Roboklon GmbH. Followed protocol provided by kit titled ‘Plant Tissue RNA Purification Protocol’ and included the optional step of the on-column DNase digestion.

cDNA Generation

cDNA generation performed using the protocol included with the AMV Reverse Transcriptase Native kit from Roboklon GmbH.

Polymerase Chain Reaction

Taq PCR	Taq PCR	Q5 PCR	Q5 PCR	Colony PCR	Colony PCR
Reaction Component:	**Volume (µL):**	**Reaction Component:**	**Volume (µL):**	**Reaction Component:**	**Volume (µL):**
10X PCR Buffer	2.5	5X PCR Buffer	10	10X PCR Buffer	2.5
dNTP solution (10 mM)	0.5	dNTP solution (10 mM)	1	dNTP solution (10 mM)	0.5
Fwd Primer (10 µM)	0.25	Fwd Primer (10 µM)	0.5	Fwd Primer (10 µM)	0.25
Rev Primer (10 µM)	0.25	Rev Primer (10 µM)	0.5	Rev Primer (10 µM)	0.25
DNA Template (1 ng-1 µg)	1.5	DNA Template (1 ng-1 µg)	3	DNA Template (1 ng-1 µg)	Colony
Taq-Polymerase	0.25	Q5-Polymerase	0.5	Taq-Polymerase	0.25
ddH2O	19.75	ddH2O	34.5	ddH2O	21.25
Final Volume	25	Final Volume	50	Final Volume	25

Thermo-Cycler Program		Taq PCR		Q5 PCR		Colony PCR (Taq)	
Program Step:		**Temperature:**	**Time:**	**Temperature:**	**Time:**	**Temperature:**	**Time:**
Initial Denaturation		95° C	2'	98° C	2'	95° C	5'
Denaturation	Steps	95° C	30''	95° C	30''	95° C	30''
Annealing	Repeated	52-58° C	30-45''	52-58° C	30-45''	52-58° C	30-45''
Elongation	X 30-35	72° C	1'/kb	72° C	30''/kb	72° C	1'/kb
Final Elongation		72° C	5'	72° C	5'	72° C	5'
Pause		16° C	∞	16° C	∞	16° C	∞

Real Time Quantitative Polymerase Chain Reaction (RT-qPCR)

Reaction Component:	Volume (µL):
10X PCR Buffer	1.5
dNTP solution (10 mM)	0.3
Fwd Primer (5 µM)	1
Rev Primer (5 µM)	1
DNA Template (1 ng-1 µg)	2
Jump Start Polymerase	0.3
ddH2O	8.6
SYBR® Green (1:400)	0.3
Final Volume	15

Thermo-Cycler Program		RT-qPCR	
Program Step:		**Temperature:**	**Time:**
Hold		95° C	6'
Denaturation	Steps	95° C	30''
Annealing	Repeated	59° C	20''
Elongation	X 45	72° C	30''
Melt		55° C - 95° C by 1° steps 90'' wait at first step and 5'' each step after	

Channel:	Source:	Detector:	Gain:
Green	470 nm	510nm	10 of 10
Yellow	530 nm	555 nm	7 of 10

RT-qPCR performed using a Rotor-Gene Q thermo-cycler using Run Wizard Advanced software and 0.1 mL 4-Strip Rotor-Gene® Style Tubes and Caps.

Bulked Segregant Analysis

See figure 14. List of primers used can be found in appendix 1.

Imaging of Plant Rosettes

Digital images of plant rosettes captured using a D3300 Nikon Digital Camera using a Tamron Aspherical LD XR DiII SP lens (AF 17-50mm f/2.8 [IF] φ67 A16).

Scanning Plant Growth Plates for Root Measurement:

After plantlets on Phyto-Agar plates reached desired days post germination, plates were scanned using RICOH MP C2503 photocopy machine, and images stored as TIFF files for subsequent analysis. Plates scanned face up on scanner with a black background cover on top.

Scanning Plant Hypocotyls for Measurement:

After plantlets on covered Phyto-Agar plates reached desired days post germination, they were transferred to an empty square Greiner plates and scanned using RICOH MP C2503 photocopy machine and images stored as TIFF files for subsequent analysis. Plates scanned face up on scanner with a black background cover on top.

Measuring Root Length

Image files form scanned plates analyzed using FIJI image analysis software (ImageJ open source software version: 2.0.0-rc-43/1.51k). 120 mm width of plates used to calibrate measurements, and then root traced with segmented line tool and measured, or Simple Neurite Tracer Plugin used to measure length.

Counting Lateral Roots

Image files form scanned plates analyzed using FIJI image analysis software (ImageJ open source software version: 2.0.0-rc-43/1.51k), and then lateral root number counted.

Measuring Hypocotyl Length

Image files form scanned plates analyzed using FIJI image analysis software (ImageJ open source software version: 2.0.0-rc-43/1.51k). 120 mm width of plates used to calibrate measurements, and then root traced with segmented line tool and measured, or Simple Neurite Tracer Plugin used to measure length.

Basic Fuchsine Staining

6 day old plantlets placed in 100 μm Nylon Cell Strainers in 6 well plates containing 10% NaOH (w/v) solution. Plate sealed with laboratory tape and left on laboratory benchtop overnight. NaOH removed and then plantlets stained with 0.01% basic fuchsine (dissolved in H_2O) solution for at least 5 minutes. Basic fuchsine removed and plantlets destained with 70% ethanol solution for 10 minutes. Ethanol removed and 50% glycerol solution added to plantlets. Plantlets then stored at 4° C (can be stored in this state almost indefinitely) until being mounted on slides in 50% glycerol for analysis via laser microscopy.

Counting metaxylem cell number

Basic fuchsine stained plantlets analyzed with fluorescent confocal microscopy using a 514 nm laser for excitation. Z stack of plantlet xylem cells in the stele imaged at the top of the root near the hypocotyl. Z stack then analyzed to count the number of metaxylem and protoxylem cells.

Agrobacterium Leaf Infiltration

Agrobacterium cultures grown overnight at 28° C in shaking incubator in 20 mL of LB-media containing appropriate selective antibiotics in Erlenmeyer flasks. Cultures spun down in 50 mL Falcon tubes at 3000 rpm for 30 minutes. Supernatant discarded and pellet washed

with 1 mL of tap water which is then removed. Pellet then resuspended in 5-10 mL of tap water and agitated for 1 to 3 hours at 28° C in shaking incubator. Measured OD_{600} and volume adjusted with tap water to a final OD_{600} of 1. Cultures mixed together when necessary and then injected in *N. benthamiana* leaves using a syringe with no needle. Leaves were first perforated using a syringe needle. Plants then left on lab bench in flat with transparent greenhouse growth cover overnight, and then transferred to growth chamber (16 hours light, 8 hours dark, 100-150 μE light intensity, 60-70% humidity, 22-23° C) or greenhouse and left overnight. Leaf disks collected and then analyzed when applicable, and then 1 gram of transformed leaf material collected and frozen in liquid nitrogen for later protein extraction.

Agrobacterium Floral Dip

Cultures of *Agrobacterium* grown overnight at 28° C in shaking incubator in 12 mL cell culture tubes. Cultures spun down in two to four 2 mL Eppendorf tubes at 3000 rpm for 10 minutes. Supernatant discarded and pellet washed with 1 mL of tap water which was then removed. Pellet then resuspended in 1.9 mL of dipping solution. *A. thaliana* flowers then exposed to solution thorough either dipping the flower into the tube, placing droplets of solution on flower with a syringe, or pouring the solution onto flowers held in gloved hand. Plants covered and moved out of direct light for 1 day and then returned to growth chamber. Mature seeds collected and then sown on selective media to identify successfully transformed plantlets.

Dipping solution: 0.002% Murashige-Skooog (MS), 2.5 mM MES buffer (pH adjusted to 5.7), 10% sucrose, and 0.05% Silwet L-77.

Protein Extraction

Frozen leaf tissue samples ground to powder under liquid nitrogen using a mortar and pestle (used 1 gram of leaf tissue when possible). Added 2 mL of ice chilled protein extraction buffer to ground leaf tissue powder and continued grinding until mix had melted enough to be pipetted into 2 mL Eppendorf tube which was done using a cut tip 1 mL micropipette. Tubes then moved to end over end mixer at 4° C for 15-30 minutes. Samples then spun-

down in temperature-controlled tabletop centrifuge set to 4° C for 15 minutes, then supernatant transferred to new 2 mL Eppendorf tube and spun again at 4° C for 15 minutes. Supernatant then transferred to new Eppendorf tube and was ready for immediate experimental use, or for storage at -20° C.

Protein Extraction Buffer: 1% IGEPAL® (Sigma-Aldrich), 50 mM Tris-HCl pH 7.5, 150 mM NaCl, 10% Glycerol, 5 mM DTT, and 1:100 (vol/vol) protease inhibitor mix (Sigma-Aldrich).

Co-Immunoprecipitation (Co-IP)

All solutions and samples kept on ice or in 4° C cold room. Equilibrated 20 µL trap-beads (GFP-trap or RFP-trap e.g.) by adding to 1 mL of protein extraction buffer (using a cut tip 200 µL micropipette) and then centrifuging at minimum speed (e.g. 500rpm) for 2 minutes, and then removing the supernatant. 60 µL of extracted protein solution placed in new Eppendorf tube and set aside on ice as Input sample. The remainder of the extracted protein solution then added to equilibrated trap-beads and then put on end over end mixer at 4° C for 1-3 hours. Samples then centrifuged at minimum speed (e.g. 500 rpm) for 2 minutes and then the supernatant removed and returned to storage for later analysis. Then added 1 mL of protein extraction buffer (protease inhibitor not added to buffer used for wash steps) and returned to end over end mixer at 4° C for 5 minutes. Then centrifuged samples like previous step and removed supernatant. This wash step was repeated 3 times. After final wash step, added double the sample volume (120 µL for input samples and 40 µL for Co-IP samples) of solution that is 1:1 mix protein extraction buffer (protease inhibitor not added to buffer used for this step) and roti-load to both the input sample and the Co-IP sample. Mixed and then boiled for 10 minutes at 95° C (70° C for 20 minutes can also be used if precipitation is a concern). Co-IP and input samples now ready for use or for storage at -20° C.

PAGE

Polyacrylamide gels prepared using 6-10% resolving gel (6-10% acrylamide, 1.5 M Tris-HCl pH 8.8, 0.4% (vol/vol) SDS) and 4.5% stacking gel (4.5% acrylamide, 0.5 M Tris-HCl

pH 6.8, 0.4% (vol/vol) SDS) and run using SDS running buffer (25 mM Tris base pH 8.5-8.8, 192 mM glycine, 1% (vol/vol) SDS). 5-20 µL of pre-stained protein ladder (PageRuler™ Thermo Fisher Scientific) and 5-20 µL of Co-IP samples loaded into sample wells (roti-load protein extraction buffer mix used in empty wells). Gels first run at 60 V for 30 minutes, and then subsequently run at 150-200 V.

Western Blot

PVDF membrane (Immobilon-P) activated by incubation for minimum of 2 minutes in 100% Methanol, and then washed in semi-dry buffer. Whatman paper incubated in semi-dry buffer (48 mM Tris base, 39 mM glycine, 20% methanol, 0.0375% SDS). Used semi-dry blotting system to transfer PAGE gel proteins to PVDF membrane (55 minutes, 0.4 Amp, 15 V)(Trans-Blot Turbo, BIORAD)(from bottom to top, 4 stack Whatman paper – PVDF membrane – Gel-4 stack Whatman paper). After transfer, incubated membrane in 1X TBST (20 mM Tris base pH 7.4, 150 mM NaCl, 0.05% Tween) containing 5% (w/vol) milk powder (Roth) for 1 hour on tabletop shaker. Primary antibodies diluted to 1:10,000 in 1X TBST containing 1% (w/vol) milk powder and incubated overnight on tabletop shaker at 4° C. Membrane then washed for 5 minutes in 1X TBST. Repeated wash step 4 times. Membranes then incubated for 1 hour in 1X TBST with 1:10,000 diluted secondary antibodies coupled with the horseradish peroxidase. Membrane then washed for 5 minutes in 1X TBST. Repeated wash step 4 times. Imaging then performed by incubating with chemiluminescence mix (SuperSignal® West Pico Chemiluminescence Substrate, SuperSignal® West Femto Trial Kit Thermo Scientific). Chemiluminscence then detected using a CCD camera imaging system (ChemCam Imager, Intas).

Confocal Laser Scanner Microscopy

Confocal microscopy performed using the Nikon AR1 Confocal Microscope at the University of Heidelberg's Nikon Imaging Center and using the Leica TCS SP5 Confocal microscope at the University of Heidelberg's Center for Organismal Studies.

GreenGate Cloning

Generation of Entry Modules: Cloning steps follow published GreenGate protocol (Lampropoulos et al., 2013). Gene of interest cloned using Q5 PCR, 8 µL of PCR product removed and used to verify appropriate product length by gel electrophoresis, and then product purified using GeneJet Gel Extraction Kit (modified protocol by not cutting band out of agarose gel but instead using PCR product solution directly). Purified fragment then ligated into vector backbone with GG-reaction (both empty plasmid vector (pGGA-I) and purified PCR product digested with Eco31I FD (Thermo Scientific) with 10X Fast Digest Buffer (Thermo Scientific). Digestion products column purified and 20-100 ng of product and 2-3 times more vector ligated together with Instant Sticky End Ligase Master Mix (5 µL of combined products and 5 µL of Instant Sticky End Ligase Master Mix) or ligated using protocol from New England Biolabs® Inc.: Ligation Protocol with T4 DNA Ligase (M0202) by New England Biolabs® inc. T4 DNA ligation reaction. Ligation reaction product put on ice for immediate use or stored at -20° C. DH5α or XL1 Blue *E. coli* cells transformed with entry module plasmid. Culture then plated, colonies selected, confirmed by PCR, culture scaled up, and then plasmid collected using Plasmid Mini-Prep Kit (Sigma) or by following Plasmid Miniprep protocol, and then stored at -20° C. Plasmid sequenced to confirm proper DNA sequence using Eurofins Genomics.

Destination Module Creation: Cloning steps follow published GreenGate protocol (Lampropoulos et al., 2013). Added 1.5 µL of necessary entry modules to 1 µL of empty destination vector pGGZ001, 2 µL of FastDigest buffer (Thermo Scientific), 1.5 µL of 10 mM ATP, 1 µL T4 DNA ligase, and 1 µL Eco31I (FastDigest). Reaction performed on thermo-cycler using following program.

GreenGate Module Creation			
Step:	Temperature:	Time:	
1	37°	2'	Repeat Steps 1 and 2 X 30-60
2	16°	2'	
3	50°	5'	
4	80°	5'	

New plasmid was then used to transform *E. coli,* culture used to propagate plasmid, and then mini-prepped (following same protocol as Generation of Entry Module) to produce

plasmid for confirmation via PCR and sequencing. Once confirmed, plasmid ready for use in transformation of *A. tumefaciens* (using *A. tumefaciens* transformation protocol).

Bacteria Cultivation

Cultures of *A. tumefaciens* (strain ASE or C5891) and *E. coli* (strain DH5α or XL1 Blue) grown with lysogeny broth (LB) media with appropriate selective antibiotics on agar plates or in liquid media. Plates put in incubator and liquid cultures put in shaking incubator. *E. coli* cultures allowed to grow for 1 day at 37° C, and *A. tumefaciens* cultures allowed to grow for 2 days at 28° C.

Transformation of *E. coli*

Chemically competent *E. coli* cells (DH5α or XL1 Blue) taken from -80° C storage and allowed to thaw on ice. 2.5 μL of plasmid for transformation added to culture and allowed to incubate for 15 minutes on ice. Culture then heat shocked at 42° C for 50 seconds and then put back on ice for 2 minutes. Then 1 mL of LB media added to transformed bacteria culture and culture placed in shaking incubator at 37° C for a minimum of 1 hour. Then culture plated on LB agar plates containing appropriate selective antibiotics and allowed to incubate overnight at 37° C. After successful colony formation, picked colonies for plasmid check via PCR and placed confirmed colonies into liquid media for overnight incubation at 37° in shaking incubator. Culture then ready for use such as for plasmid harvest.

Transformation of *A. tumefaciens*

Chemical Transformation:

Cultures of chemically competent *A. tumefaciens* cells (ASE) taken from -80° C storage and thawed on ice. 2.5-5 μL of plasmid selected for transformation added to culture which is then incubated on ice for 10 minutes. Culture then placed in liquid nitrogen for 5 minutes, then transferred to heat block at 37° C for 5 minutes of hear shock. 1 mL of LB media added to culture after heat shock. Culture then placed in shaking incubator set to 28° C for at least 2 hours. Culture then plated on selective media agar plates and left to grow for 2 days.

Colonies then selected and checked with PCR. Positive colonies transferred to liquid media and then incubated overnight in shaking incubator at 28° C. Culture now ready for use in plant transformation or storage in cold room for later use.

Electrical Transformation:

Cultures of electrically competent *A. tumefaciens* cells (C5891) taken from -80° C storage and thawed on ice. 2.5-5 µL of plasmid selected for transformation added to culture which is then incubated on ice for 1 minute. Culture transferred to electro-transformation cuvette and then shocked using a Bio-RAD MicroPulser set to the Ec1 program. Cells then chilled on ice for 30-60 seconds. Then added 1 mL LB to cuvette and pipette mixed contents before transferring to Eppendorf tube for minimum of 2 hours incubation in 28° C shaking incubator. Culture then plated on selective media agar plates and left to grow for 2 days. Colonies then selected and checked with PCR. Positive colonies transferred to liquid media and then incubated overnight in shaking incubator at 28° C. Culture now ready for use in plant transformation or storage in cold room for later use.

GeneJet Gel Extraction Kit

Product of Thermo Fisher Scientific. Followed PCR product purification protocol provided with modification that liquid PCR product was mixed with Binding Buffer solution and added directly to the column unless cloning was proving problematic, in which case the protocol was followed with no modifications.

GenElute™ Plasmid Miniprep Kit

Product of Sigma-Aldrich. Adhered to protocol for extraction and purification of plasmid DNA from *E. coli*.

Plasmid Miniprep

Bacterial cultures for miniprep were allowed to grow to high enough densities for adequate plasmid extraction. 2 mL of culture then transferred to 2 mL tube and then spun at 6800g for 2 minutes at room temperature. Supernatant then removed. 200 µL of cold P1 buffer

added and culture resuspended. 200 µL of cold P2 buffer added and culture inverted to mix. 200 µL of cold P3 buffer added and culture inverted to mix. Culture then spun for 5 minutes at full speed. Supernatant transferred to new 1.5 mL tube, 500 µL of isopropanol added, and solution inverted to mix. Solution then spun for 5 minutes at full speed. Supernatant removed and pellet washed with 500 µL of 70% Ethanol. Solution then spun for 1 minute at full speed. Supernatant then removed and pellet allowed to dry. DNA pellet dissolved in 50 µL ddH_2O and ready for immediate use or storage at -20° C.

P1 solution: 6.06 g Tris base. 3.72 g Na_2EDTA x $2H_2O$. Dissolved in 800 mL dH_2O. pH adjusted to 8.0 using HCl (approximately 8 mL of 2 N HCl solution). Final volume adjusted to 1 L with dH_2O. Solution autoclaved or filter sterilized. 10 mg of RNase A added per 100 mL of solution before use. Stored at 4° C.

P2 solution: 0.2 M NaOH and 1% SDS in dH_2O. (8 g NaOH and 10 g SDS per liter dH_2O). Solution dissolved and sterilized only though filter sterilization. Stored at room temperature.

P3 solution: 3 M Potassium acetate in dH_2O with pH of 5.5 adjusted by addition of glacial acetic acid (acetic acid will end up being almost a third of total volume). Stored at 4° C.

TECAN Plate Reader

Tecan plate reader (Infinite M1000, Tecan) used for measuring of chemo-luminescence of samples in white flat bottom 96 well plates (Perkin Elmer 96 Flat Bottom White Polystyrene). Plate reader software used was Tecan i-Control 1.10.4.

Setting for ROS burst experiment: Kinetic Measurement, Kinetic Cycles 30, Interval Time Minimal, Mode Luminescence, Attenuation None, Integration Time 1000 ms, Settle Time 100 ms. 48 wells measured at a time to limit time between measurements of same well during time course.

DNA Sequencing

EuroFins Genomics performed sequencing of DNA samples using both in house and provided primers.

Primer Design, Gene Analysis and Sequencing Data Analysis

The programs Serial Cloner (version 2.6.1) and 4Peaks (version 1.8) were used for analysis of DNA sequencing files, searching genes for restriction enzyme sites, and for primer design.

Agarose Gel Electrophoresis

Gel comprised of 1-2% agarose TAE (4.84 g/L Tris base, 0.1142% (vol/vol) acetic acid and 1 mM EDTA (pH 8) buffer solution to which 2-3 drops (~50µL) of Ethidium bromide solution (0.025% Ethidium bromide, ROTH) per 50 mL of gel was added before pouring. Used Blue Power 500 (Serva) gel electrophoresis power source to run gel. Gel then analyzed using UV light and camera from BioDocAnalyze (biometra) machine and software.

Genotyping

Plant tissue collected from plants needing to be genotyped. Then gDNA extraction protocol performed on collected plant tissue. PCR then performed on gDNA with primers testing for desired genetic sequence, or PCR product purified using GeneJet Gel Extraction kit and submitted for genetic sequencing with appropriate primers. Alternatively, seeds sown on selective media and plantlet survival assessed in order to determine segregation ratios.

Measurement of DNA or RNA Concentration using Nana-Drop

Purified DNA or RNA sample concentration measured using NanoDrop 2000C (Thermo Scientific) DNA measurement device. NanoDrop 2000/2000C software (version 1.4.2).

T-DNA Genotyping

Salk T-DNA plant line seeds received from SIGnAL (Salk Institute Genomic Analysis Laboratory). T-DNA plant lines grown and tissue collected for gDNA extraction. PCR performed with primers testing for presence of T-DNA insertion in correct gene and for homozygosity of mutation. In case of segregating T-DNA lines, plants were grown on

Phyto-agar plates containing selection antibiotic for T-DNA line. Lines showing high percentages of survival were then tested using gDNA extraction and PCR.

Root Length Abiotic Stress Phenotype Experimental Setup

Sterile seeds form desired plant lines sown on plates containing ½ Murashige-Skooog (MS) media used with 0.9% Phyto-Agar, 0-6.5% Sucrose, 0-150 mM Mannitol, 0-2% Glucose, and 0-150 mM NaCl (media pH of 5.8 adjusted with HCl and KOH) in sterile hood. Plates sealed with Millipore sterile surgical tape and put in dark at 5° C for 2 days of stratification. Plates then placed vertically in growth chambers or grow room with long day conditions (16 hours light, 8 hours dark, 100-150 µE light intensity in growth chamber and 5xPhilips Green power LED production module deep red/blue 120 LD [415 µmol/sec at distance of 40 cm] in grow rooms, 60-70% humidity, and 22-23° C) and allowed to germinate. 5 days after germination, plates imaged and root lengths measured (see Measuring Root Length method).

Drought Tolerance Experiments

Plants were first germinated on Phyto agar under short day conditions and then transferred to soil 17 DAG. Plants were grown in single pots under short day conditions (to prevent bolting) until 24 days after germination, after which watering was discontinued. 38 days after germination, plants were top watered with 10 mL each to assess their ability to recover from the initial drought stress. After this, the plants were given no water until the end of the experiment at 42 days after germination. Light intensities were 100-150 µE light intensity in growth chamber and 5xPhilips Green power LED production module deep red/blue 120 LD [415 µmol/sec at distance of 40 cm] in grow rooms.

Generation of CRISPR Mutants

CRISPR/Cas9 constructs created using pHEE401E plasmid containing egg-cell specific promotor (Wang et al., 2015b). Guide RNA (gRNA) designed using the online tool CHOPCHOP (https://chopchop.rc.fas.harvard.edu/) (Labun et al., 2019). Target sequence

selected from list provided by CHOPCHOP program. Forward primer designed as ATTG followed by 19bp from CHOPCHOP (making sure first bp is G) and reverse primer designed as compliment of 19bp from CHOPCHOP followed by GTTT. gRNA oligo duplex then annealed using annealing buffer solution with gRNA primers added (solution heated to 95° C for 5 minutes and then allowed to cool to room temperature). Oligo duplex now ready to be used in GreenGate reaction with pHEE401E plasmid. GreenGate product ready for subsequent transformation of *E. coli* to lead to later transformation of *Agrobacterium* and eventual floral dips. After floral dips, T1 seeds placed on 0.7% PA horizontal Hygromycin plates for selection (covered in paper for first 5 days in growth chamber before being exposed to regular light). Selected T1 plants then sequenced to check for mutations and confirmed mutants transferred to soil for seed collection. T2 seeds then genotyped and plants homozygous for mutation and lacking Cas9 gene selected. CRISPR derived mutant line now ready for use.

5x Annealing Buffer: 5 M NaCl, 0.5 M EDTA, and 1 M Tris-HCL pH 7.5.

Oligo duplex solution: 10 µL of 100 µM forward primer, 10 µL of 100 µM reverse primer, and 5 µL of 5x annealing buffer.

ROS Bust Experiment

Desired plant lines grown under short day conditions to prevent bolting until rosette stage (20-40 DAG). 4 mm leaf disks collected from youngest fully matured sample leaves, placed in sterile water, and covered with aluminum foil to equilibrate for at least 2 hours. After equilibration, leaf disks transferred delicately using flat forceps to a 96 well plate (Perkin Elmer 96 Flat Bottom White Polystyrene) with 1 leaf disk and 150 µL sterile water per well. Plate covered with aluminum foil and put back in growth chamber or grow room overnight. Next day, chemiluminescence and elicitor solutions prepared. Sample plate kept covered while moving to room with plate reader and preparing experiment. All lights turned off except for green light which was used for experiment set up beyond this point. Plates uncovered and sterile water removed from first 4 rows of plate using micropipette (this was done to keep the length between sample time points to ~60 seconds), being careful not to damage the leaf disks. Next added 100 µL of the L-012 and HRP solution to each well of

the first 4 rows, and made sure the leaf disks are fully submerged (needed to push the leaf disk down with a pipette tip and concluded it was alright if it floated back to the surface after it was pushed down). Before starting the next step, made sure the plate reader was open with the correct acquisition program loaded and ready to begin since as little delay as possible between the next step and the beginning on sample acquisition was desired. Then added 50 µL of the HRP elicitor solution to the first 4 sample well rows (being sure to use a multichannel pipette for this step since wanted to begin recording sample results as fast as possible and wanted all samples to be exposed to elicitors at roughly the same time) and placed the uncovered plate in the plate reader. Began sample data acquisition (see plate reader for protocol for program settings). After successful collection of data, repeated the process starting from the removal of sterile water for the bottom 4 sample rows.
L-012 and HRP Solution: 0.75 µM L-012 and 15 µg/mL HRP in ddH_2O.
Elicitor solution: 300 nM flg22 or elf18 in ddH_2O.
Final solution concentrations: 0.5 µM L-012, 10 µg/mL HRP, and 100 nM flg22 or elf18 in ddH_2O.

Normalization of Root Length Data

Root length data normalized by comparison to control treatment for respective plant line. Average root length of control group set to 100%, and all recorded root lengths converted to percent by dividing them by the average control root length and multiplying by 100.

Plate Growth Inhibition Experiment

Experiments using Phyto-Agar Plates: Phyto-agar media prepared as usual. Media allowed to cool after autoclaving to point where media was still liquid, but the bottle could be handled without heat protective equipment. Elicitors then added to media under sterile conditions and mixed. After this point plates poured as usual. After plates allowed to cool, seeds germinated on the elicitor infused Phyto-agar plates after 2-3 days vernalization, and roots measured 14 DAG.
Experiments using 48 well plates: Seeds germinated on Phyto-agar plates and allowed to grow for 4-5 days after germination. Plants then transferred under sterile conditions to 48

well plates. One plant per well with 400 µL of liquid media per well. Media contained 0-100 nM elf18 or flg22 elicitor. Plates sealed with Millipore sterile surgical tape and returned to growth chamber. After 7-10 days the plates were removed from the growth chamber and the fresh weights of the individual plants were recorded.

Experiments using 100 mL Erlenmeyer flasks: Seeds germinated on Phyto-agar plates and allowed to grow for 4-5 days after germination. Plants then transferred under sterile conditions to 100 mL Erlenmeyer flasks (10-30 per flask). Flasks then sealed with sterile aluminum foil, being sure not to cut off gas flow completely, and placed in growth chamber on Heidolph UNIMAX 2010 orbital shaker set to shake slowly. After 7-10 days the flasks were removed from the growth chamber. Filter paper was first labeled using a pencil and then weighed, making sure to have one filter per flask. After this, all plants from one flask were placed on appropriately labeled filter paper. Plants on filter paper then placed in oven at 60-70° C and allowed to dry overnight or until completely dry. After drying complete, filters with plants were removed from oven and allowed to cool before dry mass was recorded for each filter paper plant combination. Weight of filter was subtracted from final combined weight to determine sample dry mass.

Data Analysis Using RStudio

Used RStudio Version 1.2.5019 © 2009-2019 RStudio, Inc.

FIJI (ImageJ)

Version: 2.0.0-rc-69/1.52p

Elicitor RT-qPCR Gene Impact Experiment

Seeds germinated on Phyto-agar plates and allowed to grow for 5 days after germination. Plants then transferred to 100 mL Erlenmeyer flasks (30 per flask) containing 20 mL of liquid ½ Murashige-Skooog (MS) media each. Then added 5 mL of liquid ½ MS media containing 5x final elicitor concentration (regular ½ MS media with no elicitors for negative controls) to each flask (making sure not to pour directly on the plants). Flasks then sealed with aluminum foil, being sure not to cut off gas flow completely, and placed in growth

chamber on Heidolph UNIMAX 2010 orbital shaker set to shake slowly. After 1 hour, plantlets removed from media and frozen together in liquid nitrogen. Process repeated for all flasks, keeping different treatments separate. Samples then ready for RNA extraction, cDNA generation, and RT-qPCR analysis.

References

Amano, Y., Tsubouchi, H., Shinohara, H., Ogawa, M., and Matsubayashi, Y. (2007). Tyrosine-sulfated glycopeptide involved in cellular proliferation and expansion in *Arabidopsis*. Proceedings of the National Academy of Sciences **104**: 18333–18338.

Asai, T., Tena, G., Plotnikova, J., Willmann, M.R., Chiu, W.-L., Gomez-Gomez, L., Boller, T., Ausubel, F.M., and Sheen, J. (2002). MAP kinase signaling cascade in *Arabidopsis* innate immunity. Nature **415**: 977–983.

Augustin, S. (2015). Structure-function analysis of the *Arabidopsis thaliana* Receptor-Like Protein 4 (AtRLP4). Master Thesis, Heidelberg University.

Bai, C., Sen, P., Hofmann, K., Ma, L., Goebl, M., Harper, J.W., and Elledge, S.J. (1996). SKP1 Connects Cell Cycle Regulators to the Ubiquitin Proteolysis Machinery through a Novel Motif, the F-Box. Cell **86**: 263–274.

Berardini, T.Z., Reiser, L., Li, D., Mezheritsky, Y., Muller, R., Strait, E., and Huala, E. (2015). The arabidopsis information resource: Making and mining the "gold standard" annotated reference plant genome: Tair: Making and Mining the "Gold Standard" Plant Genome. genesis **53**: 474–485.

Brady, S.M., Orlando, D.A., Lee, J.-Y., Wang, J.Y., Koch, J., Dinneny, J.R., Mace, D., Ohler, U., and Benfey, P.N. (2007). A High-Resolution Root Spatiotemporal Map Reveals Dominant Expression Patterns. Science **318**: 801–806.

Bu, Q., Li, H., Zhao, Q., Jiang, H., Zhai, Q., Zhang, J., Wu, X., Sun, J., Xie, Q., Wang, D., and Li, C. (2009). The *Arabidopsis* RING Finger E3 Ligase RHA2a Is a Novel Positive Regulator of Abscisic Acid Signaling during Seed Germination and Early Seedling Development. Plant Physiol. **150**: 463–481.

Burgh, A.M. van der, Postma, J., Robatzek, S., and Joosten, M.H.A.J. (2019). Kinase activity of SOBIR1 and BAK1 is required for immune signaling. Molecular Plant Pathology **20**: 410–422.

Caesar, K., Elgass, K., Chen, Z., Huppenberger, P., Witthöft, J., Schleifenbaum, F., Blatt, M.R., Oecking, C., and Harter, K. (2011). A fast brassinolide-regulated response pathway in the plasma membrane of *Arabidopsis thaliana*: A BL-regulated plasma membrane response pathway. The Plant Journal **66**: 528–540.

Chaiwanon, J. and Wang, Z.-Y. (2015). Spatiotemporal Brassinosteroid Signaling and Antagonism with Auxin Pattern Stem Cell Dynamics in *Arabidopsis* Roots. Current Biology **25**: 1031–1042.

El-Brolosy, M.A. and Stainier, D.Y.R. (2017). Genetic compensation: A phenomenon in search of mechanisms. PLoS Genet **13**: e1006780.

Fiers, M., Golemiec, E., Xu, J., Geest, L. van der, Heidstra, R., Stiekema, W., and Liu, C.-M. (2005). The 14–Amino Acid CLV3, CLE19, and CLE40 Peptides Trigger Consumption of the Root Meristem in Arabidopsis through a CLAVATA2-Dependent Pathway. The Plant Cell **17**: 2542–2553.

Fritz-Laylin, L.K., Krishnamurthy, N., Tör, M., Sjölander, K.V., and Jones, J.D.G. (2005). Phylogenomic Analysis of the Receptor-Like Proteins of Rice and *Arabidopsis*. Plant Physiology **138**: 611.

Garnelo Gómez, B. (2017). Phosphorylation of RLP44: Shifting between subcellular localization and receptor complexes. PhD Thesis, Heidelberg University.

Gómez-Gómez, L. and Boller, T. (2000). FLS2: An LRR Receptor–like Kinase Involved in the Perception of the Bacterial Elicitor Flagellin in *Arabidopsis*. Molecular Cell **5**: 1003–1011.

Gurevich, V.V. and Gurevich, E.V. (2015). Analyzing the roles of multi-functional proteins in cells: the case of arrestins and GRKs. Critical reviews in biochemistry and molecular biology **50**: 440.

Hartwig, T., Corvalan, C., Best, N.B., Budka, J.S., Zhu, J.-Y., Choe, S., and Schulz, B. (2012). Propiconazole Is a Specific and Accessible Brassinosteroid (BR) Biosynthesis Inhibitor for *Arabidopsis* and Maize. PLoS ONE **7**: e36625.

He, Y., Zhou, J., Shan, L., and Meng, X. (2018). Plant cell surface receptor-mediated signaling – a common theme amid diversity. J Cell Sci **131**: jcs209353.

Hillmer, R.A., Tsuda, K., Rallapalli, G., Asai, S., Truman, W., Papke, M.D., Sakakibara, H., Jones, J.D.G., Myers, C.L., and Katagiri, F. (2017). The highly buffered Arabidopsis immune signaling network conceals the functions of its components. PLoS Genet **13**: e1006639.

Hohmann, U., Lau, K., and Hothorn, M. (2017). The Structural Basis of Ligand Perception and Signal Activation by Receptor Kinases. Annu. Rev. Plant Biol. **68**: 109–137.

Holzwart, E. (2018). The role of RLP44 in cell wall signalling integration and vascular cell fate determination in *Arabidopsis thaliana*. PhD Thesis, Heidelberg University.

Holzwart, E., Huerta, A.I., Glöckner, N., Garnelo Gómez, B., Wanke, F., Augustin, S., Askani, J.C., Schürholz, A.-K., Harter, K., and Wolf, S. (2018). BRI1 controls vascular cell fate in the *Arabidopsis* root through RLP44 and phytosulfokine signaling. Proc Natl Acad Sci USA **115**: 11838–11843.

Igarashi, D., Tsuda, K., and Katagiri, F. (2012). The peptide growth factor, phytosulfokine, attenuates pattern-triggered immunity: Attenuation of PTI by PSK. The Plant Journal **71**: 194–204.

Jamieson, P.A., Shan, L., and He, P. (2018). Plant cell surface molecular cypher: Receptor-like proteins and their roles in immunity and development. Plant Science **274**: 242–251.

Jeong, S., Trotochaud, A.E., and Clark, S.E. (1999). The *Arabidopsis* CLAVATA2 Gene Encodes a Receptor-like Protein Required for the Stability of the CLAVATA1 Receptor-like Kinase. The Plant Cell **11**: 1925–1933.

de Jong, W.W., Zweers, A., and Cohen, L.H. (1978). Influence of single amino acid substitutions on electrophoretic mobility of sodium dodecyl sulfate-protein complexes. Biochemical and Biophysical Research Communications **82**: 532–539.

Klepikova, A.V., Kasianov, A.S., Gerasimov, E.S., Logacheva, M.D., and Penin, A.A. (2016). A high resolution map of the *Arabidopsis thaliana* developmental transcriptome based on RNA-seq profiling. Plant J **88**: 1058–1070.

Komori, R., Amano, Y., Ogawa-Ohnishi, M., and Matsubayashi, Y. (2009). Identification of tyrosylprotein sulfotransferase in *Arabidopsis*. Proceedings of the National Academy of Sciences **106**: 15067–15072.

Kung, J.E. and Jura, N. (2016). Structural Basis for the Non-catalytic Functions of Protein Kinases. Structure **24**: 7–24.

Kuroda, H., Yanagawa, Y., Takahashi, N., Horii, Y., and Matsui, M. (2012). A Comprehensive Analysis of Interaction and Localization of Arabidopsis SKP1-LIKE (ASK) and F-Box (FBX) Proteins. PLoS ONE **7**: e50009.

Kutschmar, A., Rzewuski, G., Stührwohldt, N., Beemster, G.T.S., Inzé, D., and Sauter, M. (2009). PSK-α promotes root growth in *Arabidopsis*. New Phytologist **181**: 820–831.

Labun, K., Montague, T.G., Krause, M., Torres Cleuren, Y.N., Tjeldnes, H., and Valen, E. (2019). CHOPCHOP v3: expanding the CRISPR web toolbox beyond genome editing. Nucleic Acids Research **47**: W171–W174.

Ladwig, F., Dahlke, R.I., Stührwohldt, N., Hartmann, J., Harter, K., and Sauter, M. (2015). Phytosulfokine Regulates Growth in *Arabidopsis* through a Response Module at the Plasma Membrane That Includes CYCLIC NUCLEOTIDE-GATED CHANNEL17, H^+-ATPase, and BAK1. Plant Cell **27**: 1718–1729.

Lampropoulos, A., Sutikovic, Z., Wenzl, C., Maegele, I., Lohmann, J.U., and Forner, J. (2013). GreenGate - A Novel, Versatile, and Efficient Cloning System for Plant Transgenesis. PLoS ONE **8**.

Lempe, J., Lachowiec, J., Sullivan, A.M., and Queitsch, C. (2013). Molecular mechanisms of robustness in plants. Current opinion in plant biology **16**: 62.

Li, J. and Chory, J. (1997). A Putative Leucine-Rich Repeat Receptor Kinase Involved in Brassinosteroid Signal Transduction. Cell **90**: 929–938.

Li, J. and Nam, K.H. (2002). Regulation of Brassinosteroid Signaling by a GSK3/SHAGGY-Like Kinase. Science **295**: 1299–1301.

Li, J., Wen, J., Lease, K.A., Doke, J.T., Tax, F.E., and Walker, J.C. (2002). BAK1, an *Arabidopsis* LRR Receptor-like Protein Kinase, Interacts with BRI1 and Modulates Brassinosteroid Signaling. Cell **110**: 213–222.

Liebrand, T.W.H., Berg, G.C.M. van den, Zhang, Z., Smit, P., Cordewener, J.H.G., America, A.H.P., Sklenar, J., Jones, A.M.E., Tameling, W.I.L., Robatzek, S., Thomma, B.P.H.J., and Joosten, M.H.A.J. (2013). Receptor-like kinase SOBIR1/EVR interacts with receptor-like proteins in plant immunity against fungal infection. PNAS **110**: 10010–10015.

Lorbiecke, R. and Sauter, M. (2002). Comparative analysis of PSK peptide growth factor precursor homologs. Plant Science **163**: 321–332.

Matsubayashi, Y., Ogawa, M., Kihara, H., Niwa, M., and Sakagami, Y. (2006). Disruption and Overexpression of *Arabidopsis* Phytosulfokine Receptor Gene Affects Cellular Longevity and Potential for Growth. Plant Physiol. **142**: 45–53.

Matsubayashi, Y., Ogawa, M., Morita, A., and Sakagami, Y. (2002). An LRR Receptor Kinase Involved in Perception of a Peptide Plant Hormone, Phytosulfokine. Science **296**: 1470–1472.

Matsubayashi, Y. and Sakagami, Y. (1996). Phytosulfokine, sulfated peptides that induce the proliferation of single mesophyll cells of *Asparagus officinalis* L. Proc. Natl. Acad. Sci. USA: 5.

Nam, K.H. and Li, J. (2002). BRI1/BAK1, a Receptor Kinase Pair Mediating Brassinosteroid Signaling. Cell **110**: 203–212.

Pickart, C.M. (2001). Mechanisms Underlying Ubiquitination. Annu. Rev. Biochem. **70**: 503–533.

Roux, M., Schwessinger, B., Albrecht, C., Chinchilla, D., Jones, A., Holton, N., Malinovsky, F.G., Tör, M., de Vries, S., and Zipfel, C. (2011). The *Arabidopsis* Leucine-Rich Repeat Receptor–Like Kinases BAK1/SERK3 and BKK1/SERK4 Are Required for Innate Immunity to Hemibiotrophic and Biotrophic Pathogens. Plant Cell **23**: 2440–2455.

Santiago, J., Henzler, C., and Hothorn, M. (2013). Molecular Mechanism for Plant Steroid Receptor Activation by Somatic Embryogenesis Co-Receptor Kinases. Science **341**: 889–892.

Sauter, M. (2015). Phytosulfokine peptide signalling. EXBOTJ **66**: 5161–5169.

Segonzac, C., Macho, A.P., Sanmartín, M., Ntoukakis, V., Sánchez-Serrano, J.J., and Zipfel, C. (2014). Negative control of BAK 1 by protein phosphatase 2A during plant innate immunity. EMBO J **33**: 2069–2079.

Shi, Y., Mowery, R.A., Ashley, J., Hentz, M., Ramirez, A.J., Bilgicer, B., Slunt-Brown, H., Borchelt, D.R., and Shaw, B.F. (2012). Abnormal SDS-PAGE migration of cytosolic proteins can identify domains and mechanisms that control surfactant binding. Protein Sci **21**: 1197–1209.

Shiu, S.-H. and Bleecker, A.B. (2003). Expansion of the Receptor-Like Kinase/Pelle Gene Family and Receptor-Like Proteins in *Arabidopsis*. Plant Physiol. **132**: 530–543.

Shiu, S.-H. and Bleecker, A.B. (2001). Plant Receptor-Like Kinase Gene Family: Diversity, Function, and Signaling. Sci. STKE **2001**: re22–re22.

Shpak, E.D., Lakeman, M.B., and Torii, K.U. (2003). Dominant-Negative Receptor Uncovers Redundancy in the *Arabidopsis* ERECTA Leucine-Rich Repeat Receptor–Like Kinase Signaling Pathway That Regulates Organ Shape. Plant Cell **15**: 1095–1110.

Srivastava, R., Liu, J.-X., and Howell, S.H. (2008). Proteolytic processing of a precursor protein for a growth-promoting peptide by a subtilisin serine protease in *Arabidopsis*: *Peptide hormone processing*. The Plant Journal **56**: 219–227.

Stone, S.L. (2014). The role of ubiquitin and the 26S proteasome in plant abiotic stress signaling. Front. Plant Sci. **5**.

Stührwohldt, N., Dahlke, R.I., Steffens, B., Johnson, A., and Sauter, M. (2011). Phytosulfokine-α Controls Hypocotyl Length and Cell Expansion in *Arabidopsis thaliana* through Phytosulfokine Receptor 1. PLoS ONE **6**.

Sun, Y. et al. (2010). Integration of Brassinosteroid Signal Transduction with the Transcription Network for Plant Growth Regulation in *Arabidopsis*. Developmental Cell **19**: 765–777.

Szekeres, M., Németh, K., Koncz-Kálmán, Z., Mathur, J., Kauschmann, A., Altmann, T., Rédei, G.P., Nagy, F., Schell, J., and Koncz, C. (1996). Brassinosteroids Rescue the Deficiency of CYP90, a Cytochrome P450, Controlling Cell Elongation and De-etiolation in *Arabidopsis*. Cell **85**: 171–182.

Tena, G., Boudsocq, M., and Sheen, J. (2011). Protein kinase signaling networks in plant innate immunity. Current Opinion in Plant Biology **14**: 519–529.

Wang, G. et al. (2008). A Genome-Wide Functional Investigation into the Roles of Receptor-Like Proteins in *Arabidopsis*. Plant Physiol. **147**: 503–517.

Wang, J., Li, H., Han, Z., Zhang, H., Wang, T., Lin, G., Chang, J., Yang, W., and Chai, J. (2015a). Allosteric receptor activation by the plant peptide hormone phytosulfokine. Nature **525**: 265–268.

Wang, Z.-P., Xing, H.-L., Dong, L., Zhang, H.-Y., Han, C.-Y., Wang, X.-C., and Chen, Q.-J. (2015b). Egg cell-specific promoter-controlled CRISPR/Cas9

efficiently generates homozygous mutants for multiple target genes in *Arabidopsis* in a single generation. Genome Biol **16**: 144.

Wang, Z.-Y., Nakano, T., Gendron, J., He, J., Chen, M., Vafeados, D., Yang, Y., Fujioka, S., Yoshida, S., Asami, T., and Chory, J. (2002). Nuclear-Localized BZR1 Mediates Brassinosteroid-Induced Growth and Feedback Suppression of Brassinosteroid Biosynthesis. Developmental Cell **2**: 505–513.

Wolf, S. et al. (2014). A receptor-like protein mediates the response to pectin modification by activating brassinosteroid signaling. Proc Natl Acad Sci USA **111**: 15261–15266.

Wolf, S., Mravec, J., Greiner, S., Mouille, G., and Höfte, H. (2012). Plant Cell Wall Homeostasis Is Mediated by Brassinosteroid Feedback Signaling. Current Biology **22**: 1732–1737.

Wu, J., Liu, Z., Zhang, Z., Lv, Y., Yang, N., Zhang, G., Wu, M., Lv, S., Pan, L., Joosten, M.H.A.J., and Wang, G. (2016). Transcriptional regulation of receptor-like protein genes by environmental stresses and hormones and their overexpression activities in *Arabidopsis thaliana*. EXBOTJ **67**: 3339–3351.

Yang, H., Matsubayashi, Y., Nakamura, K., and Sakagami, Y. (2001). Diversity of *Arabidopsis* Genes Encoding Precursors for Phytosulfokine, a Peptide Growth Factor. Plant Physiol. **127**: 842–851.

Yin, Y., Wang, Z.-Y., Mora-Garcia, S., Li, J., Yoshida, S., Asami, T., and Chory, J. (2002). BES1 Accumulates in the Nucleus in Response to Brassinosteroids to Regulate Gene Expression and Promote Stem Elongation. Cell **109**: 181–191.

Yu, X., Li, L., Zola, J., Aluru, M., Ye, H., Foudree, A., Guo, H., Anderson, S., Aluru, S., Liu, P., Rodermel, S., and Yin, Y. (2011). A brassinosteroid transcriptional network revealed by genome-wide identification of BESI target genes in *Arabidopsis thaliana*: Brassinosteroid transcriptional network. The Plant Journal **65**: 634–646.

Zhang, W., Fraiture, M., Kolb, D., Löffelhardt, B., Desaki, Y., Boutrot, F.F.G., Tör, M., Zipfel, C., Gust, A.A., and Brunner, F. (2013). Arabidopsis RECEPTOR-LIKE PROTEIN30 and Receptor-Like Kinase SUPPRESSOR OF BIR1-1/EVERSHED Mediate Innate Immunity to Necrotrophic Fungi. The Plant Cell **25**: 4227–4241.

Zheng, N. and Shabek, N. (2017). Ubiquitin Ligases: Structure, Function, and Regulation. Annu. Rev. Biochem. **86**: 129–157.

Zipfel, C., Kunze, G., Chinchilla, D., Caniard, A., Jones, J.D.G., Boller, T., and Felix, G. (2006). Perception of the Bacterial PAMP EF-Tu by the Receptor EFR Restricts *Agrobacterium*-Mediated Transformation. Cell **125**: 749–760.

Zipfel, C., Robatzek, S., Navarro, L., Oakeley, E.J., Jones, J.D.G., Felix, G., and Boller, T. (2004). Bacterial disease resistance in *Arabidopsis* through flagellin perception. Nature **428**: 764–767.

Appendix

Appendix 1: Table containing PCR primers used in the experiments of this thesis.

Primer Set:	Forward Sequence:	Reverse Sequence:	Function:
PS1	CGTTGCAGCAGTTTTACTTAGC	GACGAGCCACTGAAGCAAG	RT-qPCR of PSKL1
PS2	GCGTGCACCTAAAGAGATGG	GCGGTTTTGGAGGATGTGTT	RT-qPCR of PSKL1
PSKL1 gRNA 1	ATTGGACTCTCCAGAGCAAATCAA	AAACTTGATTTGCTCTGGAGAGTC	PSKL1 CRISPR/CAS9 guide sequence
PSKL1 gRNA 2	ATTGGTAACTTTAGGTGCACGCGG	AAACCCGCGTGCACCTAAAGTTAC	PSKL1 CRISPR/CAS9 guide sequence
PSKL1 CRISPR Confirmation	AACATTCTTATCGTTGCAGCAG	AACCAAACTCTCCATAGATGCAA	Sequencing of CRISPR/CAS9 targeted DNA
PSKL1 sequencing	CGCAACGCAATTAATGTGAG	CAGATTGTACTGAGAGTGCACC	Sequencing of cloned PSKL1 gene
RLP44 TDNA Genoyping Gene Primers	ACCTCACTTCTGCTAAAACGC	AGACCTAATTGCTGCGGAATC	Genotyping of RLP44 TDNA line SAIL_596_E12
RLP44 TDNA Genoyping Insert Primer	ATAACCAATCTCGATACAC	-	Genotyping of RLP44 TDNA line SAIL_596_E12
BSA Primer: CER448567	ATAGAAAGGTTTGAGGGGGC	TGCGAAGAACCACTAAACCC	BSA Primer 1 (Chromosome 1)
BSA Primer: F9L1	CTCGGAAATTCTTAGCTTTC	TTATAACTTGCCCAAAGCGAA	BSA Primer 2 (Chromosome 1)
BSA Primer: F1K23ind38	GGATTGAACATAGGGAAGGGG	GATCTGTATCTGAAACCTGGG	BSA Primer 3 (Chromosome 1)
BSA Primer: F6D8ind94	CCGTTACCCCCATACGAACG	TCGTGAGGTTATGCCGATCC	BSA Primer 4 (Chromosome 1)
BSA Primer: F5I14	CTGCCTGAAATTGTCGAAAC	GGCATCACAGTTCTGATTCC	BSA Primer 5 (Chromosome 1)
BSA Primer: CER466780	GAACCCTTATAATATGGCTGGC	GGAAGTATTCCC AAGACAAGG	BSA Primer 6 (Chromosome 2)
BSA Primer: MSAT2-36	GATCTGCCTCTTGATCAGC	CCAAGAACTCAAAACCGTT	BSA Primer 7 (Chromosome 2)
BSA Primer: F3N11	GTTAAAGCGAGGACGATTGG	AGATACTGTCGCCATCAAGG	BSA Primer 8 (Chromosome 2)
BSA Primer: MSAT2-9	TAAAAGAGTCCCTCGTAAAG	GTTGTTGTTGTGGCATT	BSA Primer 9 (Chromosome 2)
BSA Primer: nga172	AGCTGCTTCCTTATAGCGTCC	CATCCGAATGCCATTGTTC	BSA Primer 10 (Chromosome 3)
BSA Primer: CER455386	CTCTTTTGGCTCGGACAAG	GTTGTAATCGGGAAAATGC	BSA Primer 11 (Chromosome 3)
BSA Primer: CER455914	GGAGCAGAGAAAGAGAC	GAGGAAGGACAACATGGC	BSA Primer 12 (Chromosome 3)
BSA Primer: CER456071-Indel-35	AGCCATAGGTAATGTCCACG	CTCGCGGATGAGTATCATCC	BSA Primer 13 (Chromosome 3)
BSA Primer: CER470172	GTAAAACTCCTCCTCTGGGG	TGTAATCGTGGCGGAACGGG	BSA Primer 14 (Chromosome 3)
BSA Primer: nga8	GAGGGCAAATCTTTATTTCGG	TGGCTTTCGTTTATAAACATCC	BSA Primer 15 (Chromosome 4)
BSA Primer: FCA0ind25	AAGCCAACTATTGCCAAGGG	TCACTGCCCTTTACTCCGGT	BSA Primer 16 (Chromosome 4)
BSA Primer: F7J7-47	TGGTGAAGAGCTTAGTTGATGA	TCACTAGATATCTCTAGTGGCT	BSA Primer 17 (Chromosome 4)
BSA Primer: CER451534	AGCTACGGTGGAGTGTAATTTCGT	GCTGATACTTGCTTTCGCTTTGCAG	BSA Primer 18 (Chromosome 4)
BSA Primer: CER459444	AGTAGCATCGTAGCTCCTAGG	GTTGTATACGTGCACGTTCCC	BSA Primer 19 (Chromosome 4)
BSA Primer: nga151	GTTTTGGGAAGTTTTGCTGG	CAGTCTAAAAGCGAGAGTATGATG	BSA Primer 20 (Chromosome 5)
BSA Primer: nga139	GGTTTCGTTTCACTATCCAGG	AGAGCTACCAGATCCGATGG	BSA Primer 21 (Chromosome 5)
BSA Primer: T26D22-IND52/CER459812	TCCCACGAAGAGAGAAGTGC	CTATTTGCTTATGAAGGTGTCC	BSA Primer 22 (Chromosome 5)
BSA Primer: CER456772	CCATGTGACATGCACTTACAC	ACCATTCTCTACCACTCCAC	BSA Primer 23 (Chromosome 5)
BSA Primer: K6M13ind33/CER454758	ATAGATGAGATCCACTTGCC	ACAAACTGTTGCTGTGGGAG	BSA Primer 24 (Chromosome 5)
BSA Primer: MBK5ind35/CER455203	ATTCTCGGACCAGGCTTCAT	AAAGAACAGCTACTGCGTGC	BSA Primer 25 (Chromosome 5)
RLP46 RT-qPCR	TAGGTAGTCTTGTCGAACTACTG	TTGAGCTTCGTTAACCGTGA	RT-qPCR of RLP46
FRK1 RT-qPCR	ATCTTCGCTTGGAGCTTCTC	TGCAGCGCAAGGACTAGAG	RT-qPCR of FRK1
NHL10 RT-qPCR	TTCCTGTCCGTAACCCAAAC	CCCTCGTAGTAGGCATGAGC	RT-qPCR of NHL10
RLP46 gRNA	ATTGGTCAAGGAGAACAATTCATG	AAACCATGAATTGTTCTCCTTGAC	RLP46 CRISPR/CAS9 guide sequence
RLP46 CRISPR Confirmation	ATGGCTACGCGTGACATGTAAC	ATATCGAGCCACTCAAGGTATG	Sequencing of CRISPR/CAS9 targeted DNA
RLP46 Sequencing 1	CAGAACAATTTCTTGTCTTC	-	Sequencing of cloned RLP46 gene
RLP46 Sequencing 2	TTGTACTATCAAGGAACAAC	-	Sequencing of cloned RLP46 gene
RLP46 Sequencing 3	CTCTCTGAGAACAATCTTGATG	-	Sequencing of cloned RLP46 gene
RLP46 Sequencing 4	CCTAAAGGTTTTAAATCTTTC	-	Sequencing of cloned RLP46 gene
CID4 gRNA	ATTGGAAGATTGCGAGAGAGATCG	AAACCGATCTCTCTCGCAATCTTC	CID4 CRISPR/CAS9 guide sequence
CID4 CRISPR Confirmation	TGGATTTCCACTCAAAAGAGGT	TGAAATCAAACCCCCAAATTAC	Sequencing of CRISPR/CAS9 targeted DNA
UPL4 gRNA	ATTGGCACTCTTAAGTTCTGATAG	AAACCTATCAGAACTTAAGAGTGC	UPL4 CRISPR/CAS9 guide sequence
UPL4 CRISPR Confirmation	TAGTAGCACTACAGGTTGCGGA	TCCAAAGAAACCCTCCTTGATA	Sequencing of CRISPR/CAS9 targeted DNA
F-Box/RNI Like gRNA	ATTGGAACAGAGGAGAGGATATGG	AAACCCATATCCTCTCCTCTGTTC	F-Box/RNI Like CRISPR/CAS9 guide sequence
F-Box/RNI Like CRISPR Confirmation	ATACAGAAAGACAGCGTCTCCG	GATGCAGCCATTAACAGAATCA	Sequencing of CRISPR/CAS9 targeted DNA
F-Box/RNI Like TDNA Genoyping Gene Primers	ACTGGCGATTCAATCGACGG	AACAGGTCTCACTGACTATCGTTGAGGGAAAGTGTTG	Genotyping of F-Box/RNI Like TDNA line SALK 01956
F-Box/RNI Like TDNA Genoyping Insert Primer	ATTTTGCCGATTTCGGAAC	-	Genotyping of F-Box/RNI Like TDNA line SALK 01956
F-Box/RNI Like sequencing 1	GAAGCTTTCACTGGAGTCTCG	-	Sequencing of cloned F-Box/RNI Like gene
F-Box/RNI Like sequencing 2	ATTACCATGTAGTTTAGTTG	-	Sequencing of cloned F-Box/RNI Like gene
CYP77A9 gRNA	ATTGGGCGATAGAGTGGGGAATCG	AAACCGATTCCCCACTCTATCGCC	CYP77A9 CRISPR/CAS9 guide sequence
CYP77A9 CRISPR Confirmation	TCAGAGTTGATGGTCGTGAAAC	GGCCGTAGATGTTTCTCATCTC	Sequencing of CRISPR/CAS9 targeted DNA
UMAMIT9 gRNA	ATTGGGGATAGTGATGAAGAAAAG	AAACCTTTTCTTCATCACTATCCC	UMAMIT9 CRISPR/CAS9 guide sequence
UMAMIT9 CRISPR Confirmation	CAAGCTCTAAACCCTACTTCGC	AAGAAAGCAAAGGGTGCAATAA	Sequencing of CRISPR/CAS9 targeted DNA
ABCG6 gRNA	ATTGGGAAAAGCAGAATCGGATCG	AAACCGATCCGATTCTGCTTTTCC	ABCG6 CRISPR/CAS9 guide sequence
ABCG6 CRISPR Confirmation	GAAGCCTTTCGAAATCAAAGAA	CTATGAGTTGTTGTGGTCGCTC	Sequencing of CRISPR/CAS9 targeted DNA
GreenGate Sequencing Primer 1	CATCAGGGATTATACAAGGCC	-	Sequencing of GreenGate cloning constructs
GreenGate Sequencing Primer 2	GTATTCAGTCGACTGGTACCAAC	-	Sequencing of GreenGate cloning constructs
GreenGate Sequencing Primer 3	ACCTCTCGGGCTTCTGG	-	Sequencing of GreenGate cloning constructs
GreenGate Sequencing Primer 4	CGATTTTTGTGATGCTCGCT	-	Sequencing of GreenGate cloning constructs
GreenGate Sequencing Primer 5	TTGGTACCAGTCGACTGAATAC	-	Sequencing of GreenGate cloning constructs

Appendix 2: Uncropped Western Blot image from figure 36 section A.

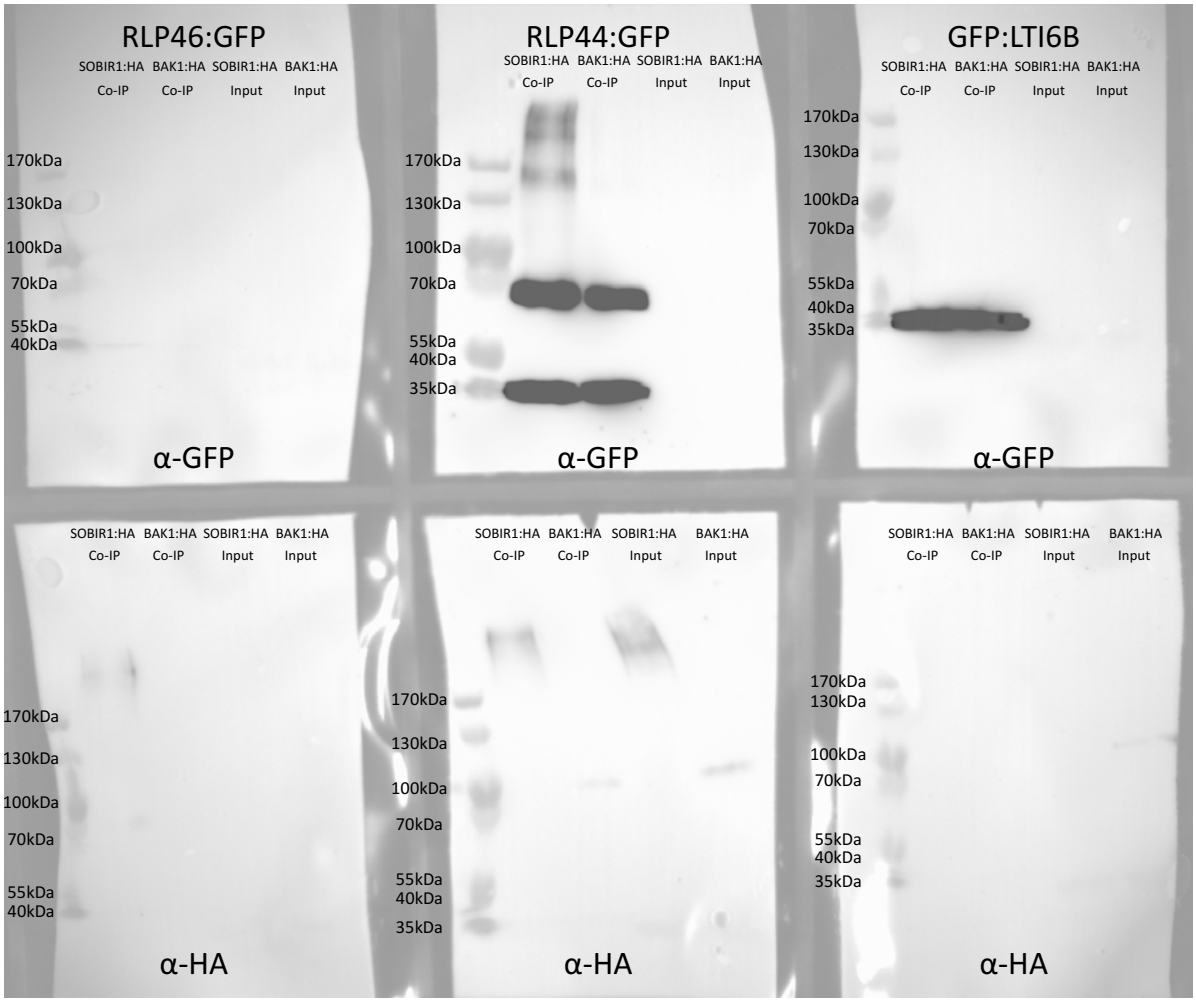

Appendix 3: Uncropped Western Blot image from figure 36 section B.

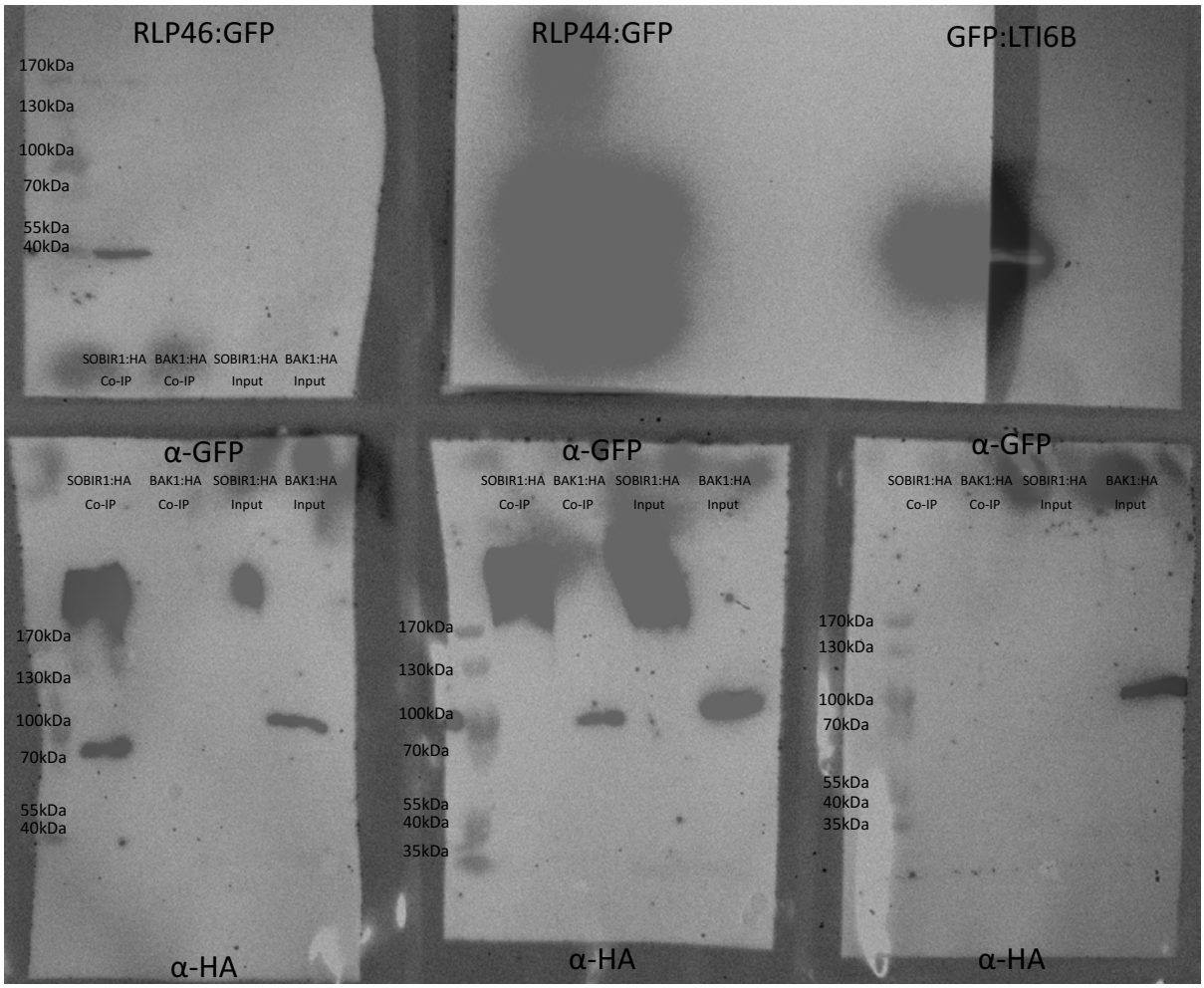

Appendix 4: Uncropped Western Blot image from figure 36 section C.

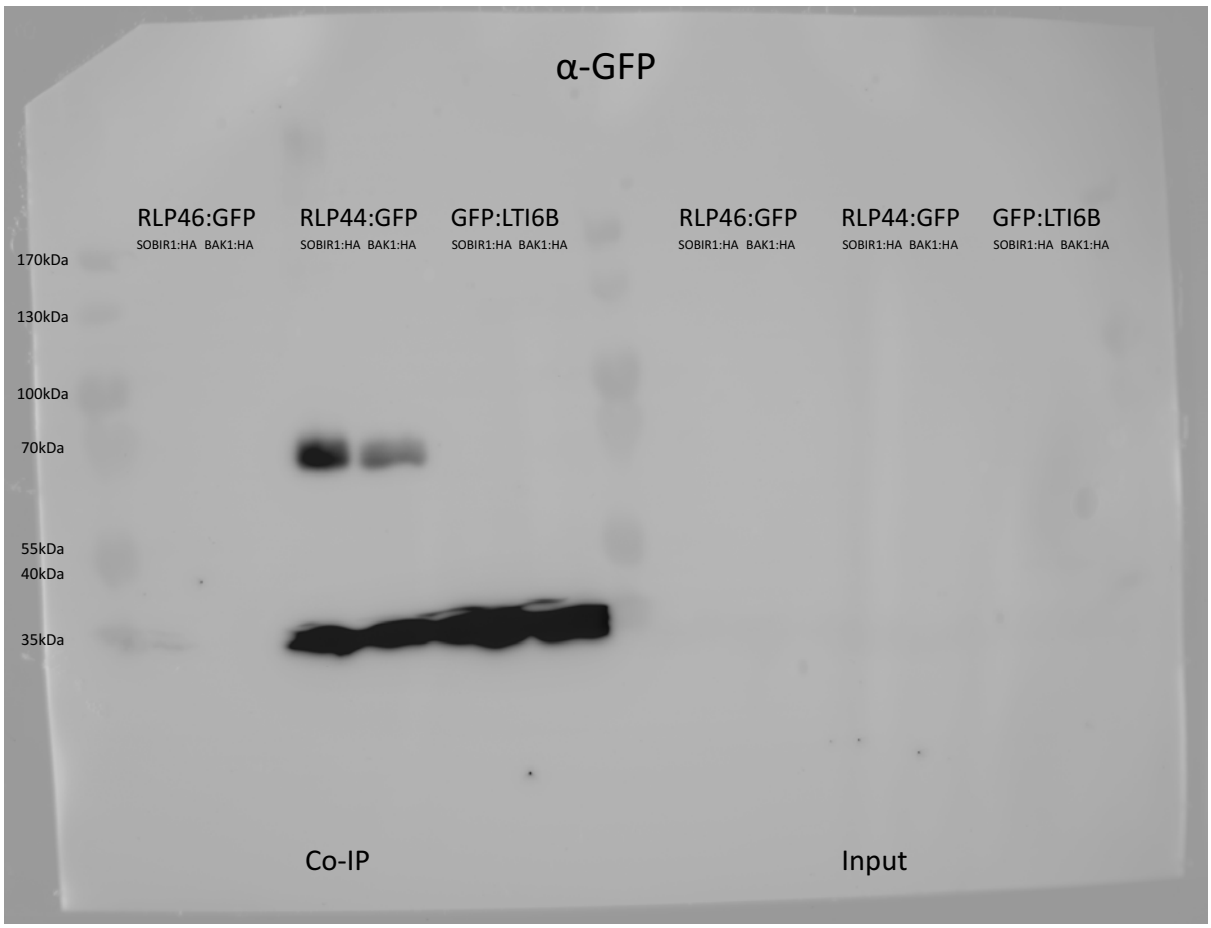

Appendix 5: Uncropped Western Blot image from figure 36 section D.

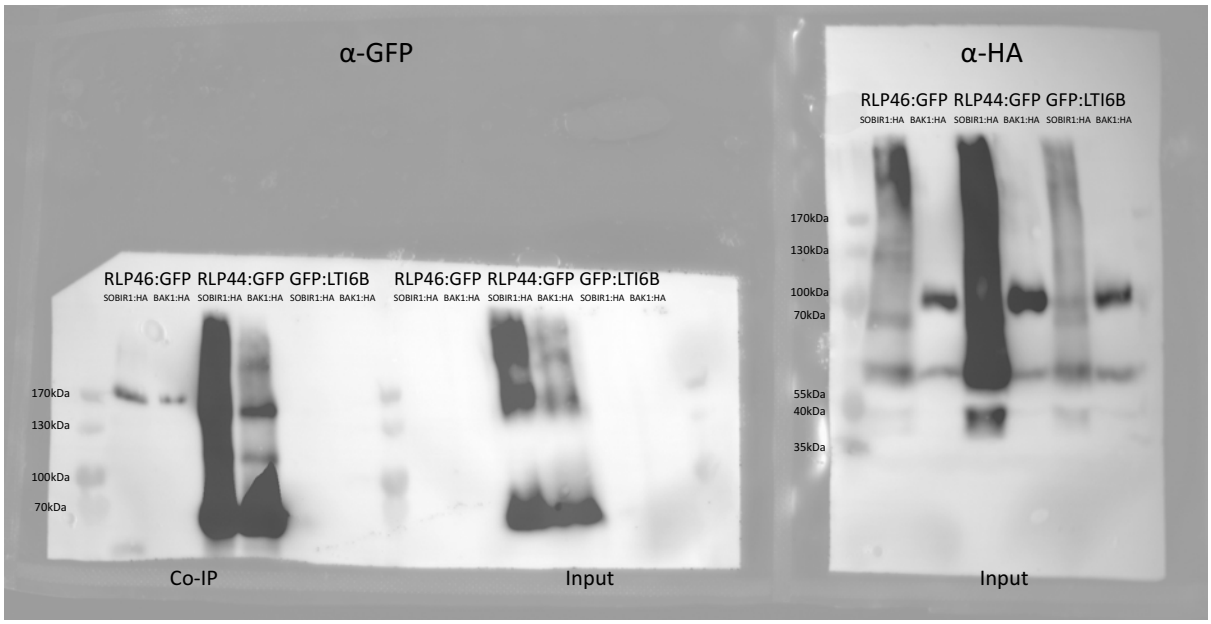

Appendix 6: Complete Tukey HSD test results from figure 7. *pskl1* mutant lines showed a significant difference in their response to PSK treatment as compared to the WT control (p value of 0.002 AND 6.1×10^{-6} respectively), however only *pskl1-058* showed a significant response to PSK (p value of 4.8×10^{-5}), which contradicts literary sources on Col-0 response (Kutschmar et al., 2009). N of 94, 93, 60, 77, 58, and 81 respectively. Data combined from 3 iterations of experiment.

	diff	lwr	upr	p adj
Col0&PSK-Col0	0.04423519	-1.0736669	1.1621373	0.9999974
pskl1_058-Col0	-0.03454475	-1.3107845	1.2416950	0.9999996
pskl1_058&PSK-Col0	2.12988075	0.9711008	3.2886607	0.0000033
pskl1_203-Col0	0.58659433	-0.6764227	1.8496113	0.7687303
pskl1_203&PSK-Col0	1.60696516	0.4443015	2.7696288	0.0012371
pskl1_058-Col0&PSK	-0.07877994	-1.3576352	1.2000753	0.9999764
pskl1_058&PSK-Col0&PSK	2.08564556	0.9239856	3.2473055	0.0000061
pskl1_203-Col0&PSK	0.54235914	-0.7233007	1.8080190	0.8238499
pskl1_203&PSK-Col0&PSK	1.56272997	0.3971959	2.7282640	0.0019604
pskl1_058&PSK-pskl1_058	2.16442550	0.8496873	3.4791637	0.0000479
pskl1_203-pskl1_058	0.62113908	-0.7863329	2.0286111	0.8050076
pskl1_203&PSK-pskl1_058	1.64150991	0.3233475	2.9596724	0.0053804
pskl1_203-pskl1_058&PSK	-1.54328642	-2.8451929	-0.2413799	0.0097457
pskl1_203&PSK-pskl1_058&PSK	-0.52291559	-1.7277124	0.6818812	0.8158514
pskl1_203&PSK-pskl1_203	1.02037083	-0.2849936	2.3257353	0.2228885

Acknowledgments

I thank all of the many colleagues and mentors that have helped me along the way to this moment. Without your support and instruction, I would not be the person I am today.

Dr. Sebastian Wolf, thank you for providing me this opportunity and being a great mentor. Prof. Dr. Karin Schumacher, thank you for accepting me into the master program in the first place.

Nabila, Polo, Rachel, and Tobi, thank you for always being rays of sunshine in the lab and good friends outside of it.

The Wolf group, thank you for being a wonderful set of colleagues to spend the last few years with.

HBIGS, thank you for accepting me into this program, and thank you all of COS for being the best institute a guy could hope to work in.

I also thank my wonderful family for everything they have done for and with me over the years. I could not have asked for a better sister or set of parents and your support has been the foundation of all my accomplishments.

To all my friends, especially Brian, Canaan, Geoff, and Kevin, thank you for always being there for me and always encouraging me to strive for what I believe in.

And lastly, thank you for everything Nora, you are an endless source of wonder. Even if coming to Germany had only resulted in meeting you it would still be the best decision I ever made. You inspire me to be the best person I can be.